Politecnico Di Milano
Facoltà di Ingegneria Industriale
Corso di Laurea in Ingegneria Meccanica Orientamento Trasporti

An Integrated Approach to a Condition Based Maintenance policy and applications

Relatore: Prof. Stefano **Beretta**

Co-relatore: Prof. Giovanni **Jacazio**

Tesi di laurea di:

Mattia Gabriele Vismara

Matr. 720285

Anno Accademico 2010/2011

Acknowledgments

I would like to thank prof. Beretta for his fairness, support and availability.

I'm also grateful for prof. Jacazio who gave me the opportunity to study in deep this innovative field and for his patience and support during these two years. without which this work would not have been possible.

I would eventually reserve my special thanks to professors Pastorelli and Sorli for their suggestions and encouragement.

Abstract

Unexpected system failures pose a significant problem in human safety and health care applications, service and manufacturing sectors, national infrastructure (nuclear power plants and civil structures), and national security (military operations). The main challenges associated with unexpected failures are related to characterizing the failure uncertainty and the stochastic nature of the degradation processes. An accurate failure time prediction and a reliability assessment are necessary if the appropriate maintenance resources (personnel, tools, spare parts, etc.) are to be assembled. For this reason the thesis presents a mathematical framework for integrating degradation-based sensor data streams with high-level logistical decision models. To achieve this goal, a software has been realized in order to simulate a discontinuous operational scenario (such as aircraft operations) in which two different maintenance policies were applied, a scheduled and a condition-based one. The former refers to a typical maintenance policy, in which no prognostic data are available, so that maintenance is scheduled basing only on prior knowledge of components' failure behavior. The latter approach, instead, implements the information given by prognostics in order to fully exploit the component's residual useful life and reduce the lead time to deliver spare parts. The last change is achieved through a revision and a modification of the entire supply chain model in a Just-In-Time-like perspective: thanks to a more precise knowledge of the time to failure, spare parts can be stored in depots so to be in the maintenance zone just before they are needed. Thus, it is possible to move these parts to higher level depots, where hold stocking costs are typically lower. As for prognostics, it has been made possible through the realisation of a RUL estimation algorithm. It is to say that many techniques have been found in literature, but none of them faced the prognostic problem with the aim of finding a closed form for RUL estimation The most promising predictive algorithm, among those developed before this work, turned out to be a Bayesian estimator based on the degradation pattern of the monitored component, under the likely assumption of exponential shape of such pattern. This algorithm has been the starting point for the one developed in this work. Leveraging on Bayesian probability theory, the up-to-date RUL probability density function of the component is evaluated at each time step, starting from the prior knowledge of the component's residual life, a stochastic parameter that is evaluated from experimental tests always done before commissioning. The

information about RUL prediction was then used to define the optimal moment at which scheduling and performing maintenance. These values were found through an objective function optimization that took into account the main drivers associated to condition-based maintenance decision making process.

Furthermore the opportunity to introduce CBM (condition based maintenance) concepts based on prognostic into a cracked railway axle management is investigated. The performances of two different prognostic algorithm are assessed on the basis of their RUL (remaining useful life) predictions accuracy. The CBM approach is compared to the classical preventive maintenance approach to railway axle maintenance management based on expensive and regular NDT. The effect of monitoring frequency and the monitoring infrastructure size error is assessed as well.

Keywords:

Prognostics, Condition Based Maintenance, Railway axles, Crack propagation

Table of Contents

Acknowledgments 3

Abstract 5

List of Tables 13

List of Figures 15

1. Introduction to CBM 23

   1.1. Diagnostics 31

   1.2. Prognostics 34

   1.3. Research Objectives and Organization 40

2. Literature Review 45

   2.1. Prognostic Algorithms in CBM 45

      2.1.1. Markov Processes 45

      2.1.2. Neural Networks 47

      2.1.3. Proportional Hazard Models 49

      2.1.4. Degradation Models 51

   2.2. Benefit of CBM policy assessment 54

3. The Integrated framework 59

   3.1. The Prognostic Algorithm 59

      3.1.1. Degradation Signal Generation 59

      3.1.2. Bayesian degradation predictive algorithm 64

   3.2. Maintenance Scheduling and replacement model 79

3.2.1. Introduction 79

3.2.2. The model 80

3.2.3. The operational scenario 87

3.2.4. Results 89

3.3. Spare Part Supply Chain model 96

3.3.1. The Model 96

3.3.2. Results and Sensitivity Analysis 102

4. Case Study 105

4.1. Introduction 105

4.1.1. Data 107

4.2. Simulation of the crack growth paths – The stochastic crack growth algorithm 107

4.3. Design of the preventive maintenance approach 114

4.3.2. Identification of the maximum inspection interval 121

4.4. Prognostic Modeling of the Crack Size Growth 125

4.4.1. Setting the threshold 125

4.4.2. Bayesian updating algorithm 129

4.4.3. Prognostic through the physical model 150

4.4.4. The size error and the updating frequency effect on TTF predictions 154

4.5. Results 160

5. Conclusions 169

6. References 173

7. Appendix 185

List of Tables

Table 1 Main Cost and benefits of CBM 27

Table 2 Values used in the case study simulation.....91

Table 3 Methodology results comparison.....94

Table 4 Results from the scheduling and replacement model for different LT ..94

Table 5 Expected demand.....102

Table 6 The 12 service time blocks.....110

Table 7 PC_{DET} with different inspection interval.....124

Table 8 $\omega 1, \beta 1, \omega 2$ and $\beta 2$ a priori pdfs parameters.....139

Table 9 Percentage prediction errors.....166

Table 10 Results – φ, $Ninsp$ and $Ninsp$ 167

List of Figures

Figure 1 The shift in condition monitoring paradigm 24

Figure 2 Maintainer's requirements 25

Figure 3 Failure progression timeline 29

Figure 4 CBM program steps 30

Figure 5 Truth and models of prior and posterior PDFs 35

Figure 6 Max Lead-Time interval for 95% confidence 37

Figure 7 Prognosis with 95% confidence and various LTIs 39

Figure 8 RUL prediction dynamics 58

Figure 9 Simulated exponential degradation signal 60

Figure 10 ti Estimation (blue line) and ti real value obtained from 50 simulations 61

Figure 11 ti estimation percentage error 62

Figure 12 Exponential interpolation using simplex least square regression 63

Figure 13 Vibration-based degradation signal of bearings 65

Figure 14 The MQE of three degradation processes: 65

Figure 15 A' normal probability plot 67

Figure 16 B normal probability plot 68

Figure 17 Updated mean and variance of the exponential model parameters 73

Figure 18 Updated correlation coefficient 73

Figure 19 RUL pdfs estimated at different time steps 74

Figure 20 Synopsis of RUL estimation (blue line), real RUL (gray line) and RUL lower bound at 97.5% level of confidence 75

Figure 21 RUL estimation confidence interval amplitude 75

Figure 22 Synopsis of reliable RUL estimation 78

Figure 23 Dynamics of maintenance decision-making process 82

Figure 24 Decreasing trend of RUL from different simulations 84

Figure 25 $f1$, $f3$, $f3$, $f4$, $f5$ computed at a given time ts 85

Figure 26 Example of $tr*$ and $ts*$ computation 86

Figure 27 Extending life by transitioning to condition based maintenance 89

Figure 28 Classical approach to safety stock problem 96

Figure 29 Ti and hi values 100

Figure 30 Number of stocked spares in the four depots as a function of tl 100

Figure 31 Number of stocked spares in the four depots as a function of σtl ... 101

Figure 32 Total stocking costs as a function of tl and σtl 101

Figure 33 Safety Stock for each scenario 103

Figure 34 Results from the supply chain model, percentage variations with respect to corrective maintenance policy 104

Figure 35 Example of a load history 111

Figure 36 Examples of simulated crack growth paths 111

Figure 37 TTF probability distribution 112

Figure 38 Lognormal fit plot for TTF pdf 113

Figure 39 The damage tolerant approach to design a preventive maintenance approach [69] 115

Figure 40 MLE results 117

Figure 41 Fastest growth crack 122

Figure 42 Calculation of the cumulative probability of detection and the fault tree of the inspection 123

Figure 43 $PCDET$ as function of the inspection intervals.....124

Figure 44 Illustration of the meaning of the size error.....126

Figure 45 The errors affecting the monitoring and prognostic system 127

Figure 46 Crack size threshold as a function of σr and $amax$.....129

Figure 47 The two exponential models.....130

Figure 48 Threshold Sth distribution.....132

Figure 49 (a) $\log\theta 1$ PDF, (c) $\log\theta 2$ PDF, (b) $\beta 1$ PDF, (d) $\beta 2$ PDF 133

Figure 50 (a) $T1$ pdf (b) $T2$ pdf 140

Figure 51 Simulated a priori TTF and a priori modeled TTF comparison – probability plot.....141

Figure 52 Simulated a priori TTF and a priori modeled TTF comparison – cdf 142

Figure 53 Correlations between the couple of model parameters.....143

Figure 54 Crack growth path.....146

Figure 55 a) updated $\mu\omega 1$ and b) updated $\mu\beta 1$.....147

Figure 56 Predicted TTF - 1st phase.....148

Figure 57 a) updated $\mu\omega 2$ and b) updated $\mu\beta 2$ 149

Figure 58 Predicted TTF – 2nd phase 150

Figure 59 TTF prediction through the NASGRO crack growth model 151

Figure 60 The approximated TTF probability plot 152

Figure 61 TTF predictions 153

Figure 62 Estimated TTF at the 0.01 and 0.98 confidence level 154

Figure 63 The effect of updating frequency on TTF predictions 156

Figure 64 The error size effect on TTF predictions 157

Figure 65 The updating frequency and size error combined effect 158

Figure 66 The 10 selected crack growth paths 160

Figure 67 Comparison of the a priori TTF pdf and the updated TTF pdf obtained from the prognostics algorithms described (green-Bayesian, blue physical based model, black - a priori) 162

Figure 68 Percentage prediction error @ 25% FT 164

Figure 69 Percentage prediction error @ 50% FT 164

Figure 70 Percentage prediction error @ 75% FT 165

Figure 71 Percentage prediction error @ 98% FT 165

Figure 72 MS of the percentage prediction errors for each residual life percentile 166

Figure 73 The size error effect on life exploited given $\delta = 90\ km$ 168

Figure 74: PHM applicability 171

1. Introduction to CBM

The area of intelligent maintenance and diagnostic and prognostic–enabled CBM of machinery is a vital one for today's complex systems in industry, aerospace vehicles, military and merchant ships, the automotive industry, and elsewhere. The industrial and military communities are concerned about critical system and component reliability and availability. The goals are both to maximize equipment up time and to minimize maintenance and operating costs. As manning levels are reduced and equipment becomes more complex, intelligent maintenance schemes must replace the old prescheduled and labor intensive planned maintenance systems to ensure that equipment continues to function. Increased demands on machinery place growing importance on keeping all equipment in service to accommodate mission-critical usage.
While fault detection and fault isolation effectiveness with very low false alarm rates continue to improve on these new applications, prognosis requirements are even more ambitious and present very significant challenges to system design teams.

A significant paradigm shift is clearly happening in the world of complex systems maintenance and support. Figure 1 attempts to show the analogy of this shift between what is being enabled by intelligent machine fault diagnosis and prognosis in the current world of complex equipment maintenance and how the old-time coal miners used canaries to monitor the health of their mines. The ''old'' approach was to put a canary in a mine, watch it periodically, and if it died, you knew that the air in the mine was going bad. The ''new'' approach would be to use current available technologies and PHM-type capabilities to continuously monitor the health of the canary and get a much earlier indication that the mine was starting to go bad. This new approach provides the predictive early indication and the prognosis of useful mine life remaining, enables significantly better mine maintenance and health management, and also lets you reuse the canary.

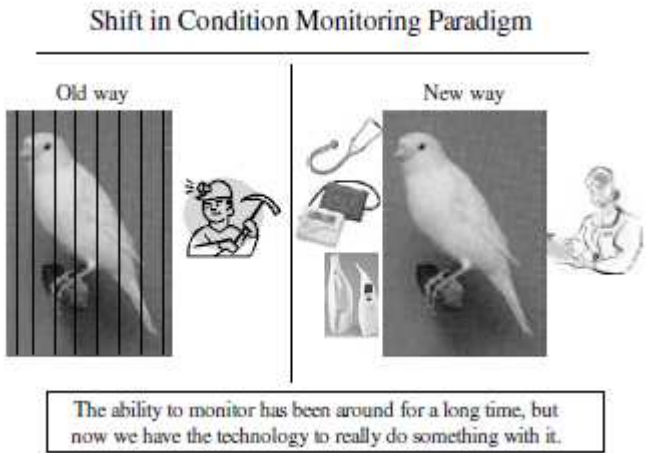

Figure 1 The shift in condition monitoring paradigm

Prognosis is one of the more challenging aspects of the modern prognostic and health management (PHM) system. It also has the potential to be the most beneficial in terms of both reduced operational and support (O&S) cost and life-cycle total ownership cost (TOC) and improved safety of many types of machinery and complex systems. The evolution of diagnostic monitoring systems for complex systems has led to the recognition that predictive prognosis is both desired and technically possible. By exploiting the data provided by the enhanced monitoring systems and turning them into information, many features relating to the health of the aircraft can be deduced in ways never before imagined. This information then can be turned into knowledge and better decisions on how to manage the health of the system.

The increase in this diagnostic capability naturally has evolved into something more: the desire for prognosis. Designers reasoned that if it were possible to use existing data and data sources to diagnose failed components, why wouldn't it be possible to detect and monitor the onset of failure, thus catching failures before they actually hamper the ability of the air vehicle to perform its functions. By doing this, mission reliability would be increased greatly, maintenance actions would be scheduled better to reduce the asset down time, and a dramatic decrease in life-cycle costs could be realized. It is with this mind-set that many of today's ''diagnostic systems'' are being developed with an eye toward prognosis.

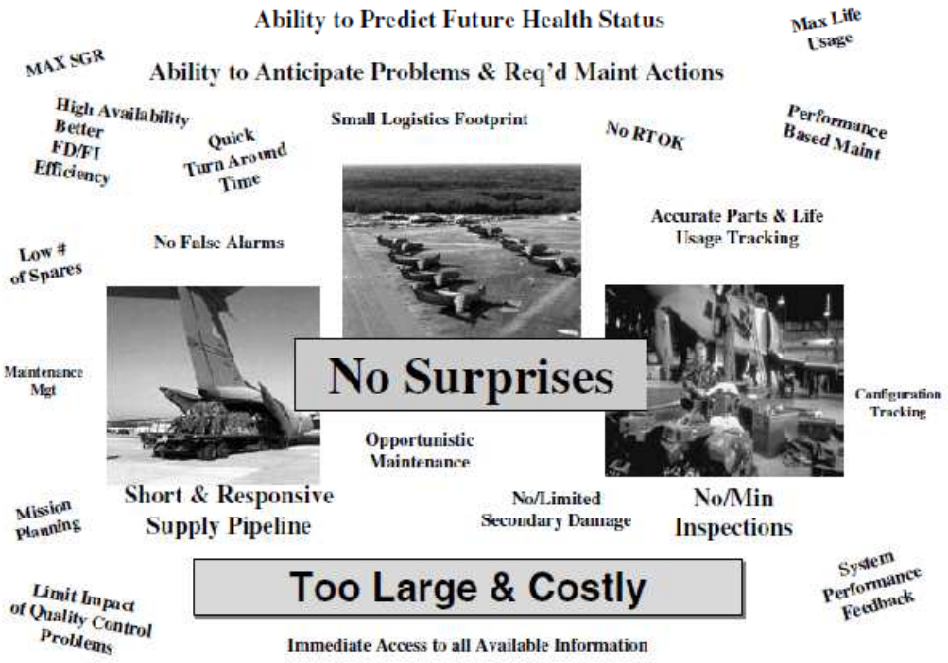

Figure 2 Maintainer's requirements [1]

If you were to ask a fleet user or maintainer what his or her most pressing needs were, you most probably would get a mixture of many answers. He or she would identify many needs, including some of the following responses: maximize sortie-generation rates and system availability, minimum or no periodic inspections, low number of spares required and small logistics footprint, quick turn-around time, maximized life usage and accurate parts life tracking, no false alarms, etc. Figure 2 depicts some of these and other fleet user needs. What the maintainer actually may want most of all is no surprises. He or she would like to be able to have the ability to predict future health status accurately and to anticipate problems and required maintenance actions ahead of being surprised by ‘‘hard downing’’ events. Capabilities that would let the maintainer see ahead of both unplanned and even some necessary maintenance events would enable a very aggressive and beneficial opportunistic maintenance strategy. These combined abilities both to anticipate future maintenance problems and required maintenance actions and to predict future health status are key enablers and attributes to any condition-based maintenance (CBM) or new logistics support concept and to ‘‘enlightened’’ opportunistic maintenance decisions. These predictive abilities and prognostic capabilities are also key enablers and very

necessary attributes to both the evolving performance-based logistics (PBL) concepts and paradigm-changing new business case approaches.

A modern and comprehensive prognosis and health management system needs to interface with the logistic information system to trigger (1) the activities of the supply-chain management system promptly to provide required replacement parts, (2) planning needed to perform the required maintenance, and (3) training of the maintainer. The main benefits and costs related to the implementation of a PHM system are [**2**][**3**]:

Reductions in the use of spare components	Accurate diagnosis of problems0 by PHM system will reduce the number of removals of parts where no trouble is found in ground testing.
Reductions in direct maintenance manpower	PHM provides several ways in which direct maintenance manpower will be reduced, including: • PHM provides a capability to predict failures in terms of remaining useful life thereby providing the opportunity to remove the component before it can contribute to an accident or failure. • PHM accurately identifies failed components so they can be quickly replaced. • Fewer removals of parts where no trouble is found with ground testing. • Less time will be spent on ground inspections because PHM will determine whether a problem exists. • Less time will be spent diagnosing and isolating failure because PHM will perform these functions. • Less time will be spent checking out repair actions because PHM will do the checkout when the repair action is complete. • Since there will be fewer repair actions because of the reduction incidents where no trouble is found, there will also be less damage inadvertently done by maintainers during removal and replacement operations. • Reduced need for maintainers to set up and use ground test equipment because PHM will provide on-board diagnostics, fault isolation and checkout, and • Since PHM will determine the condition of a component, parts previously removed on a time interval basis, some components can remain on the aircraft until their condition warrants removal. • These all contribute to reduced MTTRs and ultimately a reduction in the number of maintainers required supporting the system

Reductions in indirect maintenance manpower	With significant reductions in direct manpower, the numbers of indirect support staff can also be reduced.
Reduction in the amount of ground support equipment	Since PHM will provide an on-board diagnosis, fault isolation and checkout, there is a reduced need for ground support equipment.
Reduction in training costs	Less direct maintenance manpower means fewer people have to be trained. Lighter workloads in some specialty areas provides an opportunity to cross train people in more occupational specialties providing more flexibility in assignment of maintenance crews and further reducing the numbers of people to be trained.
Reduction in the rated of major accidents	PHM provides a capability to predict failures in terms of remaining life thereby providing the opportunity to remove the component before it can contribute to an accident.
Increased availability/reliability	Consequence of decreased average repair times due to the improved fault isolation abilities, and of reduced unnecessary repairs, removals, inspections, reduced time awaiting spares
Extended component Life	The capability of removing/repairing the component/subsystem just before failure imply an increase in component life.
Investment costs	A PHM approach requires high investments, such as: • Experimental tests (Accelerated degradation tests) • High R&D expenses required, to be replicated for each new/different component • System development (IT infrastructure, hardware, software, systems integration) • Processes reengineering
Missed and False Alarms, failure modes coverage	False alarms: • Cause extra maintenance actions • May result in unnecessary removals • Reduces User's confidence in system Missed Alarms: • Missed detections result in greater problems after PHM since Inventory levels would have been reduced so likelihood of having convenient replacement is much lower. • Significantly Reduces Users Confidence in system.

Table 1 Main Cost and benefits of CBM

Historically, such predictions would have been more of a black art than a science. Essentially, prognosis provides the predictive part of a comprehensive health management system and so complements the diagnostic capabilities that detect, isolate, and quantify the fault, and prognosis, in turn, depends on the quality of the diagnostic system.

From an operator's, maintainer's, or logistician's—the user's—point of view, what distinguishes prognosis from diagnosis is the provision of a lead time or warning time to the useful life or failure and that this time window is far enough ahead for the appropriate action to be taken. Naturally, what constitutes an appropriate time window and action depends on the particular user of the information and the overall system of systems design one is trying to optimize. Thus prognosis is that part of the overall PHM capability that provides a prediction of the lead time to a failure event in sufficient time for it to be acted on.

What, then, constitutes a prognostic method—essentially any method that provides a sufficient answer (time window) to meet the user's needs. This is an inclusive approach and one that is seen as necessary to get the system of systems-wide coverage and benefits of prognosis. Some would argue that the only true prognostic methods are those based on the physics of failure and one's ability to model the progression of failure. While this proposition has scientific merit, such an unnecessarily exclusive approach is inappropriate Within security limitations, failure data should be available to all levels, including sustaining engineering personnel, OEMs, major command staff, and unit-level war fighter personnel. Some of the benefits of such a PHM system are listed below. given the current state of the art of prognostic technologies and the most likely outcome of insufficient coverage to provide system-wide prognosis.

Thus prognostic methods can range from the very simple to the very complex. Examples of the many approaches are simple performance degradation trending, more traditional life usage counting (cycle counting with damage assessment models and useful life remaining prediction models), the physics of failure-based, sometime sensor driven and probabilistic enhanced, incipient fault (crack, etc) propagation models, and others.

To understand the role of predictive prognosis, one has to understand the relationship between diagnosis and prognosis capabilities. Envisioning an initial fault to failure progression timeline is one way of exploring this relationship. Figure 3 represents such a failure progression timeline. This timeline starts with

a new component in proper working order, indicates a time when an early incipient fault develops, and depicts how, under continuing usage, the component reaches a component or system failure state and eventually, if under further operation, reaching states of secondary system damage and complete catastrophic failure.

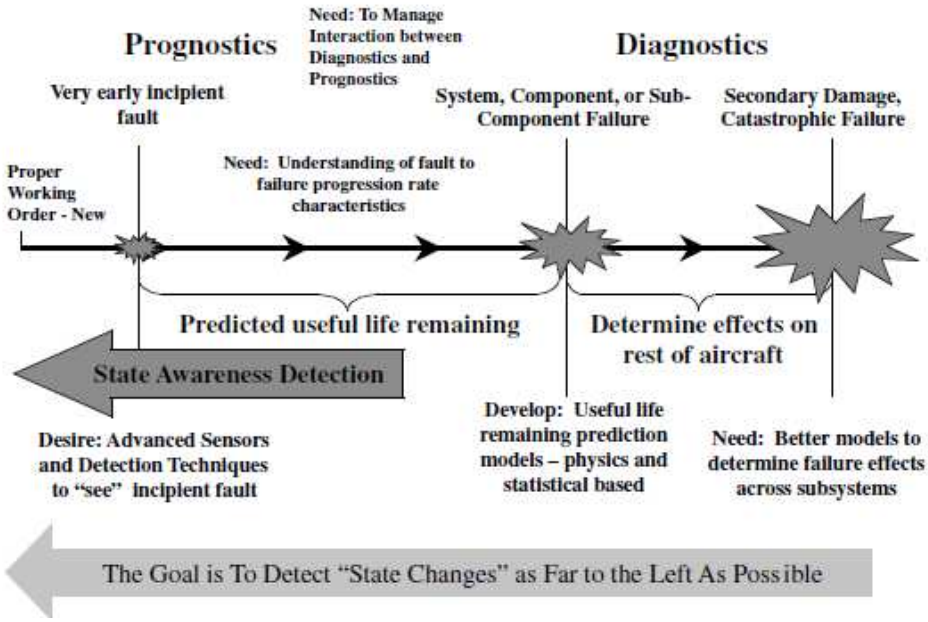

Figure 3 Failure progression timeline[1]

Diagnostic capabilities traditionally have been applied at or between the initial detection of a system, component, or subcomponent failure and complete system catastrophic failure. More recent diagnostic technologies are enabling detections to be made at much earlier incipient fault stages. In order to maximize the benefits of continued operational life of a system or subsystem component, maintenance often will be delayed until the early incipient fault progresses to a more severe state but before an actual failure event. This area between very early detection of incipient faults and progression to actual system or component failure states is the realm of prognostic technologies.

If an operator has the will to continue to operate a system and/or component with a known, detected incipient fault present, he or she will want to ensure that this can be done safely and will want to know how much useful life remains at

any point along this particular failure progression timeline. This is the specific domain of real predictive prognosis, being able to accurately predict useful life remaining along a specific failure progression timeline for a particular system or component.

To actually accomplish these accurate useful life remaining prediction capabilities requires many tools in your prognostic tool kit. Sometimes available sensors currently used for diagnosis provide adequate prognostic state awareness inputs, and sometimes advanced sensors or additional incipient fault detection techniques are required.

A CBM program consists of three key steps [**4**] (see Figure 4):

1. Data acquisition step (information collecting), to obtain data relevant to system health.
2. Data processing step (information handling), to handle and analyze the data or signals collected in step 1 for better understanding and interpretation of the data.
3. Maintenance decision-making step (decision-making), to recommend efficient maintenance policies.

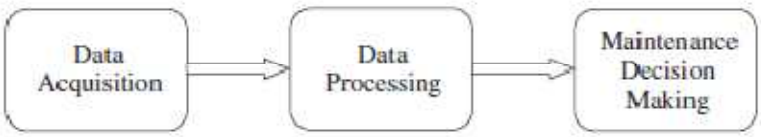

Figure 4 CBM program steps [5]

Diagnostics and prognostics are two important aspects in a CBM program. Diagnostics deals with fault detection, isolation and identification when it occurs. Fault detection is a task to indicate whether something is going wrong in the monitored system; fault isolation is a task to locate the component that is faulty; and fault identification is a task to determine the nature of the fault when it is detected. Prognostics deals with fault prediction before it occurs. Fault prediction is a task to determine whether a fault is impending and estimate how soon and how likely a fault will occur. Diagnostics is posterior event analysis and prognostics is prior event analysis. Prognostics is much more efficient than diagnostics to achieve zero-downtime performance.
Diagnostics, however, is required when fault prediction of prognostics fails and a fault occurs. A CBM program can be used to do diagnostics or prognostics, or

both. No matter what the objective of a CBM program is, however, the above three CBM steps are followed.

Data acquisition is a process of collecting and storing useful data (information) from targeted physical assets for the purpose of CBM. This process is an essential step in implementing a CBM program for machinery fault (or failure, which is usually caused by one or more machinery faults) diagnostics and prognostics. Data collected in a CBM program can be categorised into two main types: the so-called event data and condition monitoring data. Event data include the information on what happened (e.g., installation, breakdown, overhaul, etc., and what the causes were) and/or what was done (e.g., minor repair, preventive maintenance, oil change, etc.) to the targeted physical asset. Condition monitoring data are the measurements related to the health condition/state of the physical asset.

Data processing is a process of cleaning the acquired data from noise and errors (data clearing), and afterwards data analysis through appropriate algorithms (see for a list [**5**] depending on the type of data available. The aim of this phase is to compute a measure or a set of measures strictly correlated to health state of the component/subsystem/system.

Maintenance decision-making is the last step of a CBM program is maintenance decision-making. Sufficient and efficient decision support would be crucial to maintenance personnel's decisions on taking maintenance actions. Techniques for maintenance decision support in a CBM program can be divided into two main categories[**5**]: *diagnostics* and *prognostics*. As mentioned earlier, fault diagnostics focuses on detection, isolation and identification of faults when they occur.

1.1.Diagnostics

Diagnostics in engineering systems is a relatively well understood field of study. It deals with the detection of conditions of anomaly (faults or failures), the isolation of the subsystem or the interested component and, possibly, the identification of fault severity. It is important, for clarity, to introduce some definitions [**1**]:

- Fault diagnosis: Detecting, isolating and identifying a pending or incipient failure condition. The affected component (subsystem, system) is still operational even though in a degraded mode;
- Failure diagnosis: Detecting, isolating and identifying a component (subsystem, system) that has ceased to operate.
  Moreover:
- Fault/failure detection: an abnormal operating condition is detected and reported;
- Fault/failure isolation: determining which component (subsystem, system) is failing or has failed;
- Fault/failure identification: estimating the nature and extent of the fault/failure.

Many are the fields of application and consequently the number of enabling technologies that have been experimented over the time to deal with this kind of problems. However, some features are common to the major part of applications and thus can be used to give a general description of what is included within a diagnostic system:

- Sensors to collect data of the observed process variables and parameters (hardware);
- A feature extractor that reduces raw data dimensions and extracts condition indicators (features) to be
- used within the diagnostic algorithms (software);
- One or more diagnostic algorithms used to assess the current state of monitored components (software).

Diagnostic algorithms, in particular, must detect system performance, degradation levels and the eventual presence of abnormal conditions by evaluating physical property changes through detectable phenomena. For complex systems, like aircrafts, the number of possible faults is too high to create a diagnostic system having extended identification abilities. The number and type of faults to be taken into account are normally identified using of Failure Mode, Effects and Criticality Analysis (FMECA), by evaluating frequency and potential impact of failures and by cost considerations. However, detection capacities must be kept, in any case, sufficiently high.

A reduced false negative rate, indicating the frequency of undetected anomaly conditions is in fact one of the main requirements of a diagnostic system. A set of these typical requirements is presented below[**1**] :

- Maximum false positive rate, or false alarm rate;
- Maximum negative rate, to be reduced as much as possible;
- Minimum percentage of detection on monitored failures;
- Minimum percentage of identification on monitored failures;
- Minimum fault isolation rate on monitored subsystems;
- Minimum operating period between false alarms (MOPBFA);
- Maximum time window between fault initiation and detection.

The designer's objective is to achieve the best possible performances or at least to fulfill the minimum requirements. To reach this objective, it is important that some basic considerations are kept in mind during the design process. First of all, when working on diagnostic algorithms, a sufficient amount of data is always needed from both normal and faulted conditions of the monitored system. Significant results can be achieved only if massive experimental databases are available. Optimal feature selection is then another focal point. For this, good knowledge of the system is required together with a significant amount of time to be spent on experimental data analysis. The choice of the type of fault detection/identification algorithm to be used is of course another key point. One algorithm can be used for different faults or more than one algorithm can be used on the same component with the aim of improving the diagnostic abilities of the system. In the latter case, the way in which evidences coming from different algorithms are merged together (data fusion) is a crucial point too.

The enabling technologies typically fall into two major categories: model-based and data-driven. Model-based techniques rely on an accurate dynamic model of the system and are able to detect even unanticipated faults. They generate from the actual system's and model's output a residual between the two outputs that is indicative of a potential fault condition. On the other hand, data-driven techniques often address only anticipated fault conditions, where a fault model is a construct or a collection of constructs, such as neural networks, expert

systems, etc. that must be trained first with known prototype fault data before being employed online for diagnostic purpose.

1.2. Prognostics

Prognostics refers to the capability to provide early detection of the fault condition of a component, and to have the technology and means to manage and predict the progression of this fault condition to component failure[**6**].

The early-detected fault condition is monitored and safely managed from a small fault as it progresses until it warrants maintenance action and/or replacement. Impacts on other components and secondary damages are also continually monitored and considered during this fault progression process. Through this early detection and the monitoring of fault progression management the health of the component is known at any point in time and the future failure event can be safely predicted in time to prevent it. That is, useful life remaining can be predicted with some reasonably acceptable degree of confidence.
The aspect that prognostics takes place in the present requires to be a dynamic process evolving in time from the moment a component is working until it has reached failure. Prognostics is fundamentally different from a static, prior knowledge of its time to failure. In this context, prognostics is a remaining life estimation methodology that is condition-based and dynamic in both accuracy and uncertainty.

Condition-based assessments, the underpinning of the Condition-Based Maintenance philosophy, usually emphasized the diagnosis of problems rather than the prediction of remaining life. Prognoses are considerably more difficult to formulate since their accuracy is subject to stochastic processes that have not yet happened.
As a consequence of uncertainty, prognostics methods must consider the interrelationships among accuracy, precision and confidence. For our purposes, accuracy is a measure of how close a point estimate of failure time is to the actual failure time (FT), whereas precision is a measure of the narrowness of an interval in which the remaining life falls.

The interval is enclosed by upper and lower bounds. Confidence is the probability of the actual remaining life falling between the bounds defined by the precision. We use this interpretation of confidence in the figures and

discussions that follow to reflect the generic use of the term. With this in mind, consider the following paradox: the more precise the remaining life estimate, the less probable this estimate will be correct. In order to clarify this assertion, we begin by reviewing the distinction between the following four idealized Probability Density Functions (pdfs) for remaining life [7]

a) True prior pdf at time zero;
b) Modelled pdf estimating the true pdf at time zero;
c) True posterior pdf conditioned on observations during component use;
d) Modelled pdf estimating the true posterior pdf during component use.

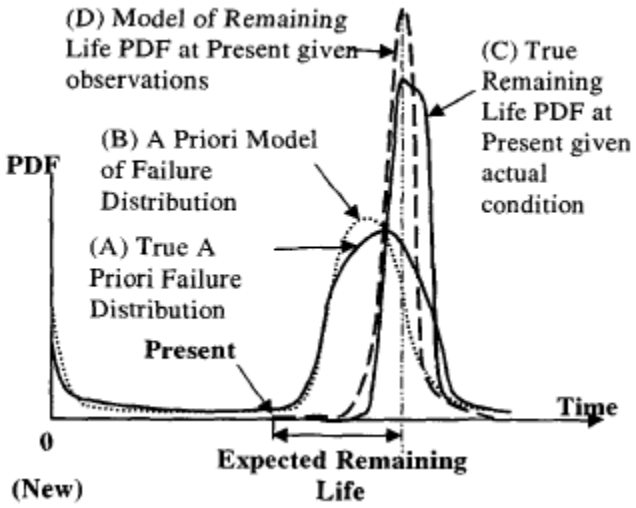

Figure 5 Truth and models of prior and posterior PDFs [6]

A notional illustration of all four is shown in Figure 5. The true prior pdf for an arbitrary component type reflects the actual frequency of lifetimes for all the components ever made (past, present and future). For obvious reasons, we usually settle for a model of this function (pdf B) that can be formed either from a limited number of samples available from real life, or similar experiences derived analytically and/or empirically. The objective of the model is to approach the true distribution so that any differences are inconsequential. Pdf B represents our best estimate of the a priori failure pdf at time zero for any new component of the given type (the so-called "bathtub curve").

Experience shows that components have variations in quality, and are subjected to different use and abuse. From the moment a component is first put into use, the a priori pdfs should be updated since the probability of infant mortality gradually diminishes with operation. In the absence of any other information, a reasonable PDF model can be formed at each moment in time by normalizing the original basic shape of the future portion of the distribution to maintain a cumulative probability of 1.0.

Intuition suggests that a better estimate of remaining life for a specific instance can be found during use by knowing the current condition of the component. This gives rise to the conditional remaining-life pdfs (pdf (c) and pdf (d)). At a given point in time and for a particular observation of component condition (i.e., the point labelled "present" in Figure 5), there exists a posterior pdf for the true remaining life (pdf (c)), and a prognostic model that approximates this truth (pdf (d)). Note that these remaining life distributions ideally are narrower and taller to maintain a total area of 1, yielding more precise but less uncertain estimates. They represent a subset of all possible instances where the distribution has been conditioned on additional information beyond the simple fact that the component is still operating. Note also that the true distributions need not be smooth or symmetrical, whereas the models are often forged into well-understood functions for computational convenience. pdfs (a) and (b) reflect the view before the component is used at time zero, while pdfs (c) and (d) reflect an instantaneous view at some point during use after some damage indication is observed. These are drawn on the same figure for comparative purposes. Remaining life estimates can be formed from prior models (pdf (b)) prior to component use, normalized prior models from the moment use begins, or refined pdfs models (i.e., pdf (d)) if something is known about component condition. Each of these remaining life estimates is covered under the broadest definition of "prognostics". Of course there are many issues associated with predicting expected remaining life, such as how do we recognize current condition and how can we derive the pdfs without a large database of failures.

To the extent that we cannot control the future, the determination of remaining life is a probabilistic computation[**6**]. Without omniscience, one cannot know exactly when a component will fail because the factors responsible for failure generally have unknown future values. Finding where an extrapolated trend meets a condemnation threshold may provide an expectation of remaining life, but it does not provide sufficient information to make a decision. The

probability of failure at this exact moment is essentially zero, and the corresponding confidence interval is unknown. The most informative solution furnishes the estimated pdf, but this is sometimes viewed as too much information. An acceptable solution might provide expected remaining life, and the lower and upper bounds that enclose an area under the PDF that equals the desired confidence. For example, suppose we are required to find the latest point in time for servicing a component that will preclude 95% of the previously experienced failures of components having a specific health condition. Figure 6 illustrates a hypothetical remaining life PDF model for components with the specified condition.

The expected point of failure is shown as the middle of the distribution, but the decision point is actually earlier and is a function of the shape of the pdf. Note that expected value is one way of describing the 'centre' of the distribution.

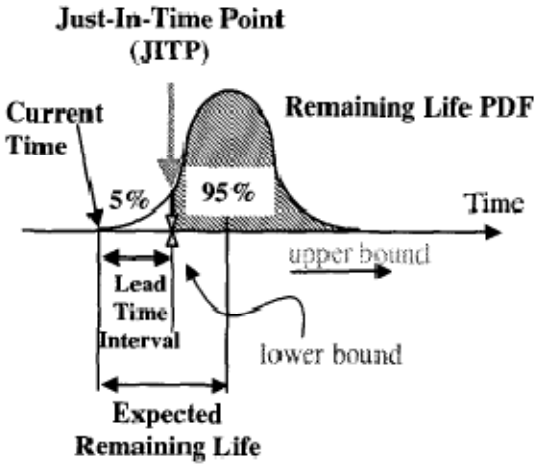

Figure 6 Max Lead-Time interval for 95% confidence [**6**]

Depending on the nature of the distribution, one might choose to use the median or the point of maximum likelihood. The place labeled Just-In-Time Point (JITP) where 5% of the pdf area has passed, is the point in time where 95% of the failures, estimated from previous experience and/or analysis, have not yet happened. The time interval from the present to the JITP is defined as the Lead-Time Interval (LTI). In this example, the upper bound is technically plus infinity indicating an estimate with poor precision. Ideally, we would prefer the distribution to be as narrow as possible so that all failures are avoided and no

unnecessary maintenance is performed. Unfortunately, the shape of the pdf is not under our control as will be explained later. Assigning values to any two of the three parameters (upper bound, lower bound, and confidence) uniquely determines the remaining parameter. As an example, Figure 7 illustrates three possible JITPs that satisfy the 95% confidence requirement, that is to say, 95% of the anticipated failures occur in the hashed in area (between the lower and upper bounds). In all three cases, the expected remaining life is the same while the LTI varies from 0 to the maximum (as shown in Figure 6).

The upper and lower bounds in each graph are indicated by the letters U and L respectively. Note that the lower bound corresponds to the JITP by our previous definition. The top graph suggests that servicing has to be done now. This most conservative philosophy has the side effect of precluding 100% of the possible failures while also having the highest unnecessary maintenance and zero component availability. The bottom graph ensures instead that 95% of the anticipated failures will be avoided. The perceived problem with the bottom graph is 10 the width of the confidence interval, spread between upper and lower bounds. Having a distant upper bound leads to the perception that unnecessary maintenance will be performed since the component may last for quite some time in the future. Of the three shown, this affords the least precision, and counter-intuitively, the least unnecessary maintenance for the same 95% confidence. Knowing only that the upper bound is far in the future does not reveal the likelihood of failures far in the future. The middle graph precludes 97.5% of anticipated failures and also has the smallest spread between upper and lower bounds and thus offers the best precision.

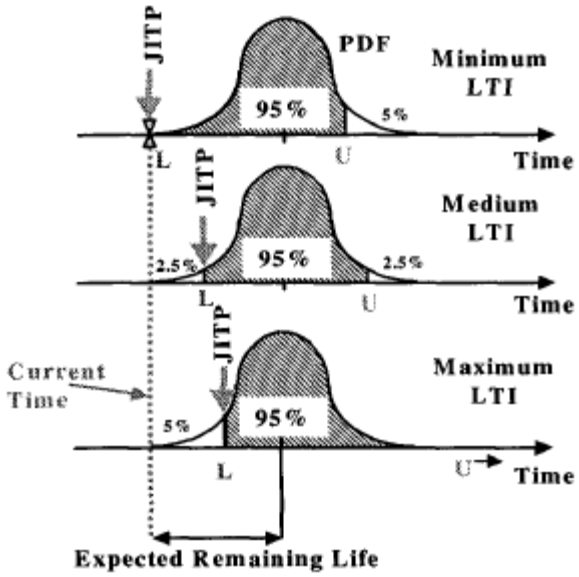

Figure 7 Prognosis with 95% confidence and various LTIs [6]

The fact that the expected remaining life is midway between the upper and lower bounds in this example is simply due to the pdf symmetry and is not necessarily true in general. These examples show that having the tightest tolerance is not always desirable from a prognostic health management point of view given criteria based on 95% confidence. In reality, as time marches along, the pdfs are updated making the LTI a moving target.

The fact that the expected remaining life is midway between the upper and lower bounds in this example is simply due to the pdf symmetry and is not necessarily true in general. These examples show that having the tightest tolerance (least uncertainty) is not always desirable from a phm point of view given criteria based on 95% confidence. In reality, as time marches along, the PDFs are updated making the LTI a moving target.

Putting the mechanics of prognostic methods aside for the moment, if 1000 components having identical conditions at a given time t_l were allowed to run to failure in a realistic environment, we should not be surprised to have 1000 different failure times. This is especially true if the damage condition at time t_l is only slight. The pdf formed by this experiment might be used to model the remaining life for the given condition. If this model were statistically accurate, it would reflect the theoretical best that any prognostics model and attendant

algorithms could achieve at time t_l. It is essential to realize that there is a theoretical limit to the accuracy and precision of any condition-based prognostic method regardless of our ability to know component condition, sensor data quality, preprocessing, feature extraction methods, remaining life projection and associated algorithms.

1.3. Research Objectives and Organization

An integrated approach to obtain and exploit the benefits related to a CBM policy is fundamental.
Seeking for an optimal solution to CBM requires an integrated approach that links maintenance scheduling and replacement decision policy to prognostic algorithm performances and to the supply chain design.

The objective of this work is to present an approach to CBM that links the prognostic algorithm, maintenance scheduling and replacement decision and supply chain design in order to demonstrate the feasibility and the benefits resulting from to a CBM approach. To perform this study a Bayesian prognostic algorithm will be applied to artificial degradation signals representing the degradation of a general LRU with an exponential degradation pattern. Form the information provided by the algorithm, a maintenance scheduling and replacement cost based decision rule will be formulated. Afterwards, the benefits resulting from the CBM approach regarding the spare part supply chain redesign will be highlighted through modeling a (1-S,S) multi-echelon spare part supply chain.

This framework will be applied to an artificial operational scenario representing an aircraft fleet equipped with the LRU mentioned above. The benefit that could arise from applying a CBM policy to the maintenance of the LRU will be qualitatively computed.

Moreover, several sensitivity analysis will be performed to assess the effect of some key variables on the maintenance scheduling and replacement decision policy and to the supply chain design.

Once introduced the integrated framework, the crack growth in railways axles issue will be tackled by a prognostic approach. A CBM approach to cracked axles could reduce the maintenance costs associated to the numerous NDI required to guarantee safety operations. This thesis will investigate the

opportunities that a prognostic approach offers to improve the maintenance of a railway cracked axle. Particularly a prognostic algorithm based on a crack propagation model and a Bayesian prognostic algorithm will be compared.

The remainder of this document is structured as follows:

Chapter 2 reviews some of the literature on prognostic algorithms applied to CBM as well as a brief review of the literature focused on CBM benefits assessment.

In Chapter 3 the integrated framework is described. After explaining how the degradation signals are generated, a Bayesian prognostic algorithm is presented and applied. Some sensitivity analysis is performed on several key variables in order to evaluate how the RUL predictions are affected. Next the maintenance scheduling and replacement decision rule is presented and applied. Sensitivity analysis are performed to evaluate the effects on the overall performances evaluated through three metrics, the lead time guaranteed and its variability, the percentage of the exploited life and the risk taken. Eventually the multi-echelon supply chain is modeled and several considerations are made on the key variables that play a key role in the supply chain design in a CBM environment.

In Chapter 4 the problem of the railway axles maintenance management is faced. The usual preventive maintenance is presented. Next, through the use of a crack propagation model based on fracture mechanics principles, two prognostics algorithm are described and eventually their predictive performance are compared. The conclusions and future research constitute Chapter 5.

2. Literature Review

The literature review is focused on two main topics. The first part is oriented to review the main prognostic algorithms used in CBM programs and how they are used in the context of maintenance management. The second part is focused on review some of the studies on CBM cost benefit assessment as well as on methodology used.

2.1. Prognostic Algorithms in CBM

2.1.1. Markov Processes

A Markov process is a special case of a stochastic process for which the distribution of a future random variable or state depends only on the present state and not on how it arrived in the present state. Since changes in parameters that define equipment degradation are generally probabilistic, as Christer [**8**] points out, many of the published theoretical CBM models adopt a Markov approach to model the degradation, where states are usually 'operating', 'operating but fault present', and 'failed'. Transitions between these states occur according to probabilistic laws, with each state being associated with the coincident occurrence of an inspection and some associated maintenance action.

Monplaisir et al. [**9**] formulated a seven-state Markov chain to model the deterioration process taking place in the crankcase locomotive diesel engines. The authors defined the state-space in terms of certain known pathologies commonly associated with lubricant deterioration. The weekly probabilistic change in physical crankcase oil condition was used as the monitored condition variable. They demonstrated the utility of the model as a maintenance decision support for fault diagnosis, specification of preventive maintenance tasks, and evaluation of alternative policies.

Coolen et al.[**10**] analyzed a basic model for the economic evaluation and optimization of inspection techniques. The model assumed that for a specific failure mode the system passed through an intermediate state, which could be detected by inspection. They presented a 2-phase semi-Markov model to determine the optimal inspection time that minimized maintenance costs. They performed sensitivity analysis to simplify their model and determined which

model parameters could be kept constant without seriously affecting optimal decision making. Assuming that the time spent in the intermediate state can be represented by a unimodel distribution, the authors concluded that an estimation of the mean and standard deviation of this state was enough to provide good decisions about the monitoring interval.

Kallen and van Noortwijk [**11**] presented a decision model for determining the optimal time between periodic inspections of an object with sequential discrete states. The deterioration model used a Markov process to model the uncertain rate of transitioning from one state to the next, allowing the decision maker to properly propagate the uncertainty of the component's condition over time. The model was illustrated by an application to the periodic inspection of road bridges. The author also showed that the model could be applied to production facilities to optimize the threshold for preventive maintenance.

Chen and Trivedi [**12**] presented a semi-Markov decision process for the maintenance policy optimization of condition-based preventive maintenance problems, and presented the approach for joint optimization of inspection rate and maintenance policy. The joint optimization of the inspection rate and maintenance policy was performed by taking the inspection rate as the input parameter to the semi-Markov decision process model. For each individual inspection rate the model was solved for the optimal maintenance policy.

Glazebrook et al. [**13**] formulated a Markov decision process to schedule maintenance routines to minimize the total expected discounted cost incurred in operating a collection of deteriorating machines over an infinite time horizon. Information on the condition of each machine was continuously available to the decision-maker and was expressed through the machine's state. The methodology was illustrated via analyses of two different machine maintenance models.

Saranga and Knezevic [**14**] developed a mathematical model for reliability prediction of condition-based maintained systems in which the component deterioration was modeled as a Markov process. A system of integral equations was used to compute the reliability of the system at any instant of operating time. When the reliability of the item reached the minimum required reliability level, it was assumed that the item has reached a critical state and hence the required maintenance activities should be carried out to restore the system to an

acceptable level. The authors suggested that a well designed condition monitoring strategy incorporated into CBM could offer improved reliability and availability at the system level.

2.1.2. Neural Networks

Artificial Intelligence techniques such as neural networks use sensory information to detect equipment defects and classify their functional condition. A neural network is a data processing system consisting of a large number of simple, highly interconnected processing elements in an architecture inspired by the structure of the cerebral cortex portion of the brain. Because of the topology of the systems and the manner in which information is stored and manipulated, neural networks are often capable of doing things that humans or animals do well but that conventional computers do poorly. For example, neural networks have the ability to recognize patterns even when the information comprising these patterns is noisy or incomplete, to do matching in high-dimensional spaces, and to effectively interpolate and extrapolate from learned data [**15**].
Perhaps the most important characteristic of neural networks is their ability to model processes and systems from actual data. The neural network is supplied with data and then "trained" to mimic the input-output relationship of the process or system. The ability of artificial neural networks to capture and retain nonlinear failure patterns make them an excellent CBM tool, since equipment condition and fault developing trends are often highly nonlinear and time-series based.

Choudhury et al. [**16**] used neural networks to monitor tool wear without having to interrupt the machining process. They presented an on-line monitoring technique to predict flank wear and concluded that flank wear values estimated by the neural network were close to the actual flank wear measured under the tool maker's microscope.

Booth et al. [**17**] used neural network-based condition monitoring techniques to evaluate and classify the operating condition of power transformers in power plants. They demonstrated that neural networks could be used to ascertain the on-line condition of the transformer through estimating the level of vibration based upon other sensor data input, and comparing this with the observed sensor output. They also showed that neural networks could be used to classify the

"health" of the transformer based upon the interrelationships between load current, and thermal and vibration parameters.

Bansal [**18**] introduced a real-time, predictive maintenance system based on the motion current signature of DC motors. They proposed a system that used a neural network to localize and detect abnormal electrical conditions in order to predict mechanical abnormalities that indicate, or may lead to the failure of the motor. The author developed a simulation model to map the system parameters to the motion current signature, and then used the mapping to generate training data for the neural network. The study showed that the classification of the machine system parameters, on the basis of motion current signature, using a neural network approach was possible.

Sinha et al. [**19**] developed a neural network model to predict the failure probability of an underground pipeline system. The neural network was trained using the results of a simulation-based reliability analysis. Several test cases were analyzed, demonstrating that the proposed network was very accurate in predicting the probability of failure directly from the in-line inspection data on depth and length of corrosion defects.

Luxhoj and Shyur [**20**] compared neural network and proportional hazard models for the problem of reliability estimation extrapolated from accelerated life testing data for a metal-oxide-semiconductor integrated circuit. Both modeling approaches were discussed, and their performance in fitting accelerated failure for metal-oxide semiconductor integrated circuits was analyzed. The neural network model resulted in a better fit to the data based upon minimizing the mean square error of the predictions when using failure data from an elevated temperature and voltage to predict reliability at a lower temperature and voltage.

Alguindigue et al. [**15**] discussed their work on developing a methodology for interpreting vibration measurements based on neural networks. The methodology made it possible to automate the monitoring and diagnostic processes for vibrating components. The authors thought that the potential of neural networks to operate in real-time and to handle data that may be distorted and noisy makes the methodology an attractive complement to traditional vibration analysis. They illustrated the effectiveness of the neural network

technique to a data set consisting of vibration data from a steel sheet manufacturing mill.

2.1.3. Proportional Hazard Models

Proportional hazard models a system's risk of failure with its working age and external operating conditions that are captured using explanatory covariates [**21**]. One of the first proportional hazard models was developed by Cox to analyze medical survival data [**22**]. Proportional hazard models were then used in various engineering applications, such as aircrafts, marine applications, and machinery [**23**][**24**][**25**] [**26**].

Kumar and Westberg [**27**] developed a PHM to estimate the optimum maintenance time interval for a system by considering planned and unplanned maintenance costs.

Kobacy et al. [**28**] used simulation techniques to schedule PM intervals for pumps used in a continuous process industry. The authors proposed a proportional hazard model to evaluate the risk of failure and demonstrated that their model lead to an increase in system availability and better performance.

Jardine *et al* [**29**] proposed a PHM with a Weibull baseline hazard function and time-dependent stochastic covariates representing monitored conditions to incorporate condition monitoring information when estimating a component's reliability. A Markov stochastic process was assumed as a model for stochastic covariates. The optimal replacement policy was either to replace at failure or replace when the hazard function exceeded a threshold level determined to minimize the expected total cost per unit time. This study was part of a continuous research effort in the area of CBM to develop software which could assist engineers to optimize decisions in a CBM environment. A case study dealing with diesel engine inspections and replacements illustrated the use of the decision model and software under development. The finished software, called EXAKT, was used by Campbell's Soup to optimize CBM decisions. A study was carried out that compared their current replacement policy of shear pump bearings with other replacement policies, including one that used EXAKT. The

results showed that replacements that are made according to the output from EXAKT resulted in a documented cost reduction of 33%.

Ghasemi *et al.* [**30**] derived an optimal CBM replacement policy that assumed that the diagnostic state of the equipment was unknown, but could be estimated based on the observed condition. The authors assumed that the information obtained at inspection times could only be used to calculate the probability that the system is in a certain diagnostic state. This assumption brought the model closer to real world situations since most information is noise corrupted and should not be treated as perfect information. In addition, in many situations a specific value of an observation can belong to more than one diagnostic state. In this paper, the equipment deterioration process was formulated by a PHM. Since the equipment's state was unknown, the optimization of the optimal maintenance policy was formulated as a partially observed Markov decision process (POMDP), and the problem was solved using dynamic programming. Combining the PHM and POMDP enabled the model to take into account two causes of system deterioration: the ageing process and the conditions under which the system was used. In addition, the model took into account the manufacturer knowledge, which is an important source of information.

Prasad and Rao [**31**] used PHM techniques to assess the failure characteristics of three different case studies. The first case was the failure analysis of electro-mechanical equipment under renewal process with type of failure (electrical, compressed air, cable) as a covariate. Non-parametric PHM methods were used to obtain failure rate ratios of the equipment at different covariates. The second case study was maintenance scheduling of a thermal power unit under a non-homogeneous poisson process with type of failure mode (boiler, electrical, turbine) as a covariate. Three different non-parametric cumulative hazard rate function estimators were discussed to evaluate rate ratios of system covariates. The last case was accelerated life testing of a small D.C. motor with voltage, load current and type of operation as covariates. In this case study, the failure behavior of the motor at different operating condition using non-parametric PHM methods was compared with the results obtained by the Weibull PHM.

Luxhoj and Shyur [**32**] compared proportional hazard and neural network models for the analysis of time-dependent dielectric breakdown data for a metal-oxidesemiconductor integrated circuit. The study showed that the neural network model presented a more accurate technique for using accelerated failure

data for estimating reliability at normal operating conditions than the proportional hazards model.

Kumar and Westberg [**27**] suggested a reliability based approach for estimating the optimum maintenance time interval for a system or threshold values of CM variables under the age replacement policy. A PHM was used to estimate the reliability function, which was based both on the failure times and the values of the monitored variables.
Then, the authors formed a maintenance cost equation based on the planned and unplanned maintenance costs and the reliability function. In order to find the optimum maintenance time interval or the threshold values of the monitored variables, a total time on test (TTT) plot was used to find the minimize the long run maintenance cost. The authors used an example based on pressure gage failure data to illustrate their approach.

Vlok et al. [**33**] described a case study in which the Weibull PHM was used to determine the optimal replacement policy for a critical item which was subject to vibration monitoring. The case study considered CBM for circulating pumps in a coal wash plant. The CBM policy recommended in this study was based on lifetime data collected over a period of 2 years, and was compared with current practice. The policy was validated using data that arose from subsequent operation of the plant.
Proportional hazard models attempt to characterize degradation processes at an aggregate level compared to other methods that focus on modeling the evolution of sensory-based condition monitoring information. In addition, these models require a baseline hazard function, which is time-based rather than condition-based[**34**]. As a result, the use of degradation models is becoming increasingly popular in CBM applications.

2.1.4. Degradation Models

Components usually degrade during their service life. The degradation of identical components can differ drastically. Degradation processes are typically accompanied by specific physical phenomena that evolve over time, such as increased vibration, temperature changes, and increased crack propagation. Generally, such physical phenomena can be observed using sensor-driven condition monitoring technology. Many components exhibit characteristic

patterns in their sensor signals known as degradation signals and these signals evolve with respect to the component's state of degradation [**35**]. If properly modeled, degradation signals can be used to predict a component's remaining life distribution. In degradation modeling, failure is defined in terms of the degradation signal reaching a predetermined failure threshold. Degradation modeling focuses on using degradation signals developed via condition monitoring techniques that capture the deterioration of a component over time. Degradation models can be used to estimate the residual life distribution of the monitored component. In particular, degradation modeling literature can be divided into two main categories based on the approaches used to evaluate degradation states of equipment.

The first category consists of random coefficients models and time series techniques to model the path followed by a component's degradation signal. Generally, the model parameters are derived from degradation characteristics associated with the component's population. Tseng et al. [**36**] studied the degradation of fluorescent lamps by monitoring their luminosity. The authors developed a linear random coefficients model of luminosity with experimental design to improve the reliability of fluorescent lamps. The degradation model was used to identify the combination of manufacturing settings that provided the slowest rate of luminous degradation. Yang and Jeang [**37**] also used a random coefficients model to study the effect of cutting tool flank wear on surface roughness in metal cutting. Tool degradation was quantified by the roughness value of the machined part. The degradation model was used to develop an inspection strategy for optimal tool replacement. Yang and Yang [**7**] developed a random-coefficient-based approach that uses the lifetimes of failed devices plus degradation information from operating devices to estimate parameters of life distributions. Goode et al. [**38**] developed a predictive model for monitoring the condition of a hot strip mill. They developed a vibration-based degradation signal that grows exponentially as the component degrades. They concluded that the degradation model dominates the reliability model. Swanson [**39**] used time-series techniques, namely Kalman filters, to track changes in vibration characteristics of degrading devices. A Wiener process has also been used to model degradation signals from accelerated tests [**40**][**41**]. In [**40**] drift and diffusion parameters changed according to the on-the-stress level. The authors illustrated how to estimate mean life under normal stress levels. Whitmore [**41**]

illustrated how the Wiener process can be used to account for measurement errors in degradation signals.

The second category of degradation modeling literature utilizes artificial intelligence approaches such as neural networks and fuzzy logic [**42**] [**43**] to model degradation. Most of these approaches focus on quantifying the level of degradation, classifying the type of defects and forecasting degradation signals to compute failure time values [**43**]. Lee et al. [**42**] developed a neural-network model based on cerebral model articulation controllers (CMAC) in order to classify machine degradation. Gebraeel et al. [**44**] developed a neural-network model that uses vibration-based degradation data from rolling element bearings to predict failure time values of partially degraded bearings. Chinnam et al. [**45**] utilized neural networks to forecast the degradation signal of individual components and evaluate their reliability characteristics given predetermined failure thresholds.

The most prominent research efforts in finding a close form for RUL distribution has been done by Lu and Meeker [**46**]. The authors developed statistics-based degradation models to estimate time-to-failure distributions for general degradation models and demonstrated some special cases for which it is possible to obtain closed form expressions. The authors assumed that the path taken by the degradation signal (a.k.a. degradation path) can be defined accurately if the values of specific degradation parameters are known. However, these parameters are based on reliability characteristics evaluated across the component's population and are not unique to individual components. In contrast, this research proposes a degradation modeling approach that establishes a linkage between reliability characteristics and condition monitoring information. Reliability characteristics capture the general characteristics common to a component's population whereas condition monitoring information captures degradation states of individual components in real time. The first paper proposing an effective solution to the prognostic problem of RUL estimation is Gebraeel[**47**], dated 2006, in which a Bayesian approach was introduced in order to predict the residual useful life of a component subject to degradation. It is to say that the Bayesian prognostic algorithm developed in this work can be considered a concrete improvement of Gebaeel's model.

2.2. Benefit of CBM policy assessment

Several studies have been carried out to assess the actual benefits and impacts that the implementation of a prognostic maintenance policy could generate, in terms of safety and inexpensiveness. This attention to the issue is due to the significant investment required to develop this kind of system, that involves extensive and expensive experimental researches on items failure modes and the reengineering of the entire maintenance operations.

Moreover, detailed analysis must be done to ensure an appropriate solution to be developed given both the technical design characteristics and the concept of operations. Different approaches have been followed to tackle this issue, that are:

- Cost Benefit Analysis [**48**][**49**][**50**][**51**] [**52**]
- Life Cycle Cost [**53**]
- Discrete Event Simulation [**54**][**55**][**56**]

The first category typically uses an analytic approach to determine the costs/benefits of implementing a prognostic maintenance policy, while the second category's approach is somehow similar to the previous one, but it's more prone to be implemented in a simulation model as one of the performance indicators. Both requires as inputs the cost data of the technologies implemented as well as maintenance process data. Conversely, the last category's main focus is that of emphasizing the dynamics of the whole modeled system. While in the first two cases performances are somehow known, in the last one the system performances assessment is the main goal.

The most important system performance indicator in a military operation environment is the assets availability[**57**] .This issue is well known and is reflected in the body of literature produced so far. Maintenance policy and operations are the main variables influencing assets availability, that is the outcome of different aspects, such as logistic support, maintenance engineering, system technology, fleet management and human factors [**49**]. All these issues have to be considered in order to design and assess the effects of a maintenance policy.

Before the introduction of new technologies that have enabled the application of prognostic paradigm in maintenance policy, simulations have been conducted to test different scenarios in which the same system variables are modified in order to find an optimum with respect to some predefined indicators or to evaluate the performance indicators deviation derived from a known variable shift, the so-called 'what if' analysis. For example [**57**] evaluates the aircraft availability at three repair levels under battlefield conditions, including the evaluation of logistic delays (spare parts, equipments and maintenance crew). In [**58**] author address the problem of human resource planning in the Continental's Line Maintenance (also called short routine maintenance) station at Newark, in which the total number of technicians working overtime was used as an objective function and the optimization algorithm was set to minimize this entity. The capability of computer simulation of handling complex requirements allows practitioners to model systems characterized by complex stochastic events and processes[**58**]. The technical driven possibility to implement prognostic techniques in performing maintenance tasks and the high costs related to its development have led to the necessity of evaluating a priori the theoretical potential benefits that can be generated, considering the operational scenario in which this approach will be implemented.

The benefits correlated to the implementation of a prognostic maintenance policy can't be pursued without considering the interaction between the maintenance related aspects mentioned before. The technology employed influences the maintenance engineering process and logistic support, which consequently influences fleet management decisions, the needed workforce and eventually the asset's readiness and availability. In other words, in order to completely exploit the potential benefits allowed by prognostics, information produced by the system has to be processed in order to make smart decisions integrating all the issues involved. Indeed, benefits will be attained only when all the components are coordinated and successfully integrated. Another component that turns the scenario to higher complexity is the high number of actors involved in the entire maintenance process. As a matter of fact, outsourcing maintenance tasks are a common issue, most of all when it is not the core business or when it is too expensive or risky to be performed in house. This highlights and enhances the coordination capabilities of the whole maintenance chain. The variables that influence the system performance are numerous and

moreover not deterministic. The information provided by prognostics, as described in paragraph 1.2, is probabilistic itself and evolves as time elapses. Prognostic maintenance decision process emphasizes the uncertain aspects that already characterize maintenance activities. Performing cost benefit analysis in this context appears to be too simplistic as far as the dynamic and uncertain aspects are not considered [**49**]. As a matter of fact, when assessing the influence of several system parameters on different system performance metrics in a prognostic environment, discrete event simulation has been chosen as the ideal candidate [**53**][**55**][**50**] [**56**] [**56**].

These studies have mainly focused on:

- [**53**] presents a model that enables the optimal interpretation of prognostics and health management (PHM) results for electronic systems. In this context, optimal interpretation of PHM results means translating PHM information into maintenance policies and decisions that minimize the LCC or maximize availability or some other utility function. The result of this model is a methodology for determining an optimal safety margin and prognostic distance for various PHM approaches in single and multiple socket systems where the LRUs, in the various sockets that make up a system, can incorporate different PHM approaches (or have no PHM structures at all).
- Case studies proposed in [**54**] were conducted using a stochastic model to predict the LCC impact associated with the application of PHM to helicopter avionics. The life cycle costs of systems that assumed unscheduled maintenance and fixed-interval scheduled maintenance were compared to the costs of precursor-to-failure and life consumption monitoring PHM approaches and the optimal safety margins and prognostic distances were determined.
- The purpose of [**56**] is to identify the overall categories for understanding the different types of impacts and benefits a PHM system can have from a logistics support perspective. This paper also discusses how prognostics can be assessed by a modelization, implemented in a legacy logistics support discrete-event simulation.
- [**55**] presents a sensory-updated-degradation-based predictive maintenance policy. The proposed maintenance policy utilizes contemporary degradation models that combine component-specific real-

time degradation signals, acquired during operation, with degradation and reliability characteristics of the component's population to predict and update the residual life distribution (RLD). By capturing the latest degradation state of the component being monitored, the updating process provides a more accurate estimate of the remaining life. Thanks to a stopping rule, maintenance routines are scheduled basing on the most recently updated RLD. The performance of the proposed maintenance policy is evaluated using a simulation model of a simple manufacturing cell. Frequencies of unexpected failures and overall maintenance costs are computed and compared with two other benchmark maintenance policies: a reliability-based and a conventional degradation-based maintenance policy (without any sensor-based updating).

- In [**35**] authors develop a sensor-driven decision model for component replacement and spare parts inventory.

Elwany et al.[**35**] integrate a framework for computing remaining life distributions using condition based sensor data with existing replacement and inventory decision models. This enables the dynamic updating of replacement and inventory decisions based on the physical condition of the equipment.

In the first three studies mentioned, the issues related to RUL prediction don't refer to a particular case study but simply describe the main dynamics. In this framework, as shown in Figure 8 a random failure event X occurs with f_X pdf, mean μ_X and standard deviation σ_X. No assumption is made regarding the pdf shape. At time Z, a PHM system predicts a random failure event J, with pdf f_Y, mean μ_Y and standard deviation σ_Y. Similar to X, no assumption is made regarding the shape. This prediction is made at random time L (with pdf f_L and mean τ) before the predicted failure (Y). A maintenance opportunity M can occur during the interval L, that is, between time of prediction Z and predicted failure Y. Logistic Lead Time is the time between event M and prediction Y. There can be one or more M events, or none, depending on the distributions of M and Y. It is assumed that a planned maintenance event can only occur if the maintenance opportunity M is to occur before predicted failure Y. In other words, until a maintenance event occurs because of a maintenance

opportunity after predicted failure Y and before actual failure X, it is not a planned event.

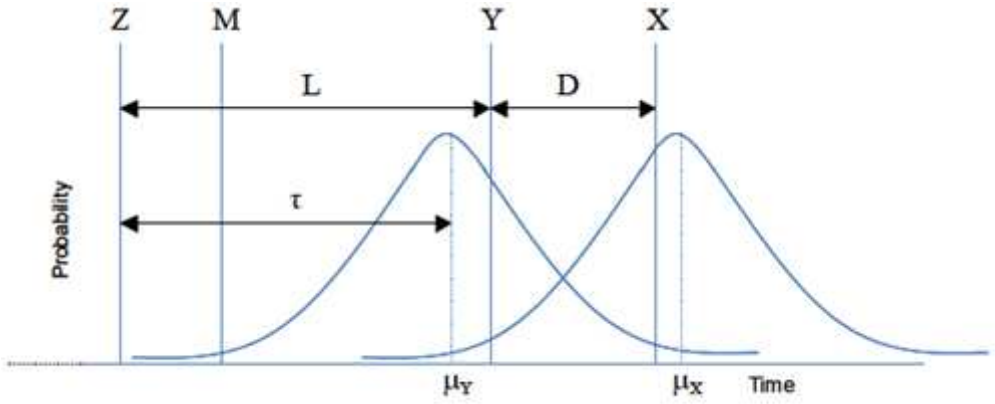

Figure 8 RUL prediction dynamics

In the first two studies, the main concepts regarding RUL estimation have been described, that are the concepts of estimate precision and accuracy but authors missed to consider the dynamic aspects of RUL estimation.

As a matter of fact, as will be done in paragraph 0 RUL estimation is not performed once in time but is continuously updated so to have information changing over time. This aspect changes the framework in which decisions have to be taken. The time at which scheduling and performing maintenance has to be decided once provided information on TTF estimation with the related confidence bounds and unknown accuracy. The dynamic aspects of RUL prediction are tackled in [**35**] and [**55**] In [**55**] a rule is presented to establish when maintenance tasks have to be performed, while in [**35**] a maintenance scheduling and repair policy is proposed. Further analyses and comments of these two approaches will be carried out in the paragraph 3.2.2.

However no literature, as far as we know, explicitly addresses the problem of the time scale mismatch between RUL prediction and maintenance scheduling and exploit decreasing RUL precision. RUL estimation is referred to a continuous time scale, that means that the TTF value is measured in operational hours and not in calendar time, as it should intuitively be. As a matter of fact, as for aircrafts, RUL estimation has to be translated in calendar time. Translating RUL estimates in calendar time can be an easy task when the utilization schedule is known, but when the usage is stochastic, such as in military environment, further analyses and assumptions are required.

3. The Integrated framework

3.1. The Prognostic Algorithm

3.1.1. Degradation Signal Generation

The problem is defined as the determination of the residual useful life of a mechanical component basing on an associated exponential degradation pattern. From literature, in fact, it is known that almost in every kind of mechanical degradation a feature can be found which evolves in time following an exponential shape. In order to initialize the prognostic algorithm, i.e. to calculate the prior RUL distribution, preliminary experimental tests were simulated by creating 50 exponential curves. These curves were realized by defining a stochastic variable which accounts for the time in which the component will break. This variable was called $\mathrm{t_f}$ and it was defined as belonging to a Gaussian distribution with mean μ_{tf} = 1800 h and a standard deviation σ_{tf} of 180 h. Then, the instant of initial failure was defined as a stochastic variable ti with normal distribution with mean μ_{ti} = 1260 h and standard deviation σ_{ti} = 88.2 h. So, from 0 to ti the component will follow the shape associated to the healthy component, whereas from $\mathrm{t_i}$ to $\mathrm{t_f}$ the exponential evolution will manifest. Moreover, a threshold has been defined indicating the amplitude of the level the signal reached before failing. This parameter was called hi and it follows a Gaussian distribution with a mean value of 1.11 and a standard deviation of 0.011. Note that this parameter has been defined as the failure amplitude obtained from experimental tests after normalization over the mean failure amplitude, so that the treatment won't loose generality with respect to all the possible components' failure this algorithm could be applied to. Then, the mentioned exponential shape was realized by interpolation. The exponential curve was defined as follows:

$$y(t, \mathrm{t_i} \leq \mathrm{t} \leq \mathrm{t_f}) = C + Ae^{Bt} \qquad \textbf{3.1}$$

where C is the constant value associated to the linear trend of safe behaviour for the component, whereas A and B are two constants which define the shape of the curve. In order to determine these coefficients, the passage through points $(\mathrm{t_i}, \mathrm{C})$

and $(\mathrm{t_f}, hi)$ was imposed. By making the logarithm of the system of equations the following linear system is obtained:

$$Mx = d$$

$$\begin{bmatrix} 1 & t_\mathrm{i} \\ 1 & t_\mathrm{f} \end{bmatrix} \begin{pmatrix} \log A \\ B \end{pmatrix} = \begin{pmatrix} \log C \\ \log hi \end{pmatrix} \qquad \textbf{3.2}$$

From inversion of matrix M, x vector is trivially obtained. Afterwards, the final shape of the signal was achieved by defining an initial behavior from $t = 0$ to t in which the component follows a linear trend.

The curve realized is composed by a horizontal line at $y = 0.11$, on which Gaussian white noise with 3 different frequencies was applied with zero mean and exponentially growing variance, so that $\sigma_{n1} = 2\ 10^{-6} t^{1.05}$. The second part of the signal is made by the exponential pattern on which white Gaussian noise is applied. That noise has zero mean and variance low-exponentially growing $\sigma_{n2} = 3.1\ 10^{-6} t^{1.1}$. The choice of giving the noise variance an exponential growth is based on the physical assumption that while failure is increasing measurements become less accurate and other non-deterministic behaviors will appear. The 3 noise periods are: 3 hr, 100 hr and 800 hr.

At the end of this procedure the signal appears as follows (Figure 9):

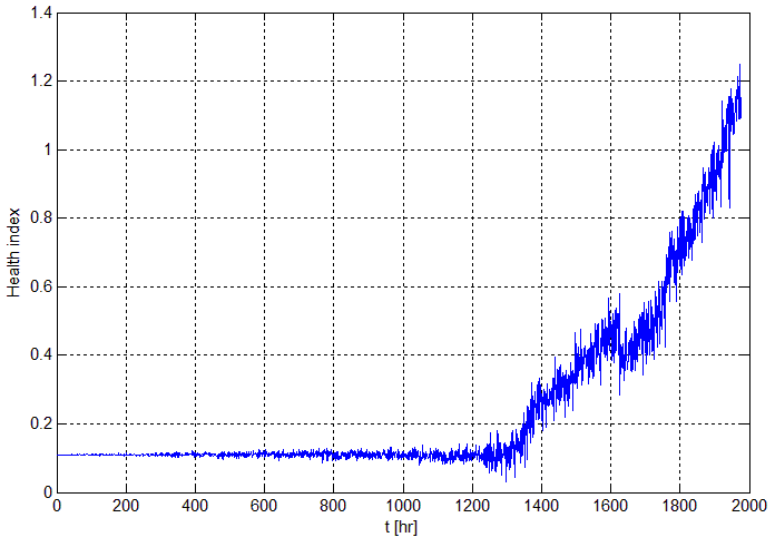

Figure 9 Simulated exponential degradation signal

Now 100 experimental signals have been created, from which the prior estimate of the coefficients will be obtained. However, actually the right time t_i in which failure starts to propagate is unknown, so an estimate of it is needed. To do so, a technique, taken from the field of signal processing, has been designed involving two connected moving averages in which the former is composed by 30 samples whereas the latter is made by the following 5 samples. Hence, at each time iteration t_n a comparison is done between the 30-samples average (called $\mu_{30\,old}$) plus six time the standard deviation of the samples considered $\sigma_{30\,old}$ and the 5-samples average (called $\mu_{5\,new}$) minus six time its standard deviation $\sigma_{5\,new}$. So the estimated instant of incipient failure $\tilde{t}_i$ is defined as the moment in which the second quantity overcomes the first one, i.e.:

$$\tilde{t}_i = t_n | \mu_{5\,new} - 6\sigma_{5\,new} \geq \mu_{30\,old} + 6\sigma_{30\,old} \qquad \textbf{3.3}$$

By doing so, the results are plotted in Figure 10 and Figure 11.

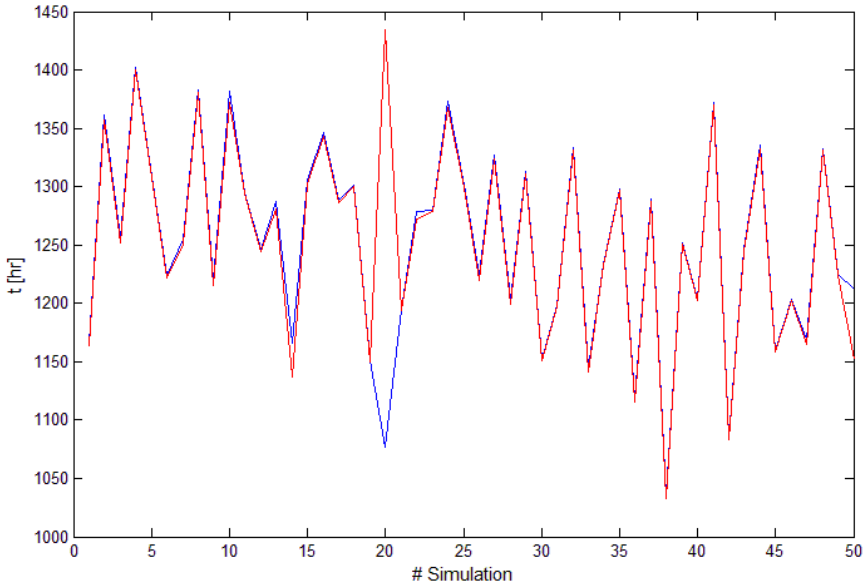

Figure 10 $\tilde{t}_i$ Estimation (blue line) and t_i real value obtained from 50 simulations

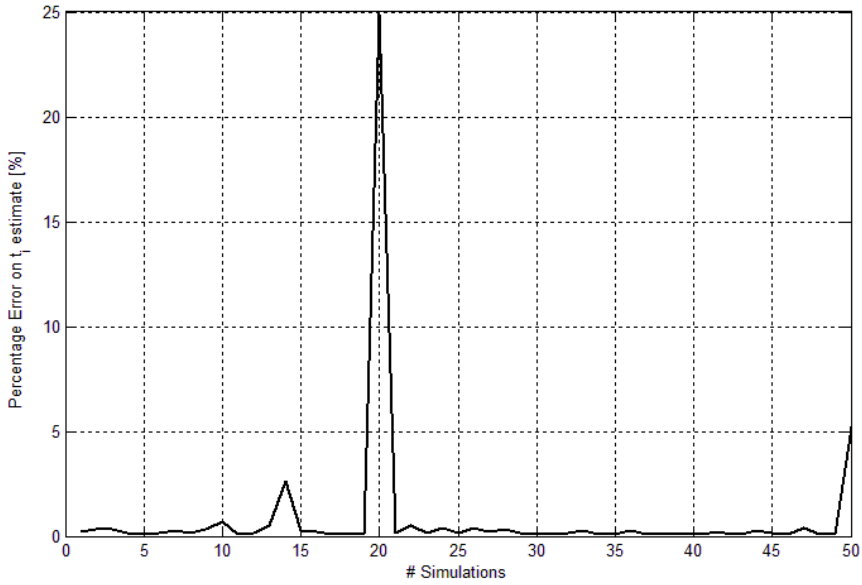

Figure 11 $\tilde{t}_i$ estimation percentage error

As it can be noticed, the error made by this estimation never goes beyond 5%. The following step consists of the estimate concerning the coefficients of the exponential curve. In order to achieve this task, a regression problem was set up in which an exponential curve has to fit the signal. The objective function used in this regression will aim to minimize the squared error between the simulated experimental signal y and the fitting signal y_{fit}, defined as:

$$y_{fit} = C + Ae^{Bt} \tag{3.4}$$

So the objective function is:

$$\min\left\{\sum_{i=1}^{n}(y_i - Ae^{Bt_i})^2\right\} = \\ = \min\left\{\sum_{i=1}^{n}\left(y_i - y_{fit}\right)^2\right\} \tag{3.5}$$

where the coefficients A and B minimizing this function have to be found. Since it is a nonlinear minimization problem, an ad hoc optimization technique has

been designed. The best performances in term of accuracy and time saving were obtained with *Nelder-Mead's downhill simplex method*.

This method is based on the concept of simplex, that is a geometric entity defined as an n-dimensional polytope with $n+1$ vertices. These vertices are used to extrapolate the behavior of the objective function in this way: the algorithm replaces the vertex in which the function assumes the highest value among the values observed by all the vertices. The new vertex will be created through a reflection through the centroid of the remaining points. If the new point is better than the old one, then the algorithm tries to stretch the simplex exponentially along this direction. If it isn't so, then the simplex is moving across a zone of minimum of the function. When this happens the algorithm has reached convergence. Note that the only drawback of this optimization strategy is that it is heuristic and it can converge to a non-stationary point when the simplex enters a low-gradient zone.
In order to avoid such a misbehavior, great attention was paid when choosing an appropriate starting point for the algorithm. As it can be stated from figure 7.6, the results obtained from the regression were acceptable.

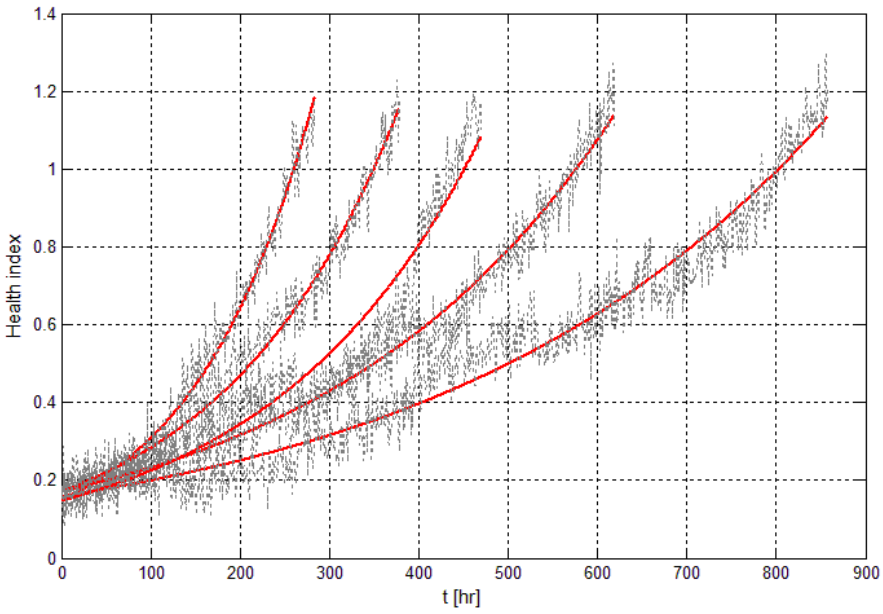

Figure 12 Exponential interpolation using simplex least square regression

Then, the set of the exponential model values were stored as well as the residuals. This set of data will represent the prior knowledge of failure mode. The following step consists in the simulation of a signal obtained from a hypothetical monitoring of a mechanical component. In order to realize such a signal, the same stochastic variables taken before were used, on which white noise was applied with the same features described above. The point of starting failure h_i is then determined by comparing two connected moving average as previously done. Then, the prognostic algorithm will be applied starting from this point, because before that time it wouldn't be able to appreciate any noteworthy variation in order to predict the residual life distribution.

3.1.2. Bayesian degradation predictive algorithm

The leading concept of Bayesian approach is that of considering probability as a measure of the state of knowledge, whereas in traditional frequentist statistics probability is considered as a physical property of a system. So, the Bayesian and the frequentist approach to a statistical hypothesis become quite different. As a matter of fact, the Bayesian approach suggests to give the hypothesis a prior probability, that will be subsequently updated basing on data provided in support or in confutation of that hypothesis. On the other side, frequentist approach doesn't associate to the hypothesis a prior probability, but the hypothesis is simply rejected or not rejected depending on the degree of frequency associated to the event the hypothesis describes. So defined, Bayesian approach results in a very powerful tool, in that it allows to formulate statistical problem in a way very close to human reasoning. As for its mathematical bases, it relies on a single wide-usage theorem, called Bayes' theorem, which is reported below:

$$P(A|B) = \frac{P(B|A)P(A)}{P(B)} \tag{3.6}$$

where $P(A)$ is the prior probability, i.e. the probability of the event A without taking into account any information concerning the event B. On the other side, $P(B)$ is the prior probability of event B and it is always taken as a normalizing factor. $P(B|A)$ is the conditional probability of B given A, while $P(A|B)$ is the posterior probability of A, i.e. the probability of A conditioned by event B. As we will see herein, this simple idea will represent the core of the prognostic algorithm.

According to [**47**][**59**] the degradation model is defined as a stochastic process $\{A(t);\ t > 0\}$ that captures the evolution of the degradation signal over time, where $A(t)$ is the amplitude of the degradation signal at time t. The degradation signal is a characteristic pattern in the sensory information that captures the physical transitions associated with the degradation process. Examples of degradation signals obtained from experimental tests are illustrated in Figure 13 and Figure 14.

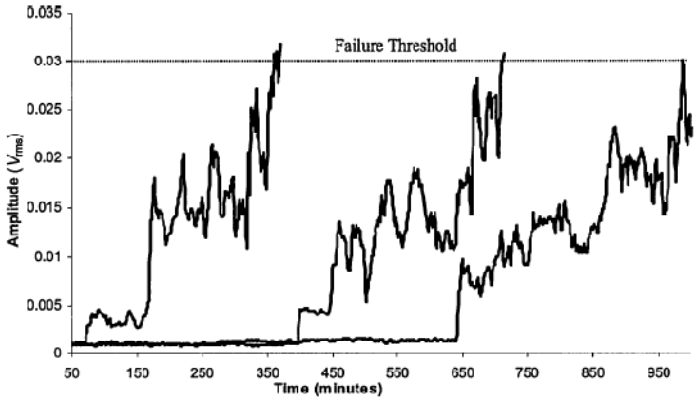

Figure 13 Vibration-based degradation signal of bearings [47]

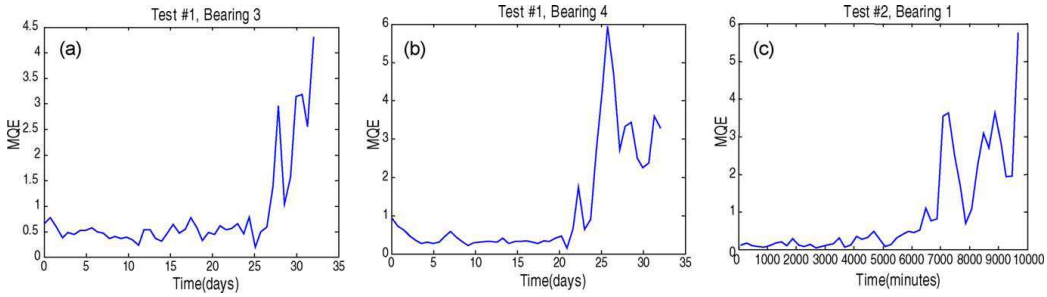

Figure 14 The MQE of three degradation processes: (a) Test 1, bearing 3; (b) Test 1, bearing 4; (c) Test 2, bearing 1 [60]

The path of the degradation signal was modeled through the stochastic equation $A(t) = h(A, B, C,\ t) + \varepsilon(t)$, denoting the value of the degradation signal at time t. The functional form $h(\cdot)$ of the signal depends on the type of component under consideration and represents a relationship between the operating time and signal amplitude. The degradation model consists of deterministic and stochastic parameters. The deterministic parameter represent a constant physical

phenomenon common to all components of a given population such as an initial degradation level for non defective components. The stochastic parameter follows a certain distribution and captures variations of the degradation processes among individual identical components.

Noise and random effects associated with the degradation signals are captured by a random error term $\varepsilon(t)$, which is modeled as a stochastic process with independent and normally distributed components. In other words, at sampling epochs $t_1 < t_2 < \cdots < t_k$ the error terms $\varepsilon(t_1), \varepsilon(t_2), \cdots, \varepsilon(t_k)$ are independent and identically distributed. The same assumption can be found in Lu and Meeker [**61**] and Gebraeel et al. [**47**], where the error in the degradation signal is considered independent and identically distributed (iid) with Gaussian distribution $N(0;\ {\sigma_n}^2)$ across the population of devices. The degradation signal is observed at discrete points in time $t_1,\ t_2,\ \cdots, t_k$ where $t_i \geq 0$ and signal amplitude at a given sampling epoch $A(t_i)$ is modeled as:

$$A(t_i) = C + Ae^{Bt_i + \varepsilon(t_i) - \frac{{\sigma_n}^2}{2}} = \\ = C + Ae^{Bt_i} e^{\varepsilon(t_i) - \frac{{\sigma_n}^2}{2}} \tag{3.7}$$

where C is a constant deterministic parameter, A and B are random variables, and $\varepsilon(t_i)$ is a normally distributed random error term with mean 0 and variance ${\sigma_n}^2$. It could be shown that $E[e^{\varepsilon(t_i) - \frac{{\sigma_n}^2}{2}}] = 1$ and, consequently $E[A(t_i)|A, B] = C + Ae^{Bt_i}$. For convenience, the logged signal L_i at time t_i will be taken, so that:

$$L(t_i) = \log(A(t_i) - C) = \log A + Bt_i + \varepsilon(t_i) - \frac{{\sigma_n}^2}{2} \tag{3.8}$$

If we let $L_i = L(t_i)$ and $A' = \log(A(t_i) - C)$ then Eq.3.8 can be rewritten as follows:

$$L_i = A' + Bt_i + \varepsilon(t_i) \tag{3.9}$$

These parameters A' and B are assumed to be jointly distributed and follow a bivariate normal distribution with ${\mu'}_0$ and μ_1, variances ${\sigma'}_0$ and σ_1, respectively,

and correlation coefficient ρ_0. The prior distribution of the stochastic parameters $A'$and B can be estimated from the 50 previously simulated signals. Once the prior distribution is evaluated, the degradation model can be used to compute an initial estimate of the residual life distribution. Sensory signals from similar components operating in the field are then used to update the prior joint distribution of the stochastic parameters. The updated degradation model is then utilized to compute an updated residual life distribution that is unique for the individual component used for the updating procedure. Hence, the Bayesian method requires two components. The first one is the conditional distribution of the degradation signal given the stochastic parameters, i.e.$f(L_i|A', B)$.
From Eq.3.12, it is clear that the conditional density function of L_i given A' and B follows a normal distribution with mean 0 and variance ${\sigma_n}^2$. The second component is the prior joint distribution of the stochastic parameters, which is assumed to follow a bivariate normal distribution $\Pi(\beta)$ with parameters (μ, Σ), where $\beta = [A' \quad B]$ is the parameters vector $\mu = [{\mu'}_0 \quad \mu_1]$ and Σ is covariance matrix. Figure 15 and Figure 16 shows the A' dataset fitted with a normal distribution on a normal probability plot and the B dataset fitted with a normal distribution on a normal probability plot respectively.

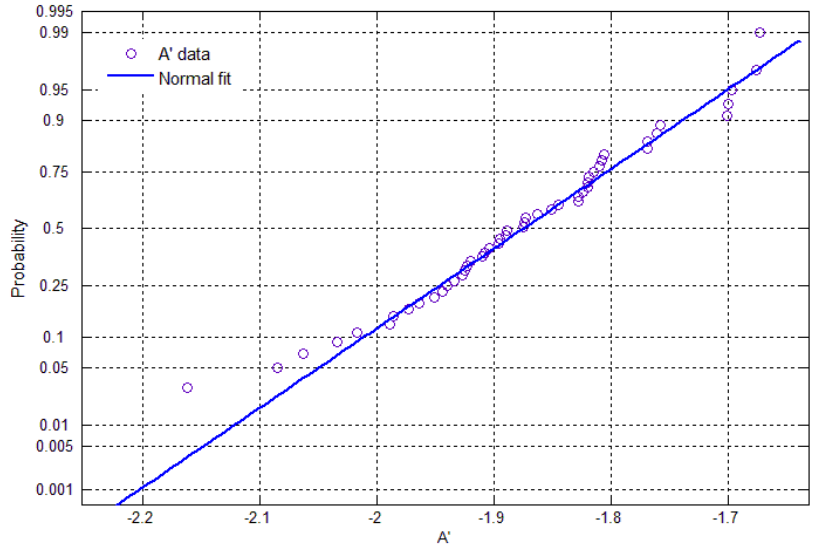

Figure 15 A' normal probability plot

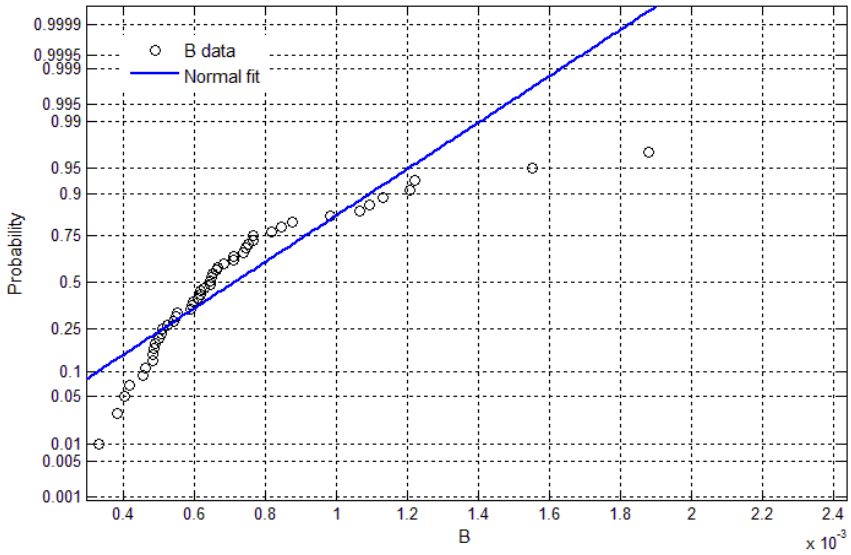

Figure 16 B normal probability plot

As can be noticed, the parameter A' is fitted with acceptable results with a normal distribution, while parameter B normal approximation doesn't lead to good results. However, for our purpose the hypothesis of normal distribution was conserved to do not increase the computational problem.

The prior information is combined with knowledge of the current degradation signal level using the Bayesian approach to compute posterior joint distribution $\widetilde{\Pi}(\beta)$.

Assuming that we have obtained a partial degradation signal $L_k = (L_1, \cdots, L_k)'$ by monitoring a component over times $t_1, \cdots, t_k$, because the error are assumed to be iid, if we know β, than the conditional joint density function of $L_1, \cdots, L_k$, given β is expressed as

$$p(L_1, \cdots, L_k | \beta) \; \alpha \; exp\left\{-\frac{1}{2{\sigma_n}^2}(L - X\beta)^2\right\} \qquad \textbf{3.10}$$

Where $X = \begin{bmatrix} 1 & t_1 \\ \vdots & \vdots \\ 1 & t_k \end{bmatrix}$.

We are interested in evaluating the posterior distribution of the vector β given that we have observed a partial degradation signal $L = (L_1, L_2 \cdots, L_k)'$. The conditional distribution of β updated at the k^{th} time epoch can be expressed as:

$$p(\beta|L_1, \cdots, L_k) \; \alpha \; f(L_1, \cdots, L_k|\beta)\Pi(\beta) \tag{3.11}$$

From [**62**] [**59**] we see that, given the observed data $L = (L_1, L_2 \cdots, L_k)'$, and the prior distribution of β is also a multivariate s-normal $N(\tilde{\mu}, \tilde{\Sigma})$ where:

$$\tilde{\mu}^T = \left(\hat{\beta}^T \frac{X^T X}{\sigma^2} + \mu^T \Sigma^{-1}\right)\left(\frac{X^T X}{\sigma^2} + \Sigma^{-1}\right)^{-1} \tag{3.12}$$

$$\tilde{\Sigma} = \left(\frac{X^T X}{\sigma^2} + \Sigma^{-1}\right)^{-1} \tag{3.13}$$

Where $\hat{\beta} = (X^T X)^{-1} X^T L$

The proof is given in [**59**] and for completeness it is reported below:

To arrive at this result, we note that given the prior distribution , and conditional joint density $\Pi(\beta)$, the posterior distribution $p(\beta^k|S)$ is given by

$$p(\beta^k|S) \; \alpha \; p(S|\beta)\Pi(\beta) \tag{3.14}$$

Where:

$$\Pi(\beta) \; \boldsymbol{\alpha} \; exp\,\{-(1/2)[(\beta - \mu)'\Sigma^{-1}(\beta - \mu)]\} \tag{3.15}$$

and

$$p(S|\beta) \; \boldsymbol{\alpha} \; \exp\{-(1/2\sigma^2)(S - X\beta)^2\} \tag{3.16}$$

By substituting in expression 3.16 , we have

$$p(\beta^k|S) \boldsymbol{\alpha} \exp\left\{-\frac{1}{2\sigma^2}(S - X\beta)^2\right\} \text{x} \exp\left\{-\frac{1}{2}[(\beta - \mu)^T \Sigma^{-1}(\beta - \mu)]\right\} \quad \textbf{3.17}$$

We let $\hat{\beta}$ be the solution for $S = X\beta$, hence $\hat{\beta} = (X^T X)^{-1} X^T S$.

$$p(\beta^k|S) \boldsymbol{\alpha} \exp\left\{-\frac{1}{2\sigma^2}\left[\left(\beta - \hat{\beta}\right)^T X^T X\left(\beta - \hat{\beta}\right) + \left(S - X\hat{\beta}\right)^T \left(Y - X\hat{\beta}\right)\right]\right\} \quad \textbf{3.18}$$

$$\text{x} \exp\left\{-\frac{1}{2}[(\beta - \mu)^T \Sigma^{-1}(\beta - \mu)]\right\}$$

$$p(\beta^k|S) \boldsymbol{\alpha} \exp\left\{-\frac{1}{2\sigma^2}\left[\left(\beta - \hat{\beta}\right)^T X^T X\left(\beta - \hat{\beta}\right) + \left(S - X\hat{\beta}\right)^T \left(Y - X\hat{\beta}\right)\right]\right\} \quad \textbf{3.19}$$

$$\text{x} \exp\left\{-\frac{1}{2}[(\beta - \mu)^T \Sigma^{-1}(\beta - \mu)]\right\}$$

$$\boldsymbol{\alpha} \exp\left\{-\frac{1}{2\sigma^2}\left[\left(\beta - \hat{\beta}\right)^T X^T X\left(\beta - \hat{\beta}\right)\right] - \frac{1}{2}[(\beta - \mu)^T \Sigma^{-1}(\beta - \mu)]\right\}$$

If we define the posterior distribution of β as $N(\tilde{\mu}, \tilde{\Sigma})$ than we can express $p(\beta^k|S)$ in the following form:

$$p(\beta_k|S) \boldsymbol{\alpha} \exp\left\{-\frac{1}{2}[(\beta - \tilde{\mu})^T \tilde{\Sigma}(\beta - \tilde{\mu})]\right\} \quad \textbf{3.20}$$

By comparing the expressions of $p(\beta^k|S)$ we see that

$$\frac{1}{\sigma^2}\left[\left(\beta-\hat{\beta}\right)^T X^T X\left(\beta-\hat{\beta}\right)\right]+\left[(\beta-\mu)^T\Sigma^{-1}(\beta-\mu)\right] \propto \boldsymbol{\alpha}\left[(\beta-\tilde{\mu})^T\tilde{\Sigma}(\beta-\tilde{\mu})\right] \quad \textbf{3.21}$$

Therefore,

$$\begin{aligned}&\frac{1}{\sigma^2}\left[\left(\beta-\hat{\beta}\right)^T X^T X\left(\beta-\hat{\beta}\right)\right]+\left[(\beta-\mu)^T\Sigma^{-1}(\beta-\mu)\right]=\\&=\beta^T\left(\frac{X^TX}{\sigma^2}\right)\beta-2\hat{\beta}T\left(\frac{X^TX}{\sigma^2}\right)\beta+\hat{\beta}^T\left(\frac{X^TX}{\sigma^2}\right)\hat{\beta}+\beta^T\Sigma^{-1}\beta\\&\quad-2\mu^T\Sigma^{-1}\beta+\mu^T\Sigma^{-1}\mu\\&=\beta^T\left[\left(\frac{X^TX}{\sigma^2}\right)+\Sigma^{-1}\right]\beta-2\left[\hat{\beta}^T\left(\frac{X^TX}{\sigma^2}\right)+\mu^T\Sigma^{-1}\right]\\&\text{x}\left[\left(\frac{X^TX}{\sigma^2}\right)+\Sigma^{-1}\right]^{-1}\left[\left(\frac{X^TX}{\sigma^2}\right)+\Sigma^{-1}\right]\beta+\left[\beta^T\left(\frac{X^TX}{\sigma^2}\right)\hat{\beta}+\mu^T\Sigma^{-1}\mu\right]\end{aligned} \quad \textbf{3.22}$$

By comparing 3.22 to the expression $(\beta-\tilde{\mu})^T\tilde{\Sigma}(\beta-\tilde{\mu})$, we find that the posterior distribution of β follows a multivariate s-normal distribution with mean, $\tilde{\mu}$, and variance, $\tilde{\Sigma}$, given by 3.12 and 3.13 respectively.

Next, we use the updated distributions of the stochastic parameters to compute the predictive distribution of the signal $L(t_k+t)$ which is Normal with the following mean and variance[**59**]:

$$\hat{\mu}_{L(t_k+t)}=\tilde{\mu}_{A'}+\tilde{\mu}_B(t_k+t) \quad \textbf{3.23}$$

$$\hat{\sigma}^2{}_{L(t_k+t)}=\tilde{\sigma}_{A'}{}^2+\tilde{\sigma}_B{}^2(t_k+t)^2+2\tilde{\rho}_0\tilde{\sigma}_B\tilde{\sigma}_{A'}+\sigma_n{}^2 \quad \textbf{3.24}$$

Where $\tilde{\mu}_A$, and $\tilde{\mu}_B$ are the updated mean of the model parameters at time t_k, i.e the first and second element of the vector $\tilde{\mu}$. $\tilde{\sigma}_B$ and $\tilde{\sigma}_A$, are the elements on the diagonal of the covariance matrix $\tilde{\Sigma}$ and $\tilde{\rho}_0$ is the updated A' and B correlation coefficient.

Using the predictive distribution of the degradation signal, we calculate the updated RLD of the component that is being monitored as the distribution of the time until the degradation signal reaches a predetermined failure threshold $\overline{hi}$. Let T be a random variable that denote the residual life of the partially degraded component. Therefore, T satisfies $L(t_k + t) = \log \overline{hi}$, and its distribution is given by:

$$F_T(t) = P(T \leq t | L_1, \cdots, L_k) = \Phi\left(\frac{\hat{\mu}_{L(t_k+t)} - \log \overline{hi}}{\hat{\sigma}_{L(t_k+t)}}\right) \qquad \textbf{3.25}$$

where $\Phi(\cdot)$ is the cumulative distribution function (cdf) of a standardized Normal random variable. Note that the domain of T is $(-\infty, +\infty)$. Since T represent the residual life time it is physically impossible that $T \leq 0$, therefore we redefine T as the truncated conditional cdf of T with the constraint $T \geq 0$. The truncated Tcdf is;

$$F_T(t) = \frac{F_T(t) - F_T(0)}{1 - F_T(0)} \qquad \textbf{3.26}$$

As highlighted by Gebraeel [**47**], T is distributed as Bernstein pdf. As demonstrated by [**63**] this distribution doesn't have a close form for its first and second moment., therefore the median is taken as the expected RUL at time epoch t_k as suggested in[**47**].

The threshold $\overline{hi}$ is set at the 1st percentile of the hi cdf because for safety reason ideally no failures should happen at health index greater than $\overline{hi}$.

Figure 17 shows an example of the updated mean and variance of the parameter A' and B pdf as function on the updating time epoch, while Figure 18 shows the updated correlation coefficient between the two variables.

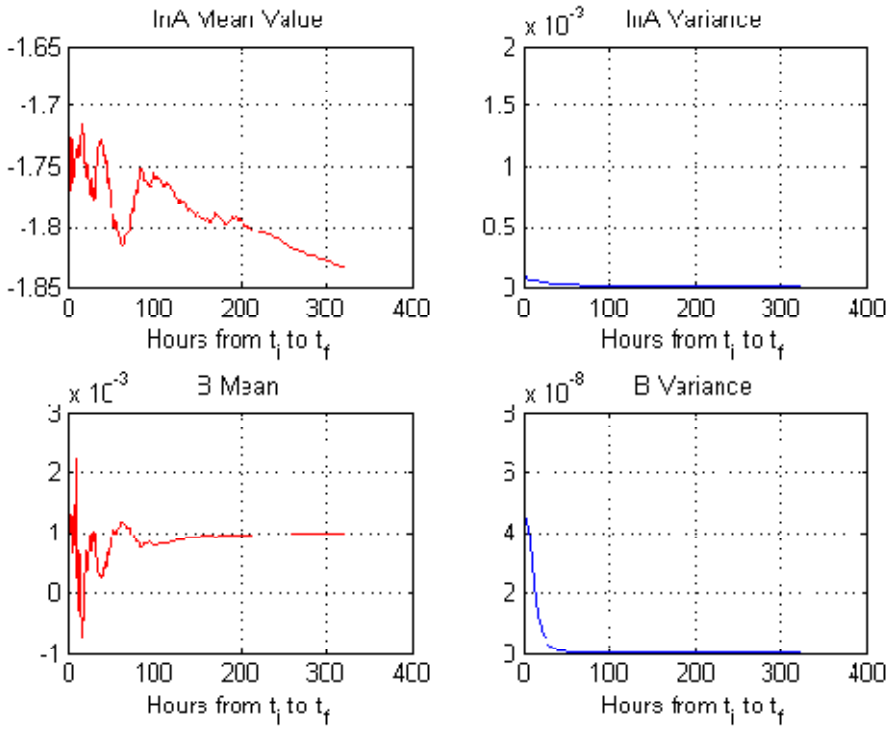

Figure 17 Updated mean and variance of the exponential model parameters

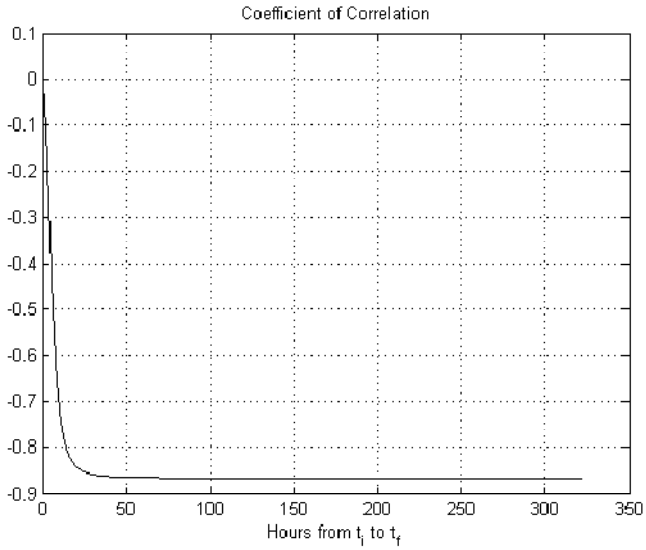

Figure 18 Updated correlation coefficient

Figure 19 shows several RUL pdfs computed at different time steps. Generally, as will be described afterwards and displayed in Figure 21, the precision (confidence interval amplitude) decreases as time elapses, therefore the plotted RUL pdfs the flatter the earlier are computed (i.e blue-green-red-cyan).

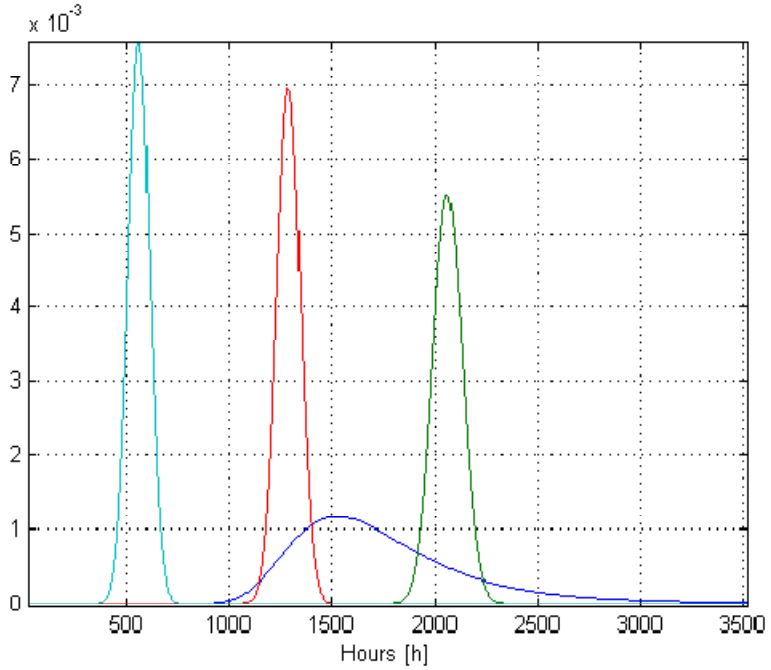

Figure 19 RUL pdfs estimated at different time steps

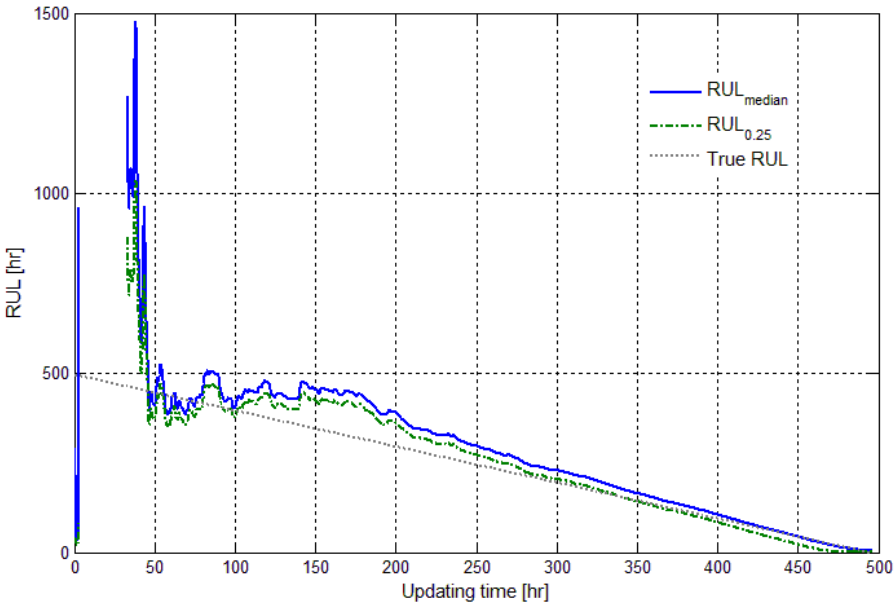

Figure 20 Synopsis of RUL estimation (blue line), real RUL (gray line) and RUL lower bound at 97.5% level of confidence

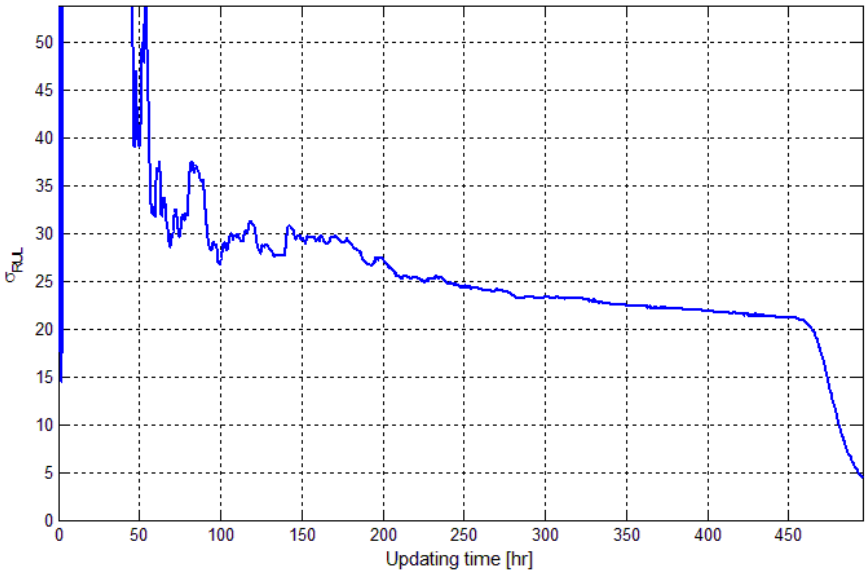

Figure 21 RUL estimation confidence interval amplitude

Figure 20 shows how RUL prediction converge on the real RUL as new measurements become available. Another interesting feature that can be seen in

Figure 21 is the decreasing pattern of the RUL predictions confidence interval amplitude. This result confirm what stated in paragraph 1.2. The RUL confidence interval is considered as the left sided confidence interval, that is the difference between RUL corresponding to the 2.5% of confidence level of the RUL cdf and the median of the RUL pdf.

Since it would be dangerous to trust overestimated predictions, a strategy to define a reliability threshold for the RUL predictions has necessarily to be defined. The objective is to find an algorithm that tells us when the RUL predictions can be trusted for maintenance scheduling decision purposes, that is for example, approximately the time epoch 250 for the instance displayed in Figure 20.

To do so, a linear moving regression of the RUL estimate can be carried out. This sub-algorithm considers at each sensor sampling time t_n, 20 previous RUL estimates, called RUL_n, and makes a linear regression $RUL = mt + q$ in order to obtain mean μ_m and variance ${\sigma_m}^2$ of the line slope m and the linear coefficient of correlation following the procedure below:

$$\mu_{tn} = \frac{\sum_{k=n-19}^{n} t_k}{20}$$

$$\mu_{RULn} = \frac{\sum_{k=n-19}^{n} RUL_k}{20}$$

$$S_{xx} = \frac{\sum_{k=n-19}^{n} (t_k - \mu_{tn})^2}{19}$$

$$S_{xy} = \frac{\sum_{k=n-19}^{n} (t_k - \mu_{tn})(RUL_k - \mu_{RULn})}{19}$$

$$m_n = \frac{S_{xy}}{S_{xx}}$$

$$q_n = \mu_{RULn} - m_n \mu_{tn}$$

$$\widehat{RUL_n} = q_n + m_n t_n$$

$$SSE = \sum_{k=n-19}^{n} (RUL_n - RUL_n)^2 \qquad \textbf{3.27}$$

$$\sigma_m = \sqrt{\frac{SSE}{18 S_{xx}}}$$

for $\bar{t}_i \leq t_n \leq \bar{t}_f$. Then, the algorithm sets the instant in which RUL prediction can be considered reliable as the moment t_a in which the slope estimate belongs to a 95% bilateral interval of confidence, centered on the expected value of the regression, and meanwhile the coefficient of correlation is greater than 90%, i.e when both the conditions in Eq 3.28 hold.

$$\begin{cases} -1 - t_{1-\alpha/2,18}\sigma_m(t_a) \leq m_n(t_a) \leq -1 + t_{1-\alpha/2,18}\sigma_m(t_a) \\ \\ R^2(t_a) = \dfrac{\sum_{k=n-19}^{n}\left(RUL_k - \mu_{RUL(t_a)}\right)^2}{\sum_{k=n-19}^{n}\left(RUL_k - \mu_{RUL(t_a)}\right)^2} \geq 0.9 \end{cases} \qquad \textbf{3.28}$$

where -1 refers to the fact that RUL real trend is a line with slope equal to -1 because at time 0[1] we have the entire useful life, whereas at the instant t_f all the component life has been wasted, so RUL is equal to 0.

The RUL predictions that are considered reliable by using this algorithm, for the same example shown in Figure 19, is shown in Figure 22. As can be noted the time epoch t_a computed using this algorithm is approximately 250 hr, that is the value identified by visual inspection from Figure 19.

[1] Time epoch at which the RUL estimation begins (estimated ti)

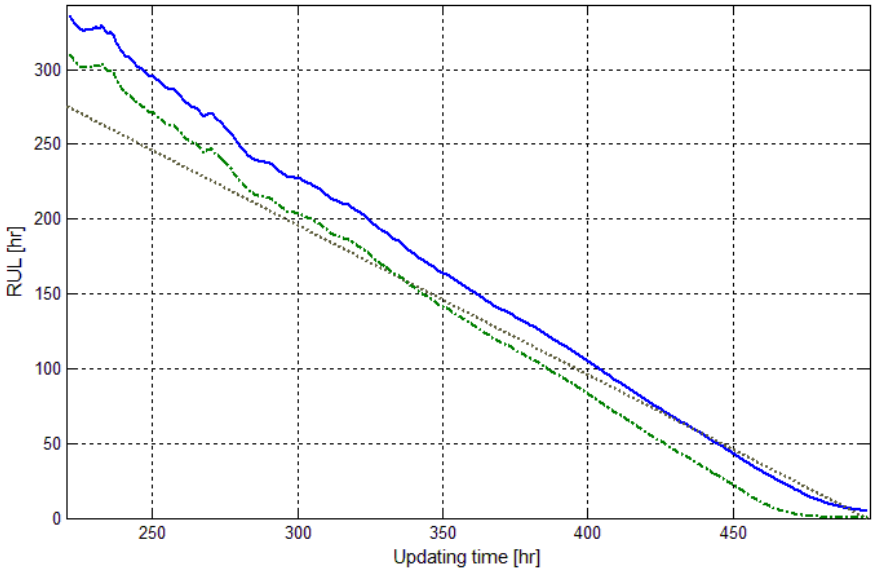

Figure 22 Synopsis of reliable RUL estimation

3.2. Maintenance Scheduling and replacement model

3.2.1. Introduction

The problem of scheduling maintenance and replacement policy in a prognostic contest has already been faced in [**64**] and [**35**]. In [**64**] the case analyzed concerns the definition of the instant in which maintenance tasks have to be performed, but as stated by the author, the policy adopted is provisional and incomplete because the information provided by the prognostic algorithm is not used properly. As a matter of fact, the instant in which maintenance is performed is the instant at which the following condition is satisfied:

$$\min_{0\leq t_n\leq\infty}\{1-[F_T(t_{n+\delta})-F_T(t_n)]\}\geq R \qquad \textbf{3.29}$$

Where R is the desired reliability level, $F_T(t_n)$ is the cdf of the remaining life updated at time t_n, where t_n is the time or epoch at which the last degradation signal was observed, and δ represents a small time increment in the future (used for calculating the cdf). Obviously, this policy can't be applied in our case because it corresponds to an unscheduled maintenance event since no prior information is given before the condition is verified.

In [**35**] ,instead, the policy is well defined. As a matter of fact, given the failure time distribution of a component, the objective of the replacement model is to find the optimum planned replacement time t_r^* . The optimal replacement time is the time that minimizes the expected costs of preventive replacement and failure replacement. The long-run average cost per cycle is expressed as

$$C_r^i=\frac{c_p\bar{F}^i(t)+c_fF^i(t_r)}{\int_0^{t_T^i}\bar{F}^i(t)dt+t_i} \qquad \textbf{3.30}$$

Once the optimal replacement time t_r^* has been computed, then it is used to decide when to order the spare unit. Due to the assumption of a single-unit storage capacity, the order quantity is always a single unit. The optimal ordering time is the ordering time that minimizes the spare parts holding costs and stockout costs. The long-run average inventory cost per cycle is expressed as

$$C_o^i = \frac{k_s \int_{t_j}^{t_0^i} F^j(t)\,dt + k_h \int_{t_0^j+L}^{t_r^i} \bar{F}^i(t)}{\int_{t_0^i}^{t_0^i+L} F^i(t)dt + \int_0^{t_r^i} \bar{F}^i(t) + t_i} \quad \textbf{3.31}$$

Where C_r^i ▫ and C_o^i are the replacement and inventory ordering cost rates per cycle, respectively, at updating time t_i. $F^i(t)$ is the updated cdf of the residual life at the updating time t_i, $\bar{F}^i(t) = 1 - F^i(t)$, $c_p$is the planned replacement cost, In other words, c_f is the failure replacement cost, k_s is the shortage cost per unit time, k_h is the holding cost per unit time and L is the fixed lead time elapsed from the moment of placing the order up till order receipt.

In other words, given that the component has survived up to time t_i and that we have observed a partial degradation signal up to time t_i, $\bar{F}^i(t)$ is the cumulative probability that the component fails after an additional t time units.The terms t_r^i and t_0^i are the optimal replacement and inventory ordering times, respectively, at the given updating epoch. Each cycle is now composed of two components, a fixed term given by the time up to which the component has survived and a random component given by the integral of the RUL. The computation is continuously performed until the following condition is verified:

$$t_r \geq t_f - LT \quad \textbf{3.32}$$

Where t_f is the median of RUL pdf. t_r is the last optimal replacement time compute and LT is Lead Time for ordering a replacement component. It is shown that the more time approaches t_f, the lower the replacement costs per unit time and the inventory costs per unit time will be.

3.2.2. The model

In the previous model Lead Time is considered as a deterministic variable, assumption that could be too simplistic. Besides, the model doesn't consider the risk associated to the amplitude of the confidence interval, i.e. it can happen that t_r is greater than t_f, a risky condition whose hazard is not taken into account by the model. In the model here proposed, instead, the time at which scheduling

and performing maintenance is determined through a function optimization. This function considers the main aspects involved in the maintenance decision-making process governed by uncertainty, that are listed below:

- Precision of RUL prediction increases in time as time goes by, resulting in a better knowledge of the component's health condition.
- Lead Time is considered as a stochastic Gaussian variable with mean μ_{LT} , that means that scheduling and performing maintenance at the same instant of time implies waiting for spare parts delivery for a certain amount of time.
- The substitution of the component due to maintenance performed at an early stage in the component's life implies a significant loose of useful life.
- Performing maintenance too close to the median of RUL estimation implies taking a risk proportional to $RUL - t_r$ and to the amplitude of the confidence interval.
- Scheduling maintenance too early with respect to t_r implies stocking spare parts for a certain amount of time, sustaining a cost proportional to the stocking cost per unit time.
- The subsystem operating time provides time windows in which to perform maintenance.

Moreover, as stated in section 2.2, RUL estimation is in the operational time domain, that means that, in order to be compared with variables expressed in the calendar time domain, it has to be converted through the knowledge of the planned flight hours. This piece of information is not always available, such as in the case in which the aircraft is employed in a mission, in which flight plans are charged for a strong stochastic component.

In these cases, the rate of increase of flight hours with respect to calendar hours has to be estimated. Figure 23 represents the main dynamics that stand at the base of the maintenance decision-making process: assuming that maintenance is scheduled at time $t = t_{s1}$ the purple solid line represents the RUL pdf estimated at time t_{s1} given the information provided by sensors until the instant t_{s1}. Blue solid line represents, instead, the probability of having spare parts available at time $t > t_{s1}$ given the fact that spare parts procurement process has started at

time t_{s1}. The integral of RUL pdf evaluated between t_{s1} and t_r represents the risk associated to performing maintenance at time t_r, while the integral of RUL pdf between t_r and ∞ represents the potential unexploited useful life. Then, if maintenance scheduling is postponed to t_{s2}, the blue dashed line becomes the new representation of LT, while the dashed purple line represents the RUL pdf computed at time t_{s2}. As can be noticed from the figure, if t_r remains the same, the risk is lower, because the precision of RUL pdf estimate has grown. Moreover, even the unexploited potential useful life has decreased, whereas at the same t_r the probability of having spare parts available has decreased because the procurement process has been postponed.

The time between t_r and t_s determines the mean time that the spare parts will have to be stocked in the depot waiting for the aircraft arrival. thus, the higher $t_r - t_s$, the greater the stocking costs.

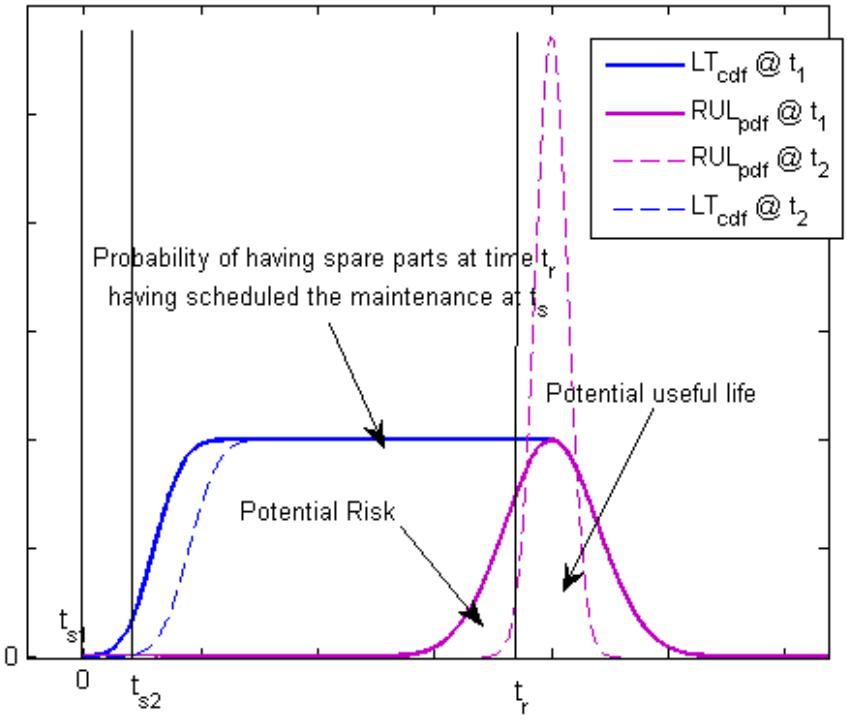

Figure 23 Dynamics of maintenance decision-making process

If the information about the system operations schedule and the component's MTTR are known, then the probability of concluding maintenance tasks before

the next planned flight, given the time t_r, can be easily computed. All these aspects, translated into formulas, become:

$$f_1 = \frac{1}{\bar{t} - t_1} \tag{3.33}$$

$$f_2 = P[TTR < (t_{start\ miss+1} - t_{end\ miss-1})] \tag{3.34}$$

$$f_3 = \int_{t_s}^{t_r} LT_{pdf}\, dt \tag{3.35}$$

$$f_4 = t_r - \frac{1}{t_r - t_s}\int_{t_s}^{t_r} LT_{pdf}\, dt \tag{3.36}$$

$$f_5 = \int_{t_s}^{t_r} \widetilde{RUL}_{pdf}\, dt \tag{3.37}$$

$$g(t_r) = \sum_{i=1}^{5} c_i f_i \tag{3.38}$$

$$t_r^* | t_s = t_r | \left(\frac{dg(t_r)}{dt_r}\right)_{t_r^*} = 0 \tag{3.39}$$

Where $\bar{t} = \frac{1}{T}\int_{t_r}^{\infty} \widetilde{RUL}_{pdf}\, dt$ and $\widetilde{RUL}_{pdf}$ is the RUL probability density function expressed in the domain of calendar hours. Finally, c_i for $i = 1,2,\cdots,5$ are the costs associated to each aspect. Then, it is to say that in the case in which the component is functioning or if the operations schedule is unknown f_2 is taken equal to zero. By multiplying each of these values by a proper coefficient, representing the cost associated to each event (i.e the stocking cost per unit time for Eq.3.36, the cost of performing unscheduled maintenance for Eq.3.37, the cost of missing a mission for Eq.3.35 and for Eq.3.34 and a the marginal

opportunity cost associated to exploiting one time unit of the LRU for Eq.3.33) a unique value can be obtained representing the potential cost related to performing maintenance at a generic time t. Obviously the time at which the function reaches its minimum should be chosen as the optimal t_r, given the time at which scheduling maintenance t_s. This computation can be performed at different time indexes, supposing to postpone the maintenance scheduling time t_s to a time $t_s + \delta$, where δ is an appropriate time index (i.e the mean time between missions) at which the standard deviation of RUL_{pdf} is equal to:

$$\sigma_{RUL_{ts+\delta}} = \sigma_{RUL_{ts}} - x(t) \qquad \textbf{3.40}$$

where $x(t)$ is a function that describes the σ_{RUL} decreasing trend. For example the function could represent the mean decreasing rate of σ_{RUL}, as reported in Figure 24. If the decreasing pattern is similar among the instances, a Bayesian approach could be used to predict the future σ_{RUL} values once measured the σ_{RUL} up the time now. This approach will be explained later in paragraph 3.2.4.

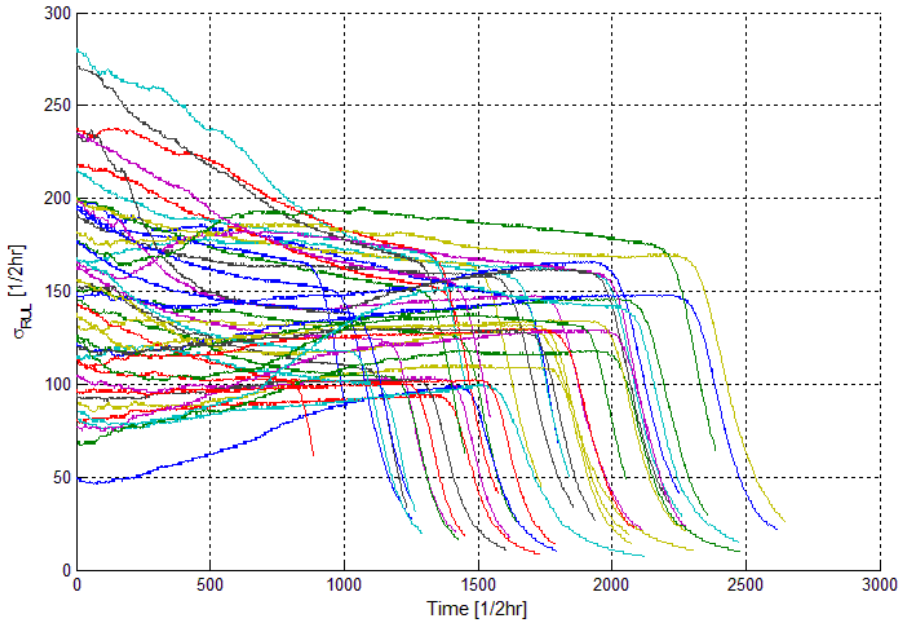

Figure 24 Decreasing trend of RUL from different simulations

The several functions for a given t_s are plotted in Figure 25.

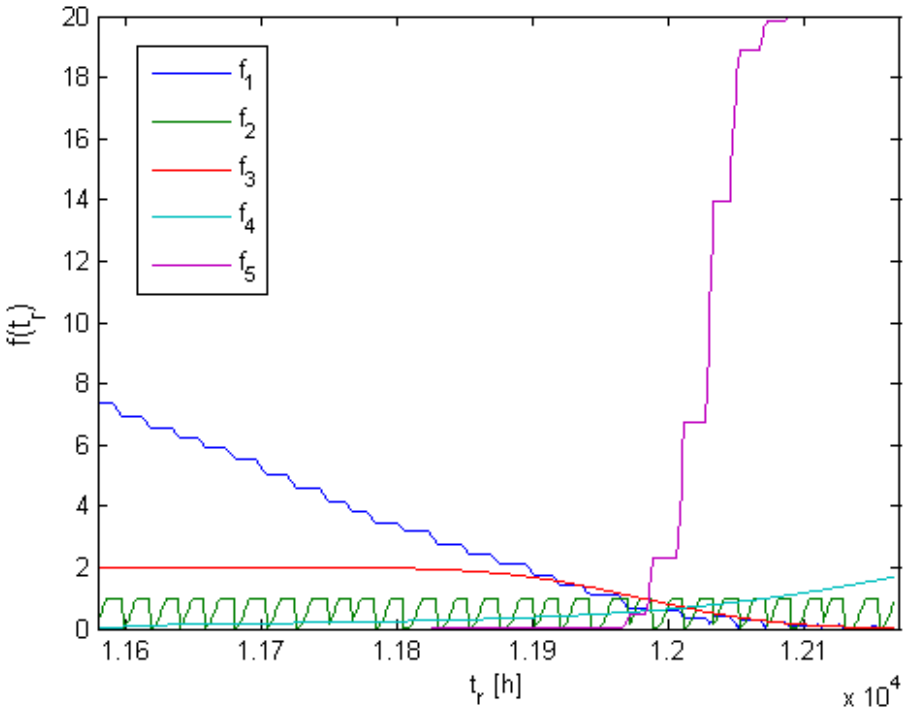

Figure 25 f_1, f_3, f_3, f_4, f_5 computed at a given time t_s

A series of t_r^* is computed at different scheduling times. At each time, the global optimum will be the instant t_s^* in which the function, given by the series of points $\left(t_s\,, F(t_r^*|t_s)\right)$, reaches the minimum, while the optimal t_r^* will be the time step at which the function f given t_s reaches its minimum, as shown in Figure 26. This computation is performed at each time step $t \in [t_a, t_f]$. So, maintenance will be scheduled at the instant t_i in which $t_i \geq t^*_{s_{ti-1}}$, where $t^*_{s_{ti-1}}$ is the time index t_s^* evaluated at time t_{i-1}. As for maintenance, it will be performed at time t_r^* given t_s^*.

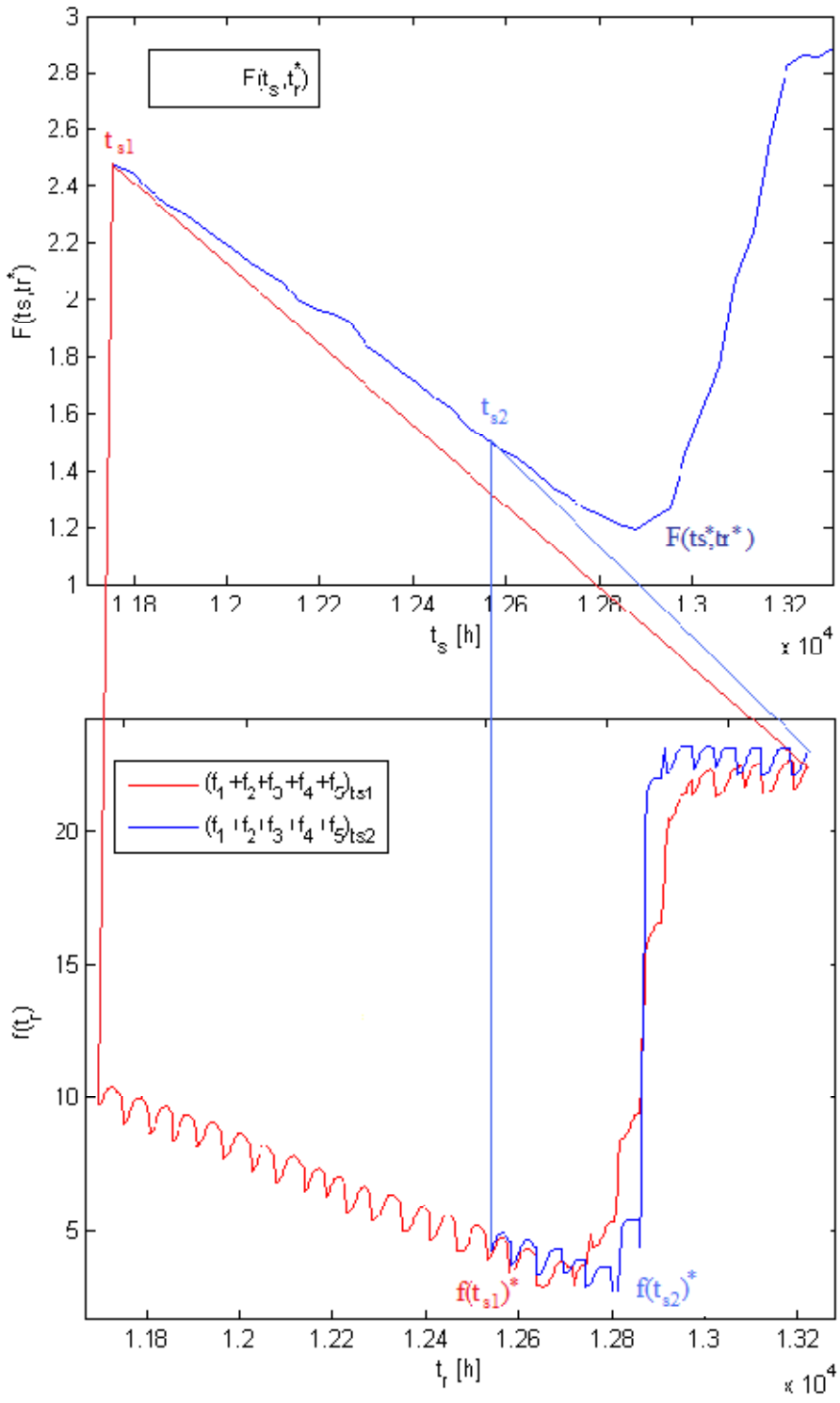

Figure 26 Example of t_r^* and t_s^* computation

3.2.3. The operational scenario

In order to demonstrate the performance of the scheduling and replacement model and the influence of some key variables, an operational scenario is defined. It is assumed that the degradation pattern described in section 3.1.1 can be representative of a degradation pattern of some logistic replacement unit (LRU) characterized by an exponential degradation pattern. The scenario chosen is a discontinuous operational scenario similar to that one that characterizes the operations of an aircraft which is described by its flight plan. Therefore a degradation pattern represents a degradation process of a component installed on an aircraft whose operations is described by a flight plan that has been defined as a connection between two stochastic variables: the flight time and the time between two flights. The former is a random variable with Gaussian distribution and its mean value has been taken equal to 2.5 hours while its standard deviation is 0.5 hours; the latter is a Gaussian random variable with mean 18 hours and standard deviation 3 hours. In this way, the flight plan is realized by simply assembling these couples of variables until the simulation time horizon is reached.

In order to evaluate how the maintenance scheduling and replacement model behaves and therefore to demonstrate the benefits that a CBM approach could generate, a set of 41 simulations have been performed. Each simulation run simulates an aircraft equipped with an unique LRU. At each time step, the LRU health index is acquired from the monitoring system and the LRU RUL is computed. If the cumulative flight hours are greater than the actual t_a[2] (different among each aircraft), then the maintenance scheduling and replacement model optimizes t_r and t_s through the function minimization described in paragraph 3.2.2. Maintenance scheduling and replacement model is interrogated at each time step until $t = t_s^*$ when the maintenance will be performed at time t_r^*. At time step t, if $t_r^* \geq t_f$, an unscheduled maintenance action is generated.

The benefits that are intended to be modeled by the 41 simulations are:

Reduced Lead Time/lower spare parts stocked

[2] Time at which the RUL predicted can be considered reliable

The key benefit of prognostics in this scenario is to identify the need for a resource that requires a non negligible lead time to acquire. An example of such a resource could be a replacement item (spare) or a maintenance resource that must come from off-site. Prognostics helps to reduce or eliminate the Lead Lime, resulting in less downtime and in the case of spares, fewer pipeline spares.

Extended Life/Reduced Maintenance Frequency/Increased Availability

The benefit of prognostics in this scenario is to implement a condition-based rather than time-based scheduled maintenance. By scheduling maintenance considering each individual item's predicted RUL versus a population statistic, the period between maintenance tasks is expected to increase, thus reducing the frequency of maintenances tasks (and its costs). This statement is well explained in Figure 27: the mean period between two maintenances tasks in a CBM environment will approach, thanks to prognostics, the mean time between failure (MTBF) of the item, as prognostics is able to predict failure with more accuracy. In time based maintenance environment (preventive) we can suppose [**56**] that maintenance tasks are performed always at the same cumulative operational hours. This threshold can be set on the basis of the a priori component TTF pdf. Once set a reliability level, i.e 99,9%, scheduled maintenance actions should be performed always at time instant t_i at which the condition $\int_{-\infty}^{t_i} TTF\, dt = 1 - R$ is satisfied.
Obviously, reducing the maintenance action frequency, also the asset availability will increase, as explained later in paragraph 3.2.4.

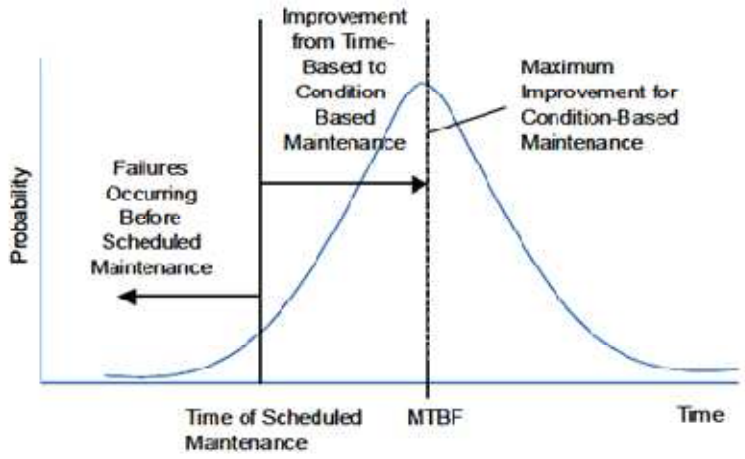

Figure 27 Extending life by transitioning to condition based maintenance

To evaluate these gains the metrics that have been chosen are:

- Availability $A = TFH/(TFH + TTR)$;
- Spares stocked total cost (see par.3.3.2);
- Unscheduled maintenance events ($t_r^* \geq t_f$)
- Life exploited
- $t_r - t_s$ variance

Where TFH stands for total flight hour flown, TTR stands for time to rapair. Life exploited percentage is defined as $LE\% = (t_f - t_r)/t_f$.

3.2.4. Results

Performing the optimization described in paragraph 3.2.2 at each time step requires long simulation times. To face this difficulty, an algorithm that speeds up the computation has been defined. Our goal is to select the right time steps at which computing the maintenance scheduling and replacement optimization among the entire time lag $t_f - t_a$. The risk related to run the optimization using wider time spans is to miss the optimum and therefore to compromise the results. Theoretically, the time that elapses between two successive time steps in which performing maintenance scheduling and replacement, should not be linear. The updating of the optimal maintenance schedule and replacement must be more frequent nearby the optimum. The solution adopted consists of defining

the time step $i+1$ as a function of the time between t_i and the previous estimation of time scheduling $t_{s_{i-1}}$. As a result, the optimization subroutine has to indicate the time step t_{i+1} so that the ratio $(t_{i+1}-t_i)/(t_i-t_{i-1})$ tends to zero as the difference $t_{s_{i-1}}-t_i$ decreases. The function chosen is reported in the following equation:

$$t_{i+1} = t_i + \varepsilon\left(t_{s_{i-1}} - t_i\right) + \mathrm{C} \qquad \textbf{3.41}$$

where the constant C is a parameter set to control the convergence velocity of the algorithm when approaching the optimal t_s value. The fact that a constant has been introduced in the advancement rule leads to a certain loss in accuracy, whose value can be qualitatively controlled by varying this constant. Once optimized the solution finding procedure, it is possible to run several simulations to praise the improvements of the approach proposed so far and consequently assess the potential benefits of a prognostic approach to maintenance. The case study framework has been described in the previous paragraph 3.2.3. Since no data were available that fitted properly to our case, we made some plausible assumptions regarding the values of the variables used (Table 2)

Simulation Variables			
Variable	*Value*	*Description*	
f_t	N (2.5,0.025)	Flight Time	[h]
f_{bf}	N (6,1.8)	Time Between Flights	[h]
LRU Failure and Feature Variables			
TTR	N (8,1)	Time To Repair	[h]
TBF	N (1800,180)	Time Between Failures	[h]
hi	N (1.11,0.0111)	Health Index at Failures	[/]
hi_{th}	$\mu_{hi} - 3\sigma_{hi}$	Health Index Threshold	[/]
t_i	N (1260,88.2)	Time to Failure Trigger	[h]

Maintenance Scheduling and Replacement Optimization Function Variables			
c_1	0.01	Marginal Opportunity Cost for Exploiting Component's Life	[/]
c_2	1	Missing Mission Cost index	[/]
c_3	0.001	Unavailability Cost index	[/]
c_4	0.00001	Marginal Spare Part Holding Cost index	[/]
c_5	40	IFSD[3] cost index	[/]
LT	450,350,350,150	Lead Time	[h]
ε	$1/3$	Computation Optimization Function Constant	[1/hr]
C	3	Computation Optimization Function Constant	[h]

Table 2 Values used in the case study simulation

In this case study the LT is considered as a deterministic variable. This is because the LT variance is not an important issue to be analyzed, it would be invariant among the simulations.

In order to study the relationship between the maintenance scheduling and replacement model and the supply chain organization, 4 different simulation runs are performed with different LTs whose values are reported in Table 2.

Before performing all the 4 simulations run, remembering Eq.3.39, a comparison between keeping $\sigma_{RUL_{ts+\delta}}$ constant and using a Bayesian approach is performed. In the first case the underlying assumption is that no inference is made upon the future values of the RUL predictions confidence interval amplitude σ_{RUL}. Therefore, σ_{RUL} future values are kept constant and equal to last computed σ_{RUL}. Whereas the second approach aims to exploit the information that σ_{RUL} decreasing patter as new measurements become available is similar

[3] IFSD (In flight Shut Down)

among different degradations paths. This is evident observing Figure 21. Assuming that from experimental tests or from the field some $\sigma_{RUL}(t)$ functions (i.e several curves as those displayed in Figure 21) are known, an approach similar to that used to predict the RUL can be followed. This upgrade can let us estimate the σ_{RUL} future values combining the a priori information and the computed σ_{RUL} value vector. Supposing that we are at time t_k and we have computed $\sigma_{RUL} = \sigma_{RUL}(t_1), \cdots, \sigma_{RUL}(t_k)$, we can estimate the future values $\sigma_{RUL}{}' = \sigma_{RUL}(t_k + 1), \cdots, \sigma_{RUL}\left[\widetilde{t_f}(t_k)\right]$ that can be used by the maintenance scheduling and replacement model to determine the optimal t_r and t_s. $\widetilde{t_f}(t_k)$ is the estimated TTF at the time epoch t_k by the prognostic algorithm. Hopefully the overall performances would be better than the performance obtained keeping $\sigma_{RUL} = cost$.

The σ_{RUL} degradation pattern is modeled as a 4th degree polynomial with random coefficients distributed as a multivariate normal with parameters $(\mu_\sigma, \Sigma_\sigma)$ and with a normal iid error with mean equal to zero and variance σ_e^2. Therefore we have:

$$\sigma_{RUL}(t) = X\gamma + E \qquad \textbf{3.42}$$

Where:

$$X = [t^4 \quad \cdots \quad t \quad 1]\,, \gamma = \begin{bmatrix}\gamma_1\\ \gamma_2\\ \gamma_3\\ \gamma_4\\ \gamma_5\end{bmatrix}, E = N(0, \sigma_e), \mu_\sigma = \begin{bmatrix}\mu_1\\ \mu_2\\ \mu_3\\ \mu_4\\ \mu_5\end{bmatrix}, \Sigma_\sigma = [5\ X\ 5] \text{ matrix}$$

Let suppose that we have computed $\sigma_{RUL} = [\sigma_{RUL}(t_1), \cdots, \sigma_{RUL}(t_k)]'$ and we have the a priori information on the γ parameters pdf $(\mu_\sigma, \Sigma_\sigma)$ the updated parameters means $\tilde{\mu}_\sigma$, remembering Eq.3.12, will be:

$$\tilde{\mu}_\sigma{}^T = \left(\hat{\beta}^T \frac{X^T X}{\sigma_e{}^2} + \mu_\sigma{}^T \Sigma_\sigma{}^{-1}\right)\left(\frac{X^T X}{\sigma^2} + \Sigma_\sigma{}^{-1}\right)^{-1} \qquad \textbf{3.43}$$

Where $\hat{\beta} = (X^T X)^{-1} X^T \sigma_{RUL}$, $X = \begin{bmatrix} t_1^6 & \cdots & 1 \\ \vdots & \ddots & \vdots \\ t_k^6 & \cdots & 1 \end{bmatrix}$

Therefore the mean $\sigma_{RUL}{}'$ future values will be:

$$\sigma_{RUL}{}'(t_k + t) = \tilde{X}\tilde{\mu}_\sigma \qquad \textbf{3.44}$$

Where $\tilde{X} = [(t_k + t)^4 \quad \cdots \quad (t_k + t) \quad 1]$.

The comparison between two methods was computed assuming a LT=250 hr. Each run is composed of 41 aircrafts, therefore a total of 82 simulations was performed.

The comparison is made using the metrics "exploited life" and $t_r - t_s$ introduced in the paragraph 3.2.3.

Table 3 shows the results of the simulations. As can be noticed, from the metric *Exploited life* point of view, the Bayesian methodology led to better results. As matter of facts the mean exploited life in the Bayesian case is equal to 95.4% while in the σ_{RUL} constant case is equal to 91.4% with a difference of 4 percentage points (72 operative.hr or 420.37 calendar hr). From the metric $t_r - t_s$ point of view the constant case should be preferred since guarantees less variable $t_r - t_s$. The reasons will be described in the following paragraph.

Method	Metric	Mean Value	Standard deviation
Const	Exploited life	0.91386	0,0339
Bayes	Exploited life	0.95470	0,0369
Const	$t_r - t_s$	248,7 [hr]	19,03 [hr]

Bayes	$t_r - t_s$	297,4 [hr]	153,83 [hr]

Table 3 Methodology results comparison

For the successive simulations, the Bayesian methodology will be used.

LT [hr]	Exploited life	σ_{EL}	Unscheduled events	% Unscheduled Events	$\sigma_{t_r - t_s}$ [days]
150	0,9548	0,0312	0	0%	6,912
250	0,9547	0,0339	0	0%	6,410
350	0,9572	0,0400	4	10%	7,259
450	0,9586	0,0426	8	20%	9,415

LT [hr]	Availability CBM	Availability SM	Δ_{avail} %	Δ_{MTBM} %
150	99,537%	99,419%	0,119%	-25,63%
250	99,537%	99,419%	0,119%	-25,62%
350	99,538%	99,419%	0,120%	-25,95%
450	99,538%	99,419%	0,121%	-26,13%

Table 4 Results from the scheduling and replacement model for different LT

The results obtained from the simulations with different LT are reported in Table 4. Particularly, if we observe the first column of the first table we can say that as LT increases the exploited life increases. For LT=150 hr we have an exploited life of 95,5 %, while for LT=450 we obtain an exploited life equal to 95,86%. Observing the second column that represent the standard deviation of the exploited life we have that σ_{EL}increases. However, to analyze correctly the result obtained, we have to consider the number of missed faults obtained. From the third column we have that for LT=350 hr we have registered 4 unscheduled maintenance events (4%) while for LT=450 hr we have registered 9 missed faults (20%). The underlying reason is that increasing the LT the model will shift backwards t_s in order to keep the optimization function low, determining a loss in precision and accuracy of RUL estimation. Due to high LT the system is forced to schedule maintenance basing on an unreliable estimation. This may cause a degradation in the performances as for missed and false alarms, since

the high LT forces the system to schedule maintenance basing on an unreliable estimation. Hence, this may cause a global degradation in the performances of the system, determining situations that can be interpreted as false alarms or missed alarms. The last column of the first table the standard deviation of the metric $\sigma_{t_r - t_s}$ is reported. This value increases as LT increases. This phenomenon has to be taken into account for spare parts supply chain design.

In the second table a comparison between a CBM approach and a Scheduled Maintenance approach is made by comparing the availability that each approach guarantee and the frequency of the maintenance actions.

In the case of Time Based Maintenance the maintenance tasks are scheduled at a given time before the prior estimate of t_f pdf. This time is established setting a reliability threshold equal to 99,9%, therefore the scheduling threshold is a fixed value. This lead to the fact that in case of time based maintenance, the exploited life is always equal to 0.76. This value is strictly correlated with the asset availability. Since this percentage is also an index of the $MTBM$ (Mean Time Between Maintenance) that is on average equal to:

$$MTBM = LE \text{ x } MTBF \tag{3.45}$$

Where LE is the average life exploited and MTBF stands for mean time between failures. Moreover, considering that the $MTTR$ (Mean time to repair) is constant in both the scheduled and condition-based maintenance scenarios, the improvement observed thanks to prognostic directly result in an increment of the availability. In fact, if we express the canonical availability equation as a function of LE, we obtain:

$$A_{CBM} = \frac{MTBM}{MTTR + MTBM} = \\ = \frac{MTBF\ LE}{MTTR + MTBF\ LE} = \\ \frac{MTBF}{\frac{MTTR}{LE} + MTBF} \tag{3.46}$$

Since $LE_{CBM} > LE_{SM}$, the availability in a CBM framework is greater than the availability allowed by a SM policy. The availability computed in a CBM scenario, in this example, is on average 0.11% greater than in a SM approach. The main benefits however comes from the decrease of the maintenance task frequency that it is proportional to the increase of MTBM, therefore the increase in LE. In this example a 25.63% decrease is computed.

3.3. Spare Part Supply Chain model

3.3.1. The Model

The cost model for the logistic supply chain is focused on the level of safety stock required, at each depot to support the assets and the on-time repairs with the desired quality-of-service level basing on a prior estimate of the average rate of repair and the its variance. The impact of a prognostic maintenance policy on the spare parts supply chain has been described in [**65**], adapting the classical approach to safety stock problem as displayed in Figure 28 [**66**].

In [**65**] it is assessed the influence of prognostics on the distribution and the level of spare parts safety stock along the supply chain, which is considered as a serial network of 6 nodes with deterministic transfer times between them. In the model proposed, the safety stock level optimization, both in the scheduled maintenance, corrective maintenance and in the conditional maintenance policy scenario, follows the approach proposed in[**66**] considering the additional lead time provided by the CBM as a random variable $(t_r - t_s)$ and not as a constant. Considering $t_l = t_r - t_s$ as a stochastic variable is necessary since, as demonstrated in the previous paragraph, its variance could be not negligible.

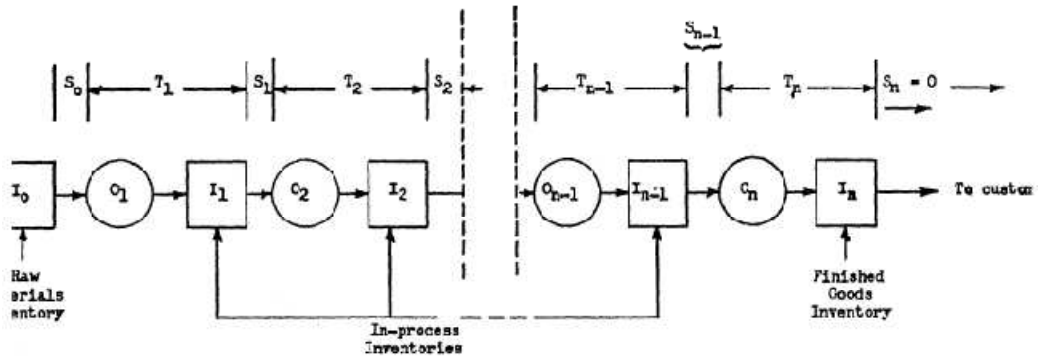

Figure 28 Classical approach to safety stock problem**[**66**]**

The baseline model, i.e. without PHM, consists of a 4-stage serial system ($N = 4$). This system is composed of the Spare parts manufacturer depot, depot I, depot II and the base depot with node i supplying node $i + 1$, for $0 < i <$ N, characterized by the $(s, 1 - S)$ inventory policy. Node 0 represents a location of plentiful supply from which resources may be drawn with zero delays and node 4 (Base depot) represents the repair site. There are no capacity constraints limiting the amount of resources that may be held at node i.
Intermediate nodes are potential depots in which resources may be best aged and pre-processed en route to the repair site. The overall number of repairs in the fleet at each period is an independent Poisson-distributed random variable with mean λ and variance λ. T_i represents the time required to transfer resources from depot T_i to depot T_{i+1} once they are available, and to process them for the delivery to the next node. The incremental holding cost for resources at node i, following whatever processing is required, is h_i. Typically, nodes in the supply chain closer to the end have smaller transfer lead times T_i but greater stocking costs h_i [**65**].

Each node quotes and guarantees a service time S_i, which is the maximum delay to supply parts for delivery to the next node. In the baseline model (Scheduled maintenance or corrective maintenance), $S_0 = S_{\mathrm{N}} = 0$, since it is presumed that there are no delays at node 0, and that the goal is to enable a repair as soon as a fault is detected to maximize availability of the asset. The variables $S_1 \cdots S_N$ are independent variables. To determine the total stock required at a given node, we define k as the quality of service level for node i, which denotes the percentage of time service guarantees that are met.

The safety stock I_i, at node i must be sufficient to address demand during the time gap from the service time guarantee S_i and the time to replenish stock $S_{i-1} + \mathrm{T_i}$ according to the following equation ([**66**][**65**][**67**]):

$$I_i = k\lambda\sqrt{S_{i-1} + \mathrm{T_i} - S_i} \qquad \textbf{3.47}$$

Further, we can deduce some bounds on the service time S_i, that at a given node is at best zero, in which case the stock is always sufficient to supply deliveries, and at worst it always requires replenishment from the previous node, which

takes time $S_{i-1} + \mathrm{T_i}$. This leads to the following problem statement for the baseline supply chain model:

$$\min \sum_{i=1}^{N} h_i I_i \qquad \textbf{3.48}$$

$$\begin{gathered} I_i = k\lambda\sqrt{S_{i-1} + \mathrm{T_i} - S_i} \quad i = 1, \cdots, N \\ 0 \le S_i \le S_{i-1} + \mathrm{T_i} \quad i = 1, \cdots, N \\ S_0 = S_N = 0 \end{gathered} \qquad \textbf{3.49}$$

The supply chain problem defines an optimization of a nonlinear function over a region of convex constraints. The classical analysis of Simpson [**66**], however demonstrated in the following theorem:

If $\boldsymbol{f}$ *is a function of* $\boldsymbol{N-1}$ *real variables* $\boldsymbol{S_1 \cdots S_{N-1}}$ *of the form* $\boldsymbol{f(S_1 \cdots S_{N-1}) = c + \sum_{i=1}^{N} r_i\sqrt{S_{i-1} + T_i - S_i}}$ *(where* $\boldsymbol{S_0}$*,* $\boldsymbol{S_N}$*,* $\boldsymbol{c}$ *and* $\boldsymbol{r_i}$ *are constants) whose domain* $\boldsymbol{D}$ *is the* $\boldsymbol{n-1}$ *dimensional polyhedron obtained by restricting the variables in such a way that each radicand above is nonnegative and each variable* $\boldsymbol{S_i}$ *is nonnegative then the minimum of the function* $\boldsymbol{f}$ *occurs at one of the vertices of* $\boldsymbol{D}$.

As a result, the problem has its unique optimal solution on a vertex of the boundary such that $S_i^* \epsilon \{0, \boldsymbol{S_{i-1} + T_i}\}$ therefore the scan over service times becomes a binary choice. The solution has to be chosen between all the possible combinations of S_i, the optimal value is the one that minimizes the function in Eq.3.48.

Considering the case in which PHM system provides additional lead time at the terminal node, equal to $t_r - t_s$, the supply chain can use it to reduce costs. However, this prediction is not deterministic, but it has a stochastic component as demonstrated in paragraph 3.2.4. The higher the variance of this variable, the lower the gains, as depicted in Figure 32. This modifies the terminal boundary conditions to[4]:

$$S_4 = t_l \qquad \textbf{3.50}$$

[4] Assuming t_l as a normal random variable

$$I_i = k\lambda\sqrt{S_3 + \mathrm{T}_4 - t_l + {\sigma_{tl}}^2\lambda}$$

where t_l is the lead time afforded by PHM and σ_{tl} is its standard deviation. Plotting the number of stocked spare parts at each four depots as function of t_l (keeping σ_{tl} constant) and supposing that $\mathrm{T_i}$ and h_i assume the values in Figure 29 we obtain Figure 30. As can be noticed the number of stocked parts that guarantees the same service level k decrease as t_l increases. The required spare parts are pushed backwards along the supply chain. Meanwhile, as can be noticed from Figure 31, keeping t_l constant and varying σ_{tl} the required stocked parts increases to guarantee the same service level.

Figure 32 represents the spare parts holding costs as function of σ_{tl} and t_l.

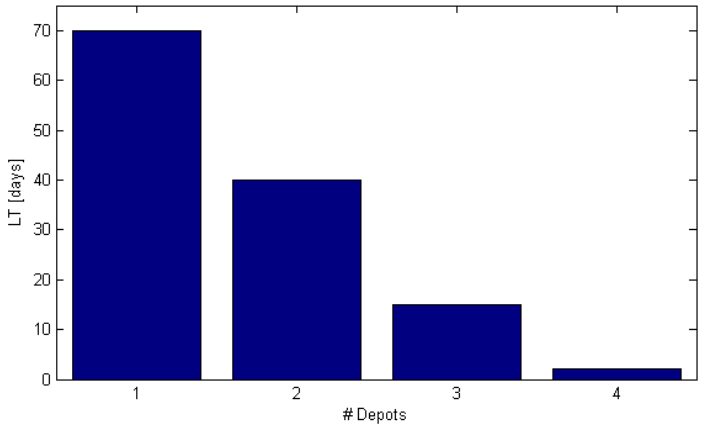

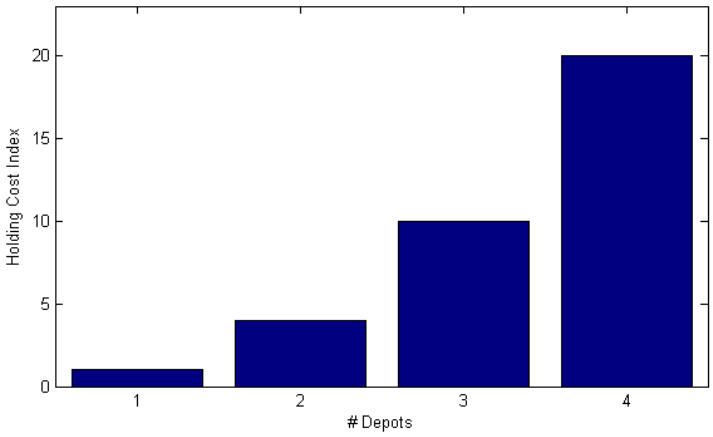

Figure 29 T_i and h_i values

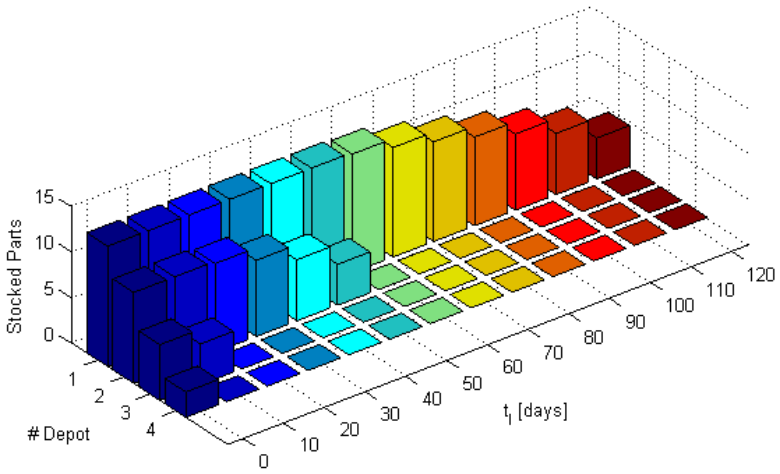

Figure 30 Number of stocked spares in the four depots as a function of t_l

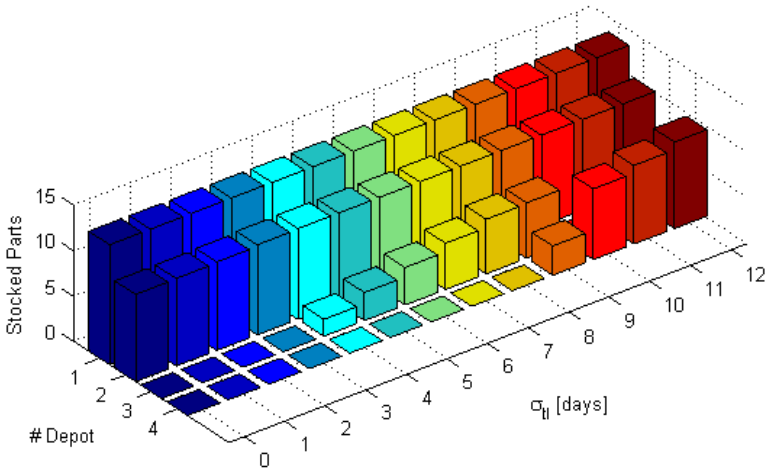

Figure 31 Number of stocked spares in the four depots as a function of σ_{tl}

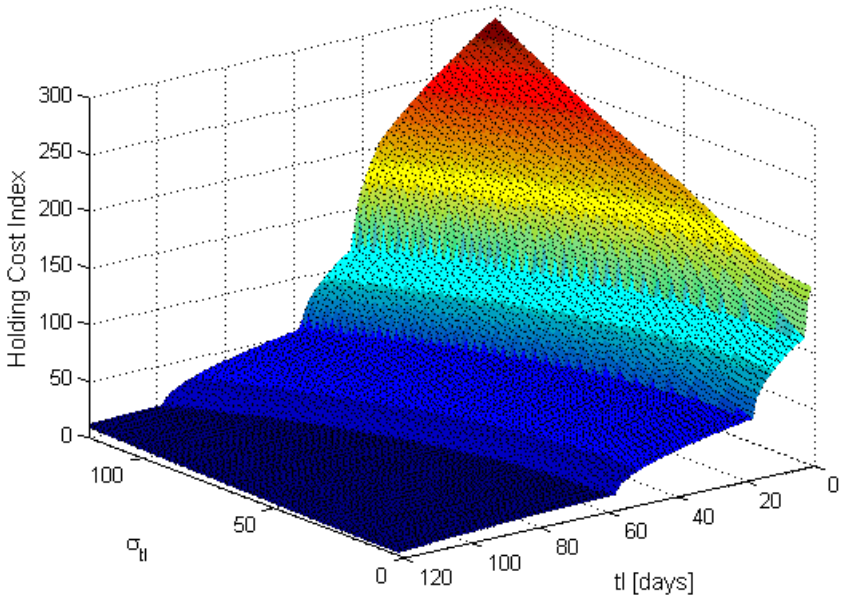

Figure 32 Total stocking costs as a function of t_l and σ_{tl}

3.3.2. Results and Sensitivity Analysis

The optimal supply chain design has been computed for all the simulations performed, that is 4 simulation runs, on for each LT. The maintenance scheduling and replacement model gave us the σ_{tl} for each simulation run, as reported in Table 4. Moreover, we obtained the values of the mean exploited life LE. This value is necessary to compute the expected spare part demand. It is assumed that the spare parts supply chain has to support a fleet composed of 40 elements of the same type.

The mean spare parts demand is proportional to the MTBM through a coefficient that represents the ratio between the actual hours flown and the calendar hours, since the aircraft utilization is discrete. The steady state expected demand for each scenario is reported in Table 5.

Maintenance Policy	Demand (λ) [parts/day]
CBM_150	0,191579
CBM_250	0,191551
CBM_350	0,191095
CBM_450	0,190847
Time Based	0,240838
Corrective	0,1829

Table 5 Expected demand

As we can observe the expected demand is lower for a CBM policy than the demand in a SM policy case since LE is greater in the CBM scenario. The table reports also the expected demand when LE=1, that is the case of a corrective maintenance. Given the LT and σ_{tl} values for each scenario (assumed to be zero for the SM and corrective maintenance scenario) we can compute the safety stock required for each depot. The results are displayed in Figure 33. As we can observe the benefits resulting from a CBM policy are not completely evident especially in the CBM scenario with LT=150 hr and LT=250 hr. This is due to the fact that, even if $tl > 0$ its variance dissipate its benefits.

Figure 34 sums up the most important results for each scenario. The blue bars represent the expected demand percentage variation with respect to the

corrective maintenance policy. As we can observe the worst case is the SM (Time based) policy since has the lowest LE. The expected demand is 31% greater that the case of corrective maintenance policy. Meanwhile, the red bars represent the spare parts holding costs variation with respect to the corrective maintenance policy. We can observe that generally the CBM policy can lower the total spare parts stocked. However several considerations have to be made upon the correct lead time that is used as an input for the maintenance scheduling and replacement model.

From these results we can conclude that, considering only the supply chain holding costs, the CBM approach imposing a LT equal to 350 hr represent the optimum. In other words the combination of the expected demand, σ_{tl} and tl for the CBM_350 scenario minimizes the spare parts holding costs. Obviously this is not the global optimum because other metrics has to be considered, such as those introduced in the paragraph 3.2.4.

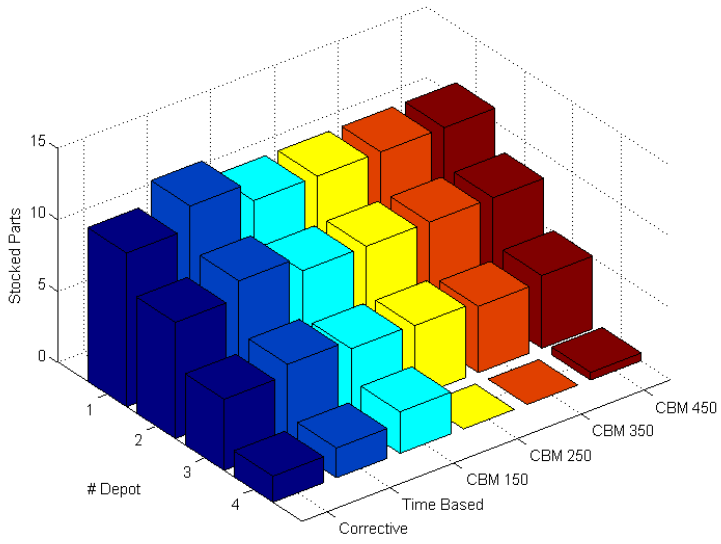

Figure 33 Safety Stock for each scenario

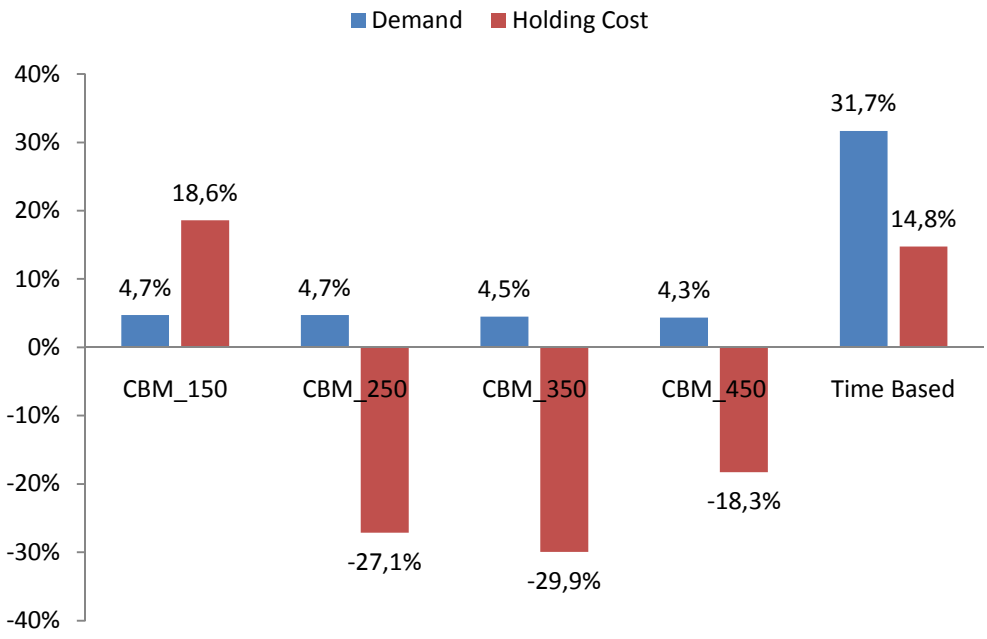

Figure 34 Results from the supply chain model, percentage variations with respect to corrective maintenance policy

4. Case Study

4.1. Introduction

Railway axles are designed to have an infinite lifetime[**68**]. However occasional failures have been and are observed in service. The typical failure positions are the press-fits for wheels, gears, and brakes or the axle body close to notches and transitions. Such failures always occur as fatigue crack propagations whose nucleation can be due to different causes [**69**]. In the case of railway axles, the presence of widespread corrosion[**70**][**71**] or the possible damage due to the ballast impacts [**72**] may constitute such causes.

This kind of failures is usually tackled by employing the 'damage tolerance' methodology, whose philosophy consists [**69**][**73**] in determining the most opportune inspection interval given the 'probability of detection' (PoD) of the adopted non-destructive testing (NDT) technique or, alternatively, in defining the needed NDT specifications given a programmed inspection interval.

The negligible number of axle failures is reached thanks to role played by inspections carried out with the aim of keeping developing fatigue problems at bay. As reported by [**74**] in the United Kingdom there have been about 1.6 axle failures per year over the last 25 years, out of a population of about 180,000 axles. (A similar number of new axles are introduced every year in PR China, where some 2.5 x 10^6 wheelsets are in fleet service.) These large numbers of axles are subjected to inspections in order to try to identify cracks before failures occur. In general, the examinations are expensive, time consuming and not particularly effective in finding cracks. Furthermore, the dismantling needed to examine axles, such as the drawing-off of bearings, can cause scratching damage that is sufficiently severe to cause an axle to be retired. The rationale behind the frequency of testing is that the largest crack that would not be detected in an inspection should not grow to failure during the service interval to the next inspection. This implies that crack propagation calculations should be performed with sufficient accuracy to set the inspection interval. However, as stated by [**74**] some difficulties arises:

1. Because of the difficulty in determining the reliability and sensitivity of the inspection techniques, the initial crack length chosen for the life calculation

must be set larger, leading to shorter intervals between inspections than are really necessary.

2. The service loads are much more stochastic in nature than the well-defined hypothetical loads used for the initial design rule suggest. In many cases, in the absence of experimental measurement, the magnitudes and frequencies of these events are unknown, thus making cycle-by-cycle crack growth predictions unreliable.

3. Important inputs to fatigue calculations are material properties such as crack growth data, fatigue limits and fatigue thresholds, which are very sensitive to material condition, manufacturing route, surface treatment, orientation and load sequence. In many cases these data are lacking, particularly from large specimens representative of axles.

5. Abnormal conditions may arise in service. There is debate about the best means of protecting axles from corrosion and the extent to which coatings may hinder inspection. The interactions between fatigue and corrosion mechanisms in extending defects are still inadequately understood. Higher speeds have led to increased examples of damage of axles from flying ballast, which may be of the form of crack-like indentations on axle surfaces that initiate premature failure.

These considerations can lead to think that maybe, instead of using a preventive maintenance approach a predictive maintenance approach based on prognostics could be convenient. Several aspects has to be considered in order to assess the technical and economical feasibility of this approach. The first and the most important is the assessment of the prognostic algorithm predictions accuracy and its sensibility to the goodness of the diagnostic and monitoring equipment used. This section constitute the first attempt to answer to this answer to this question through an explanatory assessment of two prognostic algorithms. The first one is based on statistical methods, similar to that one proposed in paragraph 3.1, the second one exploit the good understanding of the crack propagation physical process to estimate the time to fail of a cracked axle. Moreover, the predictive maintenance approach is qualitatively compared to the classical preventive approach.

4.1.1. Data

$\Delta K_{th} = N\ (11.32,0.857)\ MPa\sqrt{m}$	$n = 1.9966$	$\alpha_5 = -1.916$	$D = 160\ mm$
$\Delta K_{th0} = 5.96\ MPa\sqrt{m}$	$C_{th} = -0.02$	$\alpha_6 = -0.3927$	$K_t = 1.2$
$R = -1$	$\alpha_1 = -194.024$	$\beta = 0.656$	
$\Delta K_{crit} = 24\ MPa\sqrt{m}$	$\alpha_2 = 322.544$	$\varepsilon = 10\ MPa$	
$p = 1.3$	$\alpha_3 = -177.24$	$\vartheta = 2.5$	
$q = 0.001$	$\alpha_4 = 41.957$	$S_0 = 0.2$	

4.2. Simulation of the crack growth paths – The stochastic crack growth algorithm

In this paragraph the stochastic crack growth model used in this work is presented. The non-powered railway axle considered in the present study is manufactured in A1N steel and used in Y25 bogie with a diameter D equal to 160 mm.

Service loads acting on railway axles are the result of vertical and lateral forces [**68**] due to their normal functioning, and the maximum bending moments can be found in the area of the wheels press-fit [**69**][**72**]. On the basis of these considerations, fatigue crack growth has here been analyzed at the typical T-transition between the axle body and the press-fits.

Different algorithms for simulating the crack growth of cracked components are available in literature. Some of them consider the crack growth modeling as stochastic process, see for example [**75**],[**76**].[**77**]. However, the likelihood of lifetime calculations depends on the adopted FCG algorithm and only the most

complex algorithms are able to adequately describe crack propagation under variable amplitude loading in railway axles [**78**].

In the present work the NASGRO algorithm [**79**] will be considered. This FCG model has been chosen because it is the reference algorithms in analyses where random loadings are involved, since it takes into account the ‘‘plasticity-induced crack closure’’ phenomenon [**68**]. Moreover, NASGRO has been used in several papers addressing the propagation of fractures in railway axles [**69**] [**80**][**81**]

The considered software adopts the Paris-based crack propagation law called ‘‘NASGRO equation’’:

$$\frac{da}{dN} = C\left[\left(\frac{1-f}{1-R}\right)\Delta K\right]^{n} \frac{\left(1-\frac{\Delta K_{th}}{\Delta K}\right)^{p}}{\left(1-\frac{\Delta K}{(1-R)\Delta K_{crit}}\right)^{q}} \qquad \textbf{4.1}$$

where ‘‘C’’, ‘‘n’’, ‘‘p’’ and ‘‘q’’ are empirical constants, ‘‘R’’ is the stress ratio, ‘‘ΔK_{th}’’ is the threshold SIF range and ‘‘ΔK_{crit}’’ the critical SIF. The most important parameter is ‘‘f’’ representing the crack closure effect (Eq.4.10). Eq.4.1 is a development of the classical Forman’s formulation and incorporates all the three propagation regimes (from threshold to ΔK_{crit}). In order to introduce the dependence of thresholds on crack size and stress ratio, the ΔK_{th} parameter included in Eq.4.1 has been described by the expression:

$$\Delta K_{th} = \Delta K_{th0} \frac{1}{\left[\frac{1-f}{(1-A_0)(1-R)}\right]^{1-C_{th}R}} \qquad \textbf{4.2}$$

Where ‘‘R’’ is the stress ratio, ‘‘f’’ is the closure function, ‘‘A_0’’ (Eq.4.10), is a constant used in the formulation of ‘‘f’’(Eq.4.10), ‘‘ΔK_{th0}’’ is the threshold SIF range at $R = 0$, ‘‘C_{th}’’ is an empirical constant.

To analyze cracked bodies under combined loading, the stress intensity factor is expressed as:

$$\Delta K_{nom} = \left[\sum_{i=1}^{6} \alpha_i \left(\frac{a}{D}\right)^{i} + \beta\right](1-R)(S+\varepsilon)\sqrt{\pi a} \qquad \textbf{4.3}$$

Where α_i and β are empirical constants, S is the applied bending stress, a is the crack size and ε is a random coefficient (introduced later in the paragraph). The bending stress is considered plane since NASGRO is not able to consider rotating bending conditions. This assumption has not a significant influence on estimated life predictions as demonstrated in [**82**][**83**].

The closure function is defined as:

$$f = A_0 + A_1 R \tag{4.4}$$

Where

$$A_0 = 0.825 - 0.34\vartheta + 0.05\vartheta^2 \left[\cos\left(\frac{\pi}{2} S_0\right)\right]^{\frac{1}{\vartheta}}$$
$$A_1 = (0.415 - 0.071\vartheta) S_0 \tag{4.5}$$

ϑ is a plane stress/strain constraint and S_0 is the ratio of the maximum applied stress to the flow stress.

Since NASGRO does not consider the geometry of the typical transitions of

axles, equation 4.9 is modified in terms of the maximum SIF present at the notch root and calculated as

$$\Delta K = K_t \Delta K_{nom} \tag{4.6}$$

K_t represents the experimental stress concentration [**81**].

As demonstrated by [**78**], the crack growth randomness can be described considering the stress intensity factor threshold as a random variable. Particularly, it is demonstrated that ΔK_{th} can be considered as belonging indifferently to a lognormal distribution or normal distribution. In this work is considered as a normal variable with mean given by expression 4.2 and standard deviation $\sigma_{\Delta K_{th}}$. The empirical calibration of all the other parameters is carried out by means of dedicated fracture mechanic experiments. Their values are listed in paragraph 4.1.1

Another relevant source of uncertainty is the randomness of the applied load [**69**][**72**]. Therefore service loads have been considered derived from experimental results on a high speed train. Next, the service stress spectrum has been approximated with a simple block loading consisting of twelve blocks

(Table 6). To take into account the within block variability a random term ε is added in the Eq.4.9. It is assumed to be uniformly distributed with mean equal to 0 and with a span of 2ε.

The so defined block loadings were then applied to growth calculations with a time sequence in accordance to Gassner suggestions[**84**]. Starting from the discrete spectrum in Table 6, the random history loads sequence is built by permutations of the whole set of the blocks. Each load sequence is 3.222.887 km long, composed of 20 consecutive complete permutations. An example of load sequence is displayed in Figure 35. Some simulated crack growth path, considering all the uncertainties described (load history, ΔK_{th} and ε) are shown in Figure 36.

Cycles	Load [MPa]
1	145
8	135
75	125
825	115
15.000	105
110.025	95
357.675	85
678.900	75
1.621.725	65
3.046.500	55
8.165.775	45
39.718.275	35

Table 6 The 12 service time blocks

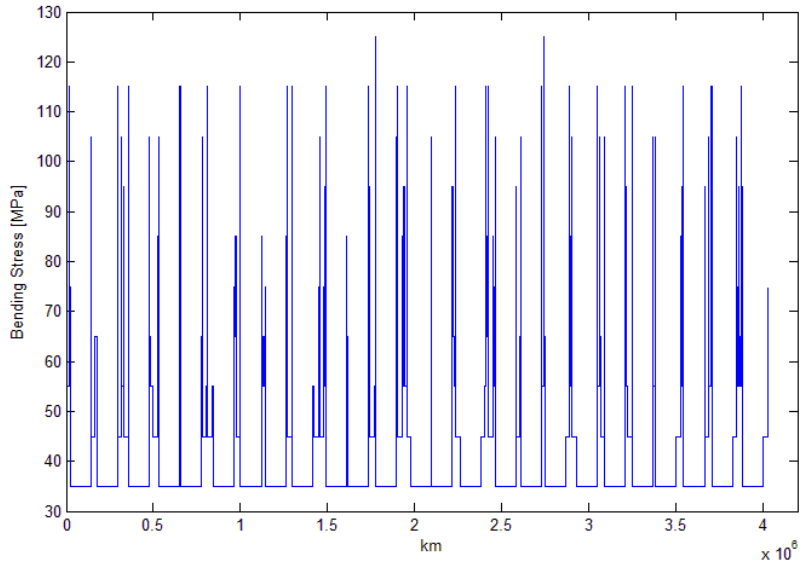

Figure 35 Example of a load history

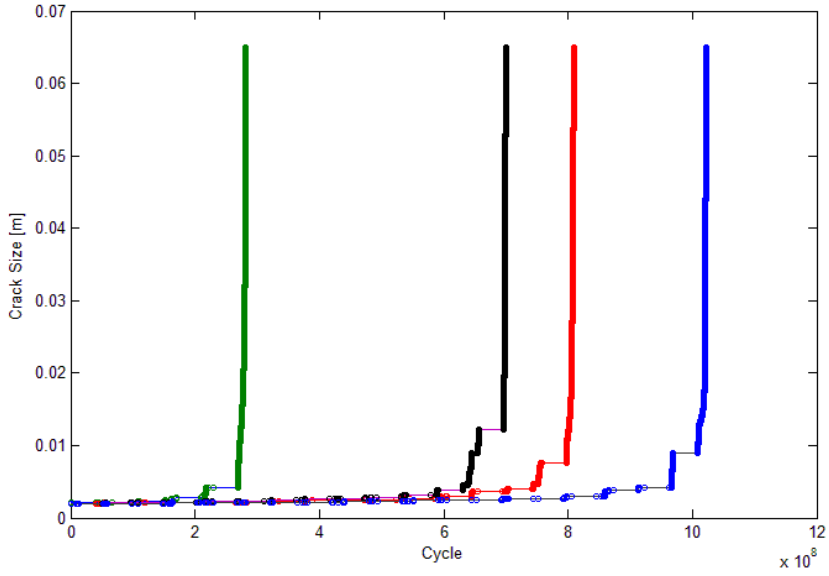

Figure 36 Examples of simulated crack growth paths

Eventually, once determined an initial crack size and a limiting crack depth value at failure, through the Monte Carlo technique is possible to estimate the TTF pdf. Each simulation run is characterized by a random ΔK_{th} and a random

load history. Considering an initial crack size of 2 mm and a limiting crack size of 60 mm, the TTF pdf is shown in Figure 37.

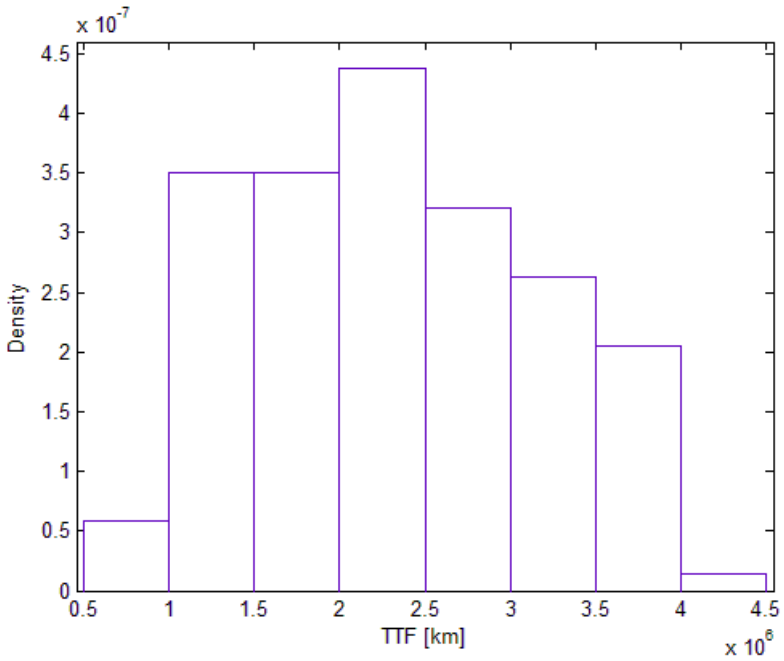

Figure 37 TTF probability distribution

The TTF pdf for the purposes of this work is considered as a lognormal distribution as can be observed in Figure 38. It can be noticed how a lognormal distribution fits well the TTF data for almost the whole TTF variability range, only the right hand tail significantly diverge for the TTF. This is demonstrated also by Beretta et al. [**78**] and Schijve [**85**].

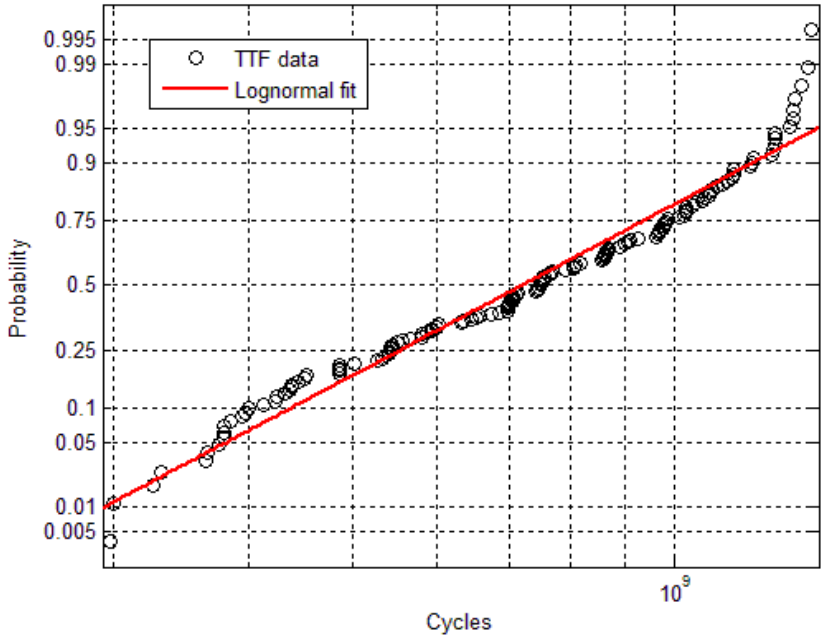

Figure 38 Lognormal fit plot for TTF pdf

4.3. Design of the preventive maintenance approach

The preventive maintenance approach is designed according to the damage tolerant approach well described by [**69**] [**73**]. Figure 39 well describe the steps that have to be followed to design a design an axle preventive maintenance plan. The steps indicated are:

1. establishment of the initial crack shape and size for further analysis
   Within a damage tolerance concept the initial crack size, a_0, is not identical to the size of a real flaw, e.g., from the manufacturing process but is a fictitious size, which usually refers to the detection limit of the NDI technique. The basic idea is that the largest crack that could escape detection is presupposed as existent.

2. simulation of sub-critical crack extension,
   This kind of crack growth is designated as sub-critical since it will not lead to immediate failure until a critical length of the crack is reached. For railway applications the common mechanism is fatigue.

3. determination of critical crack size for component failure,
   The sub-critical crack extension is terminated by the failure of the component. This may occur as brittle fracture or as unstable ductile fracture. Critical states may, however, also be defined by other events such as stable ductile crack initiation or the break-through of a surface crack through the wall or setting a maximum allowable crack size threshold.

4. determination of residual lifetime of the component,
   The residual lifetime is that time or number of loading cycles which a crack needs for extending from the initial crack size, a_0, (step 1) up to the allowable crack size, a_{max}, established in step (3).

5. specification of requirements for non-destructive testing.
   The constitution of an inspection plan is the aim of a damage tolerance analysis. From the requirement that a potential defect must be detected before it reaches its critical size it follows immediately that the time interval between two inspections has to be smaller than the residual lifetime. Sometimes inspection intervals are chosen to be smaller than half this time span. The idea is to have a second chance for detecting the crack prior to failure if it is missed in the first inspection. It is, however, also obvious that frequently even two or more inspections cannot guarantee the crack being detected since this would require a 100% probability of detection.

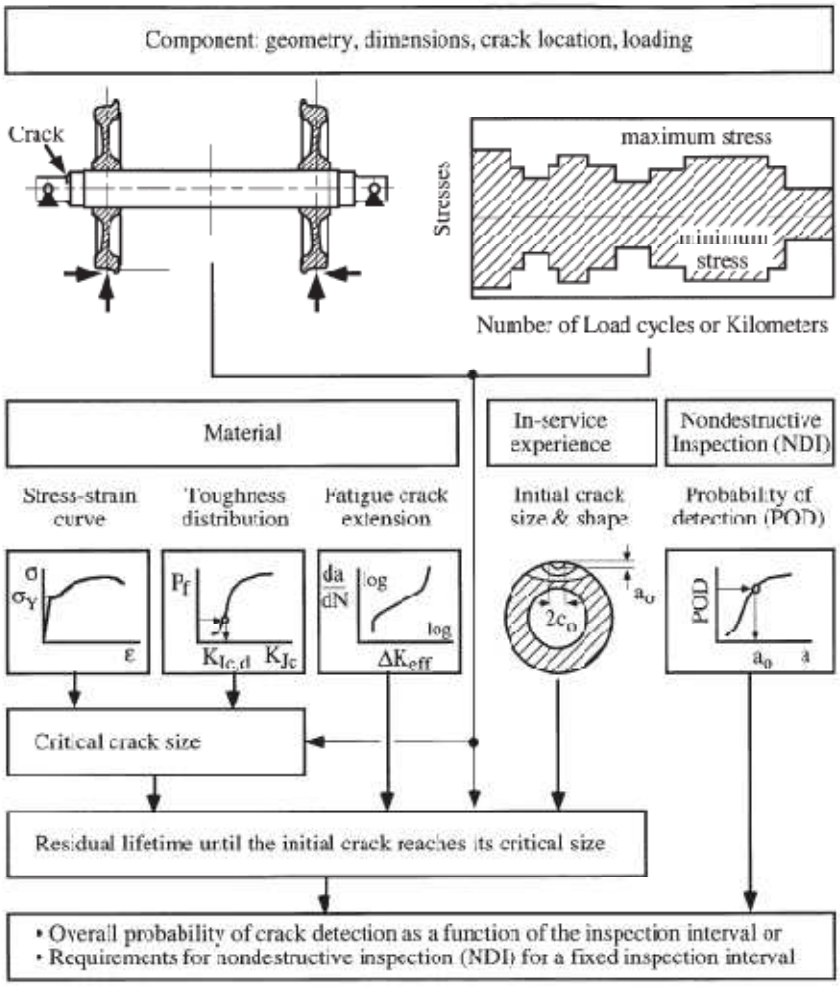

Figure 39 The damage tolerant approach to design a preventive maintenance approach[69**]**

The procedure described by [**69**] aims to define the NDT specifications following the 'last chance' approach introduce in [**72**]. In this case, the PoD is not a variable to be optimized but is given. Therefore the maximum inspection interval was defined instead of the requirements for non destructive testing. The steps from 1 to 4 has already been done in the previous paragraph.

4.3.1. The PoD curve

The PoD can be derived from the calibration function of the particular NDE equipment used that relates the crack dimension (length,depth or area) to the output. In this case, the NDE method considered is the ultrasonic inspection.

Since output from an NDE measurement process is a continuous response, the calibration curve is modeled as a linear function in which the measurement (dB of the signal) is given by a linear combination of two parameters and the crack area ($\hat{a}$ $[mm^2]$) plus a normal zero mean error with constant variance (Eq.4.7).

$$Y(\hat{a}) = \beta_0 + \beta_1 \log_{10} \hat{a} + \epsilon\,(0, \sigma_r) \qquad \textbf{4.7}$$

The parameters $\beta_0, \beta_1, \sigma_r$ are estimated through the LSE or through the MLE methods. Is assumed that 1000 dB and -1000dB are respectively the saturation and observable limits.

The data provided from which the parameters are estimated have been obtained from real inspections of railway axles. The graph in Figure 40 the data and the linear interpolating function are plotted, while the dashed blue lines are the 95% confidence interval bounds.

The parameters value are reported in Table 1.

Parameter	Value[5]
β_0	Xxo
β_1	Yyo
σ_r	Zzo

Table 1: Calibration Curve Parameters

[5] Values are omitted for confidentiality reasons

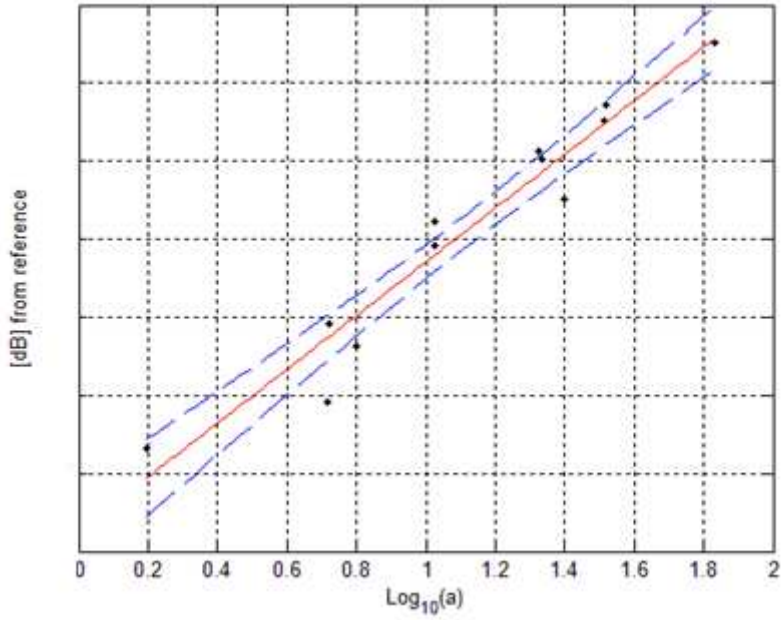

Figure 40 MLE results

In order to use the calibration curve in the following analysis, the crack size has to be expressed in term on depth instead of surface area. The crack geometry is assumed to be semicircular [**72**]. Therefore, the resulting calibration curve function becomes:

$$Y = \beta_0 + \beta_1 \log_{10}\left(\frac{\pi a^2}{2}\right) + \epsilon\,(0, \sigma_r) \qquad \textbf{4.8}$$

In order to derive the PoD function, a threshold is fixed that represents the measure's bound that if it's overcame, the presence of a crack is diagnosed. This limit is set at 50.6 dB that corresponds to a crack depth of 5.492 mm.

The reference limit and the final calibration curve with the constant $3\sigma_r$ confidence limits is shown in Figure 1.

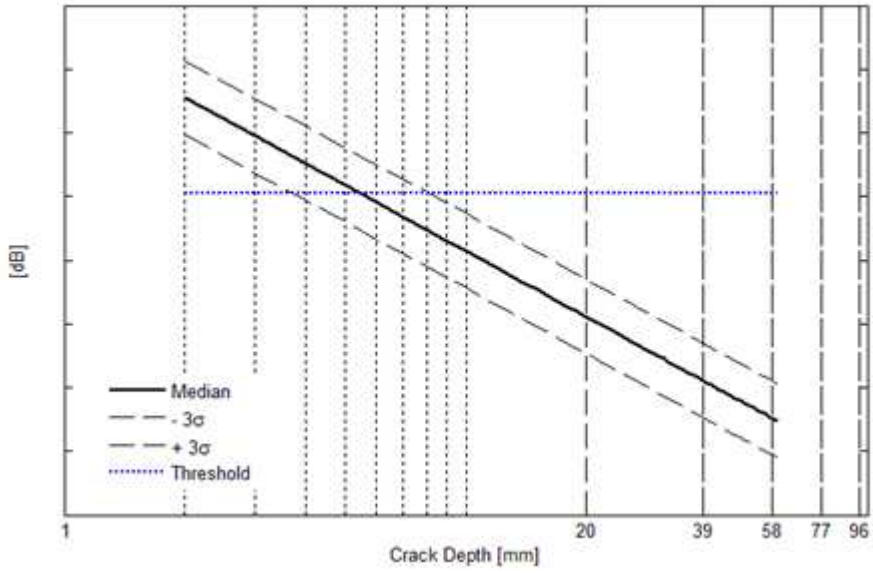

Figure 1: Final Calibration Curve

At this point the PoD curve can be derived as it represents the probability that a crack of size a can be detected, given that the threshold is set at a_{th}. According to this statement and making the hypothesis of a normal distributed error, the PoD of a crack depth a is:

$$PoD(a) = P[Y(a) > Y(a_{th})] =$$

$$= 1 - \Phi\left(\frac{Y(a_{th}) - \left(\beta_0 + \beta_1 \log_{10}\left(\frac{\pi a^2}{2}\right)\right)}{\sigma_r}\right) \qquad \textbf{4.9}$$

$$= 1 - \Phi\left(\frac{50.6 - \left(\beta_0 + \beta_1 \log_{10}\left(\frac{\pi a^2}{2}\right)\right)}{\sigma_r}\right)$$

where Φ is the standard normal cdf. In Figure 2 is shown the resulting PoD curve.

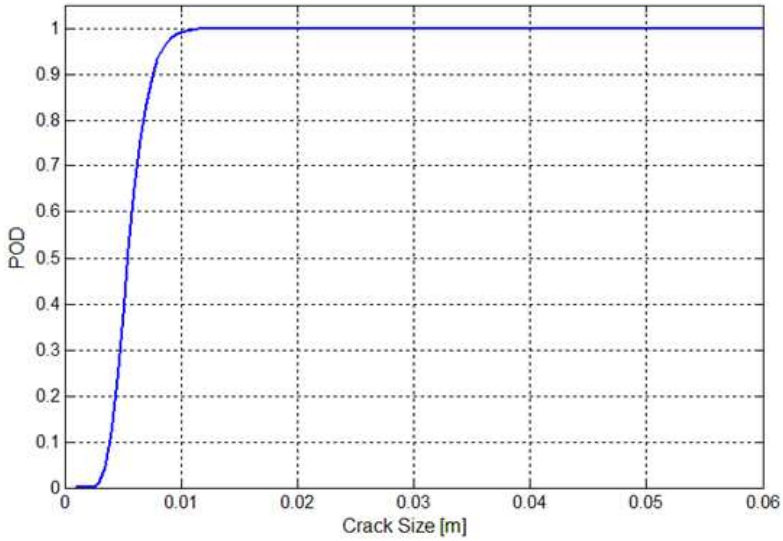

Figure 2: PoD

The PoD as discussed above in paragraph 4.3 is used to determine the maximum inspection interval in order to detect with a probability *R* the maximum allowed crack size. In the following paragraph, according to the problem defined in paragraph 4.3, the maximum inspection interval is determined.

4.3.2. Identification of the maximum inspection interval

The maximum safe inspection interval is determined through examining the effect of the interval of inspection on the overall probability of detection in the case of a fast growing crack. The inspection interval is therefore the maximum interval of inspection that allows the detection of the maximum allowable crack size with a defined reliability. The worst case is when the time (or distance) before the failure occurs (TTF) is minimum. This happen when, once the maximum defect present in the system is set, the crack growth rate is the highest. The inspection interval is therefore dependent on the largest defect present in the system, that is the defect that will eventually cause failure.

The maximum defect size is set at 2 mm as suggested by the literature reviewed[**72**][**69**] and as set in the crack growth simulations. At this point the fastest growth crack has to be chosen as the reference upon which the maximum allowable inspection interval has to defined.

Starting from the TTF distribution shown in Figure 37, the fastest growth crack has been chosen. It is the crack growth path with the minimum TTF in 300 simulations and that falls in the first bin of the TTF distribution. In Figure 41 is shown the path selected and its relative position with respect to the TTF distribution (blue line). As can be seen it falls in the left tail of TTF pdf.

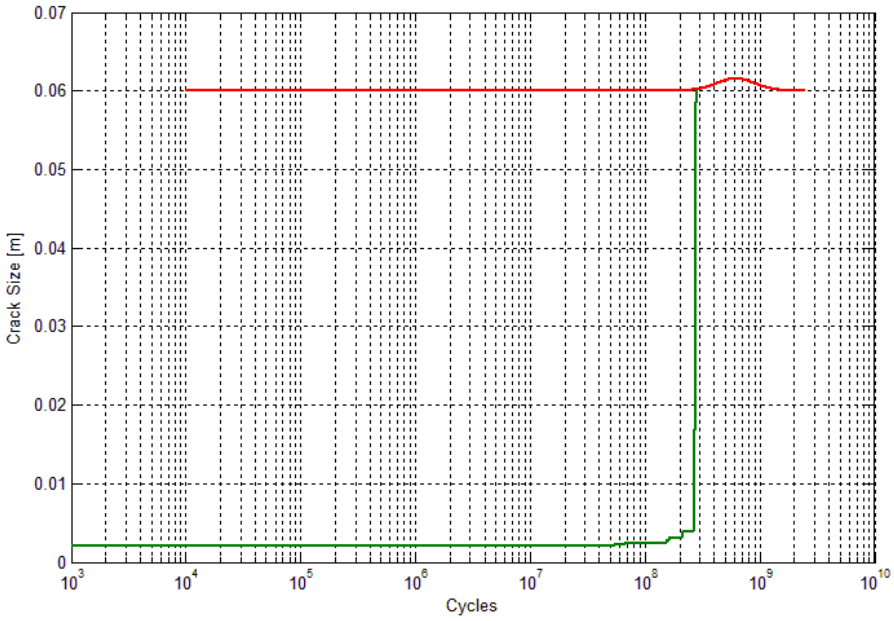

Figure 41 Fastest growth crack

Once the worst case is chosen and the reference PoD has been defined, the maximum inspection interval can be found.

Given an inspection interval, 'I', the cumulative PoD PC_{DET} of a defect, potentially observable in a given number of inspections, i, is calculated from the PoD curve of the adopted NDT technique. Figure 42 shows how the cumulative probability of detection is calculated, that in formulae results.

$$PC_{DET} = 1 - \prod_{i=1}^{n} PonD_i$$
$$PonD_i = 1 - Pod_i \qquad \textbf{4.10}$$

Here, PC_{DET} is the theoretical cumulative PoD and $PonD$ ('probability of non-detection') represents the probability of failing to detect in a given inspection.

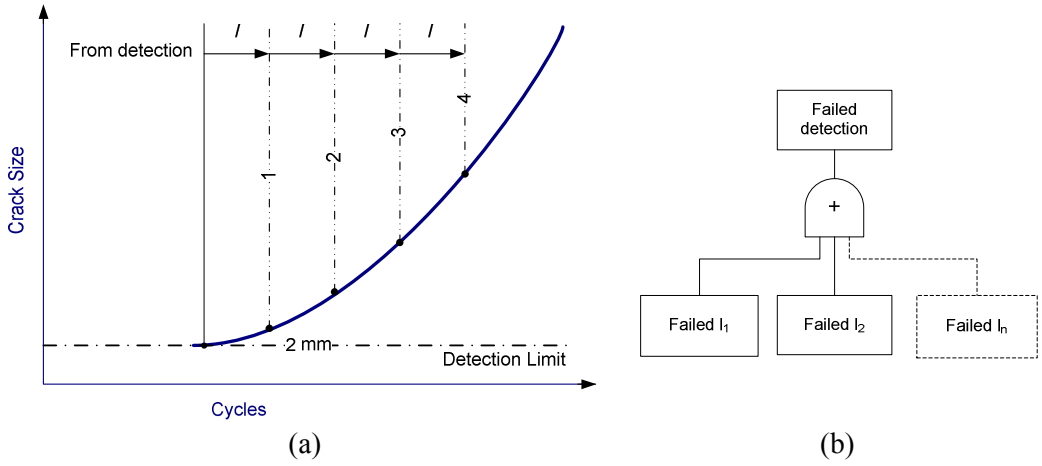

(a) (b)

Figure 42 Calculation of the cumulative probability of detection (a) and the fault tree of the inspection (b) (adopted from [72])

The PoD_i depends on the actual crack size a that corresponds to the cycle i according to the Eq.4.9. The more the inspections the more the PC_{DET} will be. Since a 100% PC_{DET} is impossible to reach theoretically, a PC_{DET} threshold was set at 0.99.

In order to determine the inspection interval the final PC_{DET} is evaluated at different intervals of inspection. Particularly, the final PC_{DET} was evaluated starting from 1 to 60 inspections that results in the same number of intervals.

The final PC_{DET} is the P_{DET} that results from the last inspection. Figure 43 shows the results of the assessment, it shows the PC_{DET} as a function of the inspection interval. The figure confirm what stated previously: as the number of inspection increases and the inspection interval decreases PC_{DET} increases. The optimal inspection interval is the largest that guarantee a $PC_{DET} = 0.99$.

From Table 7 we can see that the inspection interval at 0.99 falls between 34,988 km and 32,297 km. By linear interpolation we can find that the interval at 99% PC_{DET} is **33,663** km.

N° inspections	**Inspection Interval** [km]	PC_{DET}
1	419,856	0.000000

3	209,928	0.000014
5	139,952	0.003680
7	104,964	0.003694
9	83,971	0.007346
11	69,976	0.007360
13	59,979	0.010992
15	52,482	0.011006
17	46,651	0.026369
19	41,986	0.026967
21	38,169	0.397817
23	34,988	0.834808
25	32,297	0.999981

Table 7 PC_{DET} with different inspection interval

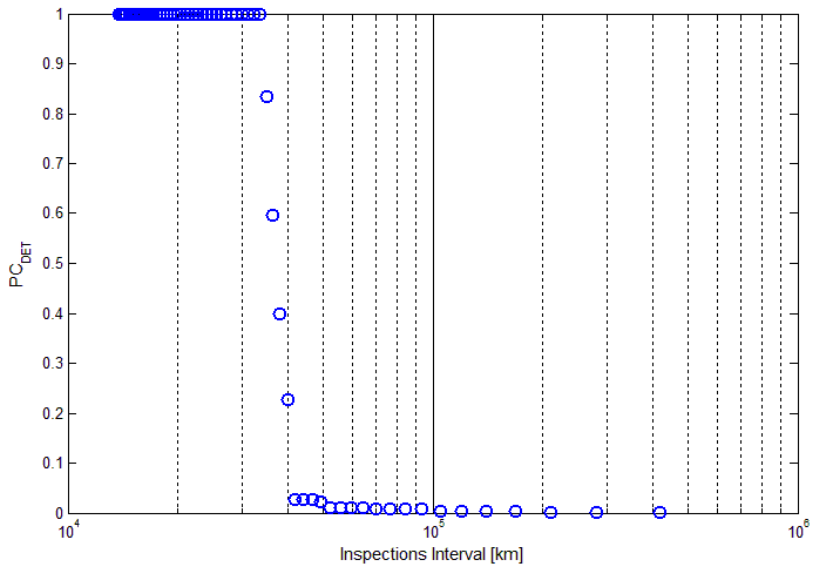

Figure 43 PC_{DET} as function of the inspection intervals

The literature reviewed [**69**][**72**] [**78**] suggests to determine the inspection intervals referring to the average crack growth path, i.e whose TTF is equal to the mean TTF. In this case, once selected the right crack propagation lifetime, the maximum inspection interval is computed as well. The result is that the optimal inspection interval should be performed each 153,197.8 km. It is worth

noting that in case of the fast crack growth crack, with an inspection interval equal to **153,197.8** km the PC_{DET} is equal to 0,2986 %.

4.4. Prognostic Modeling of the Crack Size Growth

In this section two methods able to predict the RUL of cracked railway axles are introduced and compared in term of their prediction performances.

The first model uses a statistical approach introduced in the paragraph 0 based on the Bayesian probabilistic theory and the second one uses the physical model introduced in the paragraph 4.2, the same used to generate the crack growth paths. Since the model accurately describe the real crack growth in railway axles[**78**], it can be used both to substitute experimental tests and to generate the database needed to support a statistical approach to evaluate the axles' TTF and RUL.

The aim of the section is to introduce and give evidence of the capability of a prognostic approach based on these algorithms to reduce the uncertainties associated to the prediction of the TTF of a continuously monitored cracked axle meanwhile it operates. This approach can be helpful to increase the inspection interval and, as a best result, inspects the axle only when the wheels have to be maintained without reducing the system's safety.

4.4.1. Setting the threshold

In the paragraph 1.2 as the meaning of prognostic is introduced, the concept of RUL is defined as the time units that remain till the system eventually fail.

In order to design a prognostic algorithm capable of updating the axle's TTF the concept of failure has to be clearly determined. In this case it is trivially derived since the axle is considered faulty when the maximum allowable crack size is reached. Obviously, the threshold has to fixed considering the errors that affects the whole monitoring and prognostic system. Figure 45 shows a scheme of the different types of errors that has to be considered in setting the threshold. A safety margin has to be introduced against the errors that affect the estimation. The first error was introduced in the paragraph 4.3.1.

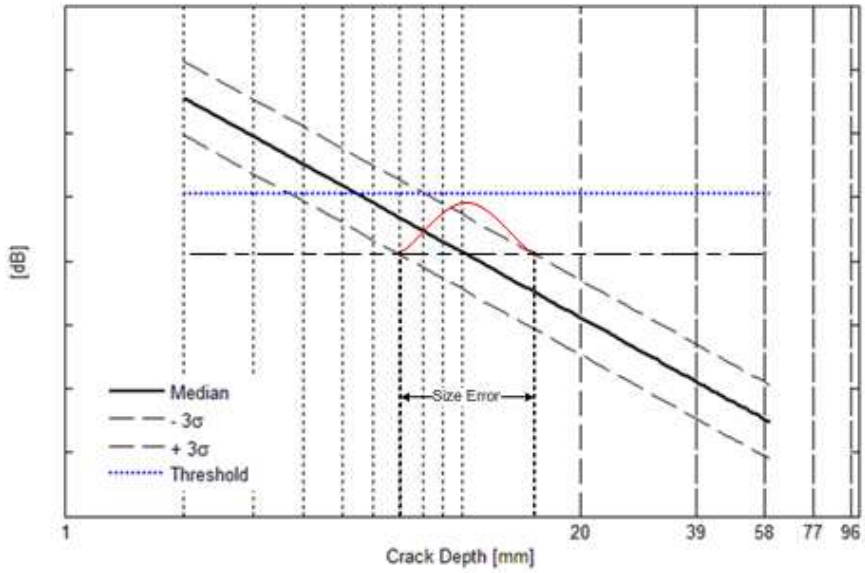

Figure 44 Illustration of the meaning of the size error

It is the error associated with the calibration curve of the ultrasonic inspection. This error introduces an uncertainty in the determination of the crack size given that the ultrasonic probe measures x dB.

Figure 44 illustrates what is meant for the size error. Given the calibration curve in Eq.4.8, the size error ε_s is defined as:

$$\varepsilon_s = \frac{\epsilon}{\beta_1}$$

$$\varepsilon_s = N\left(0, \frac{\sigma_r}{\beta_1}\right) \qquad 4.11$$

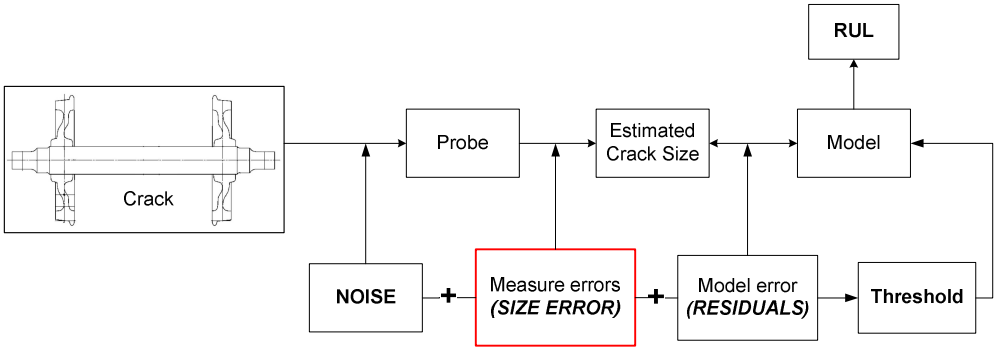

Figure 45 The errors affecting the monitoring and prognostic system

The other errors that are present are those associated with the model describing the crack growth, that are the residuals between the actual crack size and the that one predicted by the model and eventually the noise that affects the measurements process.
In this case the size error is only considered since no data are available about the other error sources. The error considered can be considered as the sum of those making the hypothesis that the used diagnostic system's performances are better.

Given a crack depth a_{max} as the maximum crack size allowed, the threshold that will be used as a reference for estimating the axle TTF is that one that guarantees at 99% of confidence that a_{max} won't be missed.

Starting from the calibration function in Eq.4.8 we have to find $\tilde{a}_{th}$ (different from that in Eq.4.10) that corresponds to $P(a_{max} \leq \tilde{a}_{th}) = 0.99$.
Starting from Eq.4.9, given the measure Y, the related crack size is:

$$a = \sqrt{\frac{2}{\pi} 10^{\frac{Y-\beta_0}{\beta_1}} 10^{\frac{\varepsilon}{\beta_1}}} \qquad \textbf{4.12}$$

Remembering that $\boldsymbol{\varepsilon_s = \frac{\epsilon}{\beta_1}}$, we have:

$$a = \sqrt{\frac{2}{\pi} 10^{\frac{Y-\beta_0}{\beta_1}} 10^{\varepsilon_s}} \qquad \textbf{4.13}$$

Given that $\hat{Y}$ corresponds to the measurement of the crack size a_{max}, we have:

$$a_{max} = \sqrt{\frac{2}{\pi} 10^{\frac{\hat{Y}-\beta_0}{\beta_1}}} \tag{4.14}$$

The crack size that corresponds to the measurement $\hat{Y}$ is:

$$a = \sqrt{\frac{2}{\pi} 10^{\frac{\hat{Y}-\beta_0}{\beta_1}} 10^{\varepsilon_s}}$$

$$a = a_{max}\, 10^{\frac{\varepsilon_s}{2}} \tag{4.15}$$

From Eq.4.15 we have that given a real crack depth of a_{max} the crack size associated a (estimated from the measurement) is a random variable distributed as a lognormal with an associated mean of $\log_{10}(a_{max})$ and a standard deviation of $\frac{\sigma_r}{2\beta_1}$.

$$\log_{10} a = \log_{10}\left(a_{max} 10^{\frac{\varepsilon_s}{2}}\right)$$

$$\log_{10} a = \log_{10}(a_{max}) + \log_{10}\frac{\varepsilon_s}{2} \tag{4.16}$$

$$\log_{10}\frac{\varepsilon_s}{2} = N\left(0, \frac{\sigma_r}{2\beta_1}\right)$$

Now we can define the threshold $\tilde{a}_{th}$:

$$P(\tilde{a}_{th} - a_{max} \leq 0) \geq 0.99$$

$$\Phi\left(\frac{\log_{10}\tilde{a}_{th} - \log_{10} a_{max}}{\frac{\sigma_r}{2\beta_1}}\right) \geq 1 - 0.99 \tag{4.17}$$

The result is $\tilde{a}_{th} = \mathbf{0.044}$.
If we let vary both σ_r and a_{max} and calculate the corresponding $\tilde{a}_{th}$ we obtain a surface plotted in Figure 46. As we can see the relation is not linear and as the standard error increases, given a maximum crack size, the corresponding crack depth threshold decreases.

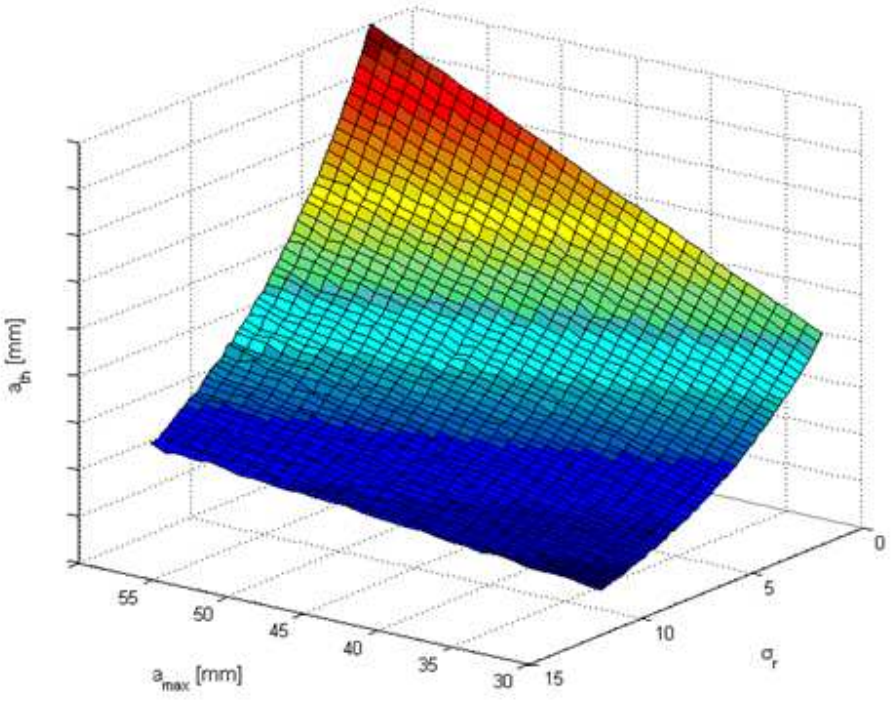

Figure 46 Crack size threshold as a function of σ_r and a_{max}

4.4.2. Bayesian updating algorithm

This section develops methods that combine two sources of information, the reliability characteristics of a axle's population and real-time sensor information from a functioning axle, to periodically update the distribution of the axles's residual life.

We first model the degradation signal for a population of axles with an appropriate model assuming error terms from an iid random error process. A Bayesian updating method is used to estimate the unknown stochastic parameters of the model for an individual component. Once we have determined the posterior distribution for these unknown parameters, we derive the residual-life distribution for the individual component.

In this case there is not simple functional form that fit well the simulated crack growth pattern. Nevertheless, an approximation of the paths can be performed by splitting the signal in two parts, that can be modeled as two exponential functions as shown in Figure 47.

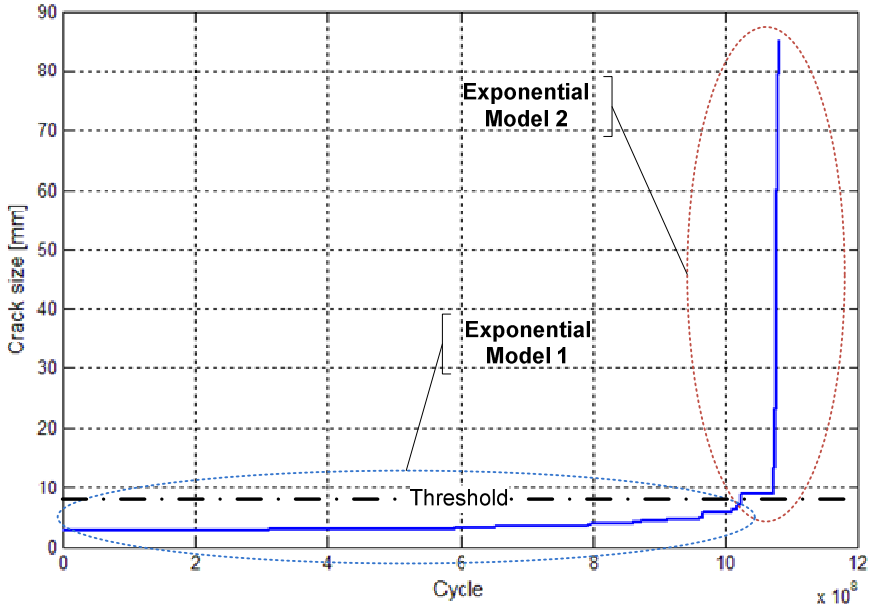

Figure 47 The two exponential models

The shift from the first model to the second is based on a crack depth threshold that is plotted in Figure 47 as a black dash dotted line. The TTF of the axle monitored is therefore defined as:

$$TTF = T_1 + T_2 \qquad \textbf{4.18}$$

Where $T_1$is a random variable that express the predicted time to reach the threshold $\tilde{S}_{th}$ and $T_2$is a random variable as well that denote the time that takes the crack to grow from the threshold to $\tilde{a}_{th}$.

Let $S(t)$ denote the degradation signal as a continuous stochastic process, continuous with respect to cycle n. We observe the degradation signal at some discrete points in cycles, n_1, n_2, . . ., where $n_i \geq 0$. Therefore, we can model the degradation signal at cycles $n_i = n_1, n_2, \ldots$, as follows:

$$\begin{cases} S(n_i) = \varphi_1 + \theta_1 \exp[\beta_1 n_i + \epsilon_1(n_i)] & S \leq \tilde{S}_{th} \\ S(n_i) = \varphi_2 + \theta_2 \exp[\beta_2 n_i + \epsilon_2(n_i)] & \tilde{S}_{th} \leq S \leq \tilde{a}_{th} \end{cases} \quad \textbf{4.19}$$

If we redefine $L_1(n_i) = S(n_i) - \varphi_1$ for $S \leq \tilde{S}_{th}$ and $L_2(n_i) = S(n_i) - \varphi_2$ for $\tilde{S}_{th} \leq S \leq \tilde{a}_{th}$ we obtain:

$$\begin{cases} L_1(n_i) = \theta_1 \exp[\beta_1 n_i + \epsilon_1(n_i)] & S \leq \tilde{S}_{th} \\ L_2(n_i) = \theta_2 \exp[\beta_2 n_i + \epsilon_2(n_i)] & \tilde{S}_{th} \leq S \leq \tilde{a}_{th} \end{cases} \quad \textbf{4.20}$$

The choice of threshold $\tilde{S}_{th}$ has to be based on an optimization rule. In this case, the threshold is that one that bound the maximum residual of the first fitted model to 0.0012. Obviously the rule can be changed, for example the threshold could be that one that minimize the overall fitting error. The value 0.0012 at which the first residual error is bounded is chosen upon that willingness to prefer a better fit in the first part of the signal in order to achieve better predictions in the first stage of the degradation process. The reason is that good predictions (more precise) in the first part of the degradation path can restrict the uncertainties on the final RUL estimation form the beginning. As matter of facts, the main part of the uncertainty on the TTF comes from the uncertainty associated with the variable T_1. In other words, the variance of the cycles taken by the crack to grow from the initial size to $\tilde{S}_{th}$ is much greater that the number of cycles taken by the crack to grow from $\tilde{S}_{th}$ to $\tilde{a}_{th}$.

After several simulations, the threshold that bound the maximum residual error of the first part of S is a random variable as shown in Figure 48.

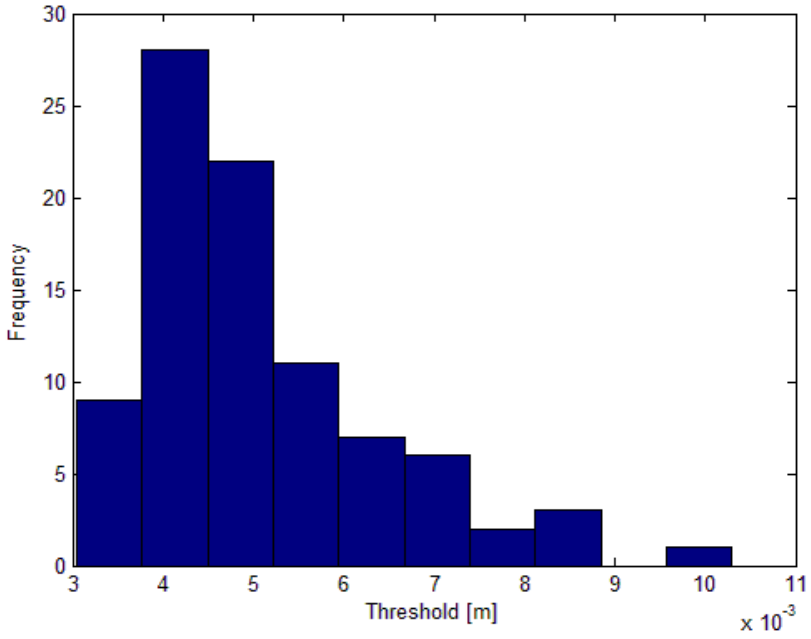

Figure 48 Threshold $\tilde{S}_{th}$ distribution

Eventually the final threshold chosen is the mean value of distribution, that is $\tilde{S}_{th} = 5,1\ mm$.

Once determined the threshold, through an appropriate number of crack growth simulations, we can build our a priori information on the crack growth behavior. Our a priori information, a part form the a priori TTF distribution shown in Figure 37, is composed of the random parameters $\theta_1, \theta_2, \beta_1$ and β_2 probability distributions. Their values are obtained through the LSE technique though fitting the crack growth functions with the models in Eq.4.19. The final distribution PDFs are plotted in Figure 49.

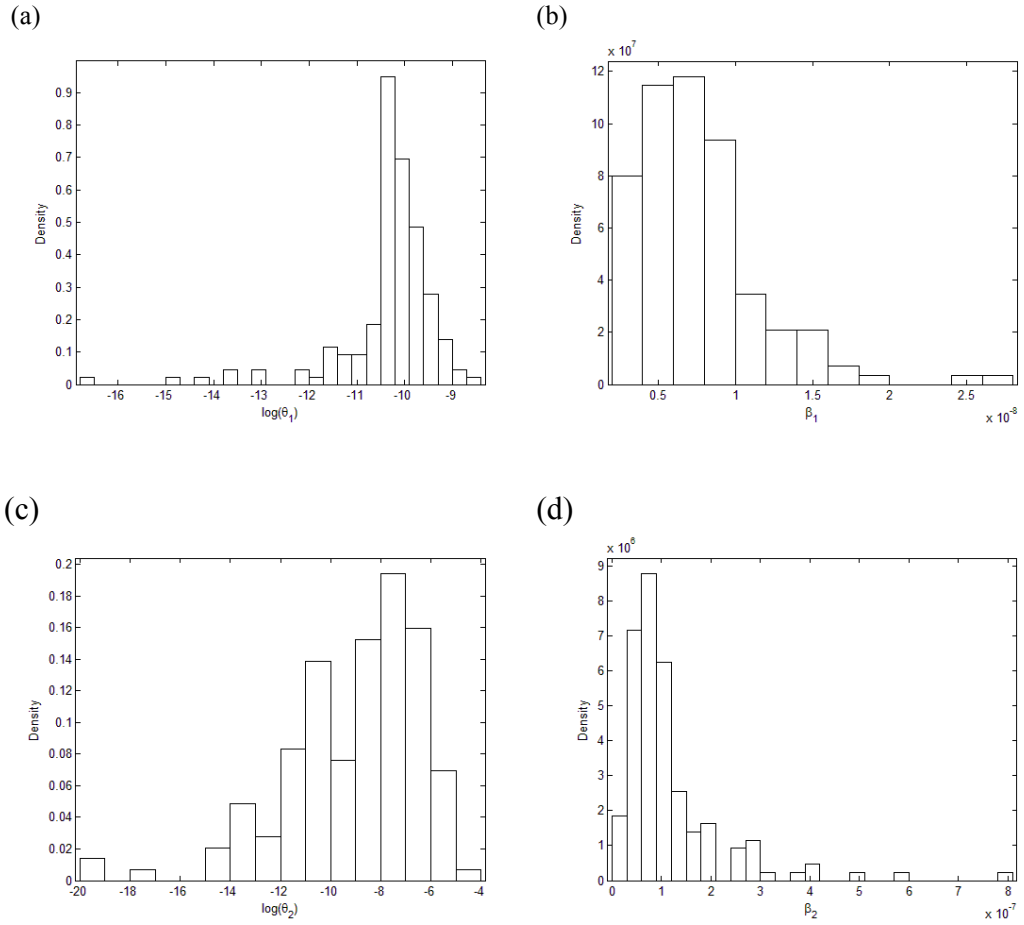

Figure 49 (a) $\log \theta_1$ PDF, (c) $\log \theta_2$ PDF, (b) β_1 PDF, (d) β_2 PDF

As can be noted from the figure above, θ_1,θ_2, β_1 and β_2 can be approximated by lognormal distributions[6] with parameters:

$$\theta_1 = LN(\mu_{\theta 1}, \sigma_{\theta 1}) \qquad \theta_2 = LN(\mu_{\theta 2}, \sigma_{\theta 2})$$

[6] In the Appendix can be found the probability charts of those distributions.

$$\beta_1 = LN(\mu_{\beta 1}, \sigma_{\beta 1}) \qquad \beta_1 = LN(\mu_{\beta 2}, \sigma_{\beta 2})$$

In the Appendix (Ch.7) are reported the probability charts of those distributions.

For these exponential models, it will be convenient to work with the logged signal S. We can then define the logged signal at cycle n_i as follows:

$$\begin{cases} LS_1(n_i) = \log\theta_1 + \beta_1 n_i + \epsilon_1(n_i) & c \le \tilde{S}_{th} \\ LS_2(n_i) = \log\theta_2 + \beta_2 n_i + \epsilon_2(n_i) & \tilde{S}_{th} \le S \le \tilde{a}_{th} \end{cases} \quad \textbf{4.21}$$

We will use the observations $LS_{i,1}$, $LS_{i,2}$[7], ..., obtained at cycles n_1, n_2 , ..., as our data. Next, suppose we have observed $LS_{i,1}$, ..., $LS_{i,k}$ at cycles n_1, ..., n_k. Since the error terms, $\in_i (n_t)$, $i = 1, 2$ and $t = 1, \ldots k$, are assumed to be iid normal random variables, if we know $\theta_{1,2}$ and $\beta_{1,2}$, then the likelihood function of $LS_{i,1}$, ..., $LS_{i,k}$, given $\theta_{1,2}$ and $\beta_{1,2}$, is:

$$f\left(LS_{1,1}, \ldots, LS_{1,k} \middle| \theta_1, \beta_1\right) = \left(\frac{1}{\sqrt{2\pi{\sigma_{r1}}^2}}\right) \exp\left(-\sum_{j=1}^{k}\left(\frac{LS_{1,j} - \log\theta_1 - \beta_1 n_j}{2{\sigma_{r1}}^2}\right)\right) \quad \textbf{4.22}$$

$$S \le \tilde{S}_{th}$$

$$f\left(LS_{2,1}, \ldots, LS_{2,k} \middle| \theta_2, \beta_2\right) = \left(\frac{1}{\sqrt{2\pi{\sigma_{r2}}^2}}\right) \exp\left(-\sum_{j=1}^{k}\left(\frac{LS_{2,j} - \log\theta_2 - \beta_2 n_j}{2{\sigma_{r2}}^2}\right)\right) \quad \textbf{4.23}$$

$$\tilde{S}_{th} \le S \le \tilde{a}_{th}$$

Assumed that θ_1,θ_2, β_1 and β_2 are lognormal random variables with parameters defined above, their a posteriori joint distributions, according to the Bayes theorem are:

[7] i is used to denote the belongings of LS to the first ($i = 1$) or second model ($i = 2$) in Eq 4.19.

$$f\left(\theta_1, \beta_1 \left| LS_{1,1}, \dots, LS_{1,k}\right.\right) = \frac{f\left(LS_{1,1}, \dots, LS_{1,k} \left| \theta_1, \beta_1\right.\right)\Pi(\theta_1)\Pi(\beta_1)}{\int_{-\infty}^{+\infty} f\left(LS_{1,1}, \dots, LS_{1,k} \left| \theta_1, \beta_1\right.\right)\Pi(\theta_1)\Pi(\beta_1)\, d\theta_1 d\beta_1}$$

$$S \leq \tilde{S}_{th} \qquad \textbf{4.24}$$

$$f\left(\theta_2, \beta_2 \left| LS_{2,1}, \dots, LS_{2,k}\right.\right) = \frac{f\left(LS_{2,1}, \dots, LS_{2,k} \left| \theta_2, \beta_2\right.\right)\Pi(\theta_2)\Pi(\beta_2)}{\int_{-\infty}^{+\infty} f\left(LS_{2,1}, \dots, LS_{2,k} \left| \theta_2, \beta_2\right.\right)\Pi(\theta_2)\Pi(\beta_2)\, d\theta_2 d\beta_2}$$

$$\tilde{S}_{th} \leq S \leq \tilde{a}_{th}$$

Where $f\left(LS_{1,1}, \dots, LS_{1,k} \left| \theta_1, \beta_1\right.\right)$ and $f\left(LS_{2,1}, \dots, LS_{2,k} \left| \theta_2, \beta_2\right.\right)$ are defined in Eq. 4.22 and Eq.4.23 respectively and:

$$\Pi(\theta_1) = \left(\frac{1}{\sqrt{2\pi {\theta_1}^2 {\sigma_{\theta 1}}^2}}\right) \exp\left(\frac{1}{2}\left(\frac{\log\theta_1 - \mu_{\theta 1}}{\sigma_{\theta 1}}\right)^2\right)$$

$$\Pi(\beta_1) = \left(\frac{1}{\sqrt{2\pi {\beta_1}^2 {\sigma_{\beta 1}}^2}}\right) \exp\left(\frac{1}{2}\left(\frac{\log\beta_1 - \mu_{\beta 1}}{\sigma_{\beta 1}}\right)^2\right)$$

$$\Pi(\theta_2) = \left(\frac{1}{\sqrt{2\pi {\theta_2}^2 {\sigma_{\theta 2}}^2}}\right) \exp\left(\frac{1}{2}\left(\frac{\log\theta_2 - \mu_{\theta 2}}{\sigma_{\theta 2}}\right)^2\right) \qquad \textbf{4.25}$$

$$\Pi(\beta_2) = \left(\frac{1}{\sqrt{2\pi {\beta_2}^2 {\sigma_{\beta 2}}^2}}\right) \exp\left(\frac{1}{2}\left(\frac{\log\beta_2 - \mu_{\beta 2}}{\sigma_{\beta 2}}\right)^2\right)$$

The a posteriori mean of the parameters can be obtained from:

$$\hat{\mu}_{\theta 1} = \int_{-\infty}^{+\infty} \theta_1 \int_{-\infty}^{+\infty} f(\theta_1, \beta_1 \,|LS_{1,1}, \dots, LS_{1,k}) d\beta_1 d\theta_1$$

$$\hat{\mu}_{\beta 1} = \int_{-\infty}^{+\infty} \beta_1 \int_{-\infty}^{+\infty} f(\theta_1, \beta_1 \,|LS_{1,1}, \dots, LS_{1,k}) d\beta_1 d\theta_1$$

$$\hat{\mu}_{\theta 2} = \int_{-\infty}^{+\infty} \theta_2 \int_{-\infty}^{+\infty} f(\theta_2, \beta_2 \,|LS_{2,1}, \dots, LS_{2,k}) d\beta_2 d\theta_2 \qquad \textbf{4.26}$$

$$\hat{\mu}_{\beta 2} = \int_{-\infty}^{+\infty} \beta_2 \int_{-\infty}^{+\infty} f(\theta_2, \beta_2 \,|LS_{2,1}, \dots, LS_{2,k}) d\beta_2 d\theta_2$$

And their a posteriori variances from:

$$\hat{\sigma}_{\theta 1} = \int_{-\infty}^{+\infty} (\theta_1 - \hat{\mu}_{\theta 1})^2 \int_{-\infty}^{+\infty} f(\theta_1, \beta_1 \,|LS_{1,1}, \dots, LS_{1,k}) d\beta_1 d\theta_1$$

$$\hat{\sigma}_{\beta 1} = \int_{-\infty}^{+\infty} (\beta_1 - \hat{\mu}_{\beta 1})^2 \int_{-\infty}^{+\infty} f(\theta_1, \beta_1 \,|LS_{1,1}, \dots, LS_{1,k}) d\beta_1 d\theta_1$$

$$\hat{\sigma}_{\theta 2} = \int_{-\infty}^{+\infty} (\theta_2 - \hat{\mu}_{\theta 2})^2 \int_{-\infty}^{+\infty} f(\theta_2, \beta_2 \,|LS_{2,1}, \dots, LS_{2,k}) d\beta_2 d\theta_2 \qquad \textbf{4.27}$$

$$\hat{\sigma}_{\beta 2} = \int_{-\infty}^{+\infty} (\beta_2 - \hat{\mu}_{\beta 2})^2 \int_{-\infty}^{+\infty} f(\theta_2, \beta_2 \,|LS_{2,1}, \dots, LS_{2,k}) d\beta_2 d\theta_2$$

Since the solution to the problem stated has not been found in the statistical literature and recognizing the computation problem associated with solving the equations numerically, we have to make other assumptions on the parameters' pdf functional forms. In order to reduce problem complexity the assumption of β_1 and β_2 as normal distributed parameters is reasonable. This assumption let us to exploit the problem solution described in the paragraph 0 and proposed by Lindley [**62**] and Gebraeel[**59**]. Therefore , $\log\theta_1$,$\log\theta_2$, β_1 and β_2 are assumed to be normal random variables with parameters:

$$\log\theta_1 = \omega_1 = N(\mu_{\omega 1}, \sigma_{\omega 1}) \qquad \log\theta_2 = \omega_2 = N(\mu_{\omega 2}, \sigma_{\omega 2})$$

$$\beta_1 = N(\mu_{\beta 1}, \sigma_{\beta 1}) \qquad\qquad \beta_1 = N(\mu_{\beta 2}, \sigma_{\beta 2})$$

Before proceeding to the formal definition of the problem statement, an assessment of the errors computed after relaxing the hypothesis of lognormal distributed β_1 and β_2 can be done through a comparison of the a priori TTF calculated by the model with β_1 and β_2 as normal random variables with the true TTF computed through the crack growth simulations.

The a priori TTF probability distribution, given the model described by the Eq. 4.20, can be computed as the probability that the degradation signal (crack size) LS is smaller than the crack maximum size allowed for each cycle $n_{\mathrm{i}} > 0$, given the a priori model parameters pdfs. The statement, remembering the Eq.4.18, can be formally written as,

$$TTF(n_{\mathrm{k}} = 0) = \widehat{T_1} + \widehat{T_2} \qquad \textbf{4.28}$$

Where $\widehat{T_1}$and $\widehat{T_2}$ are the a priori pdf distributions of T_1 and T_2. They can be expressed as:

$$\widehat{T_1}(n_{\mathrm{i}}|\mathrm{n_k} = 0) = \mathrm{P}\big(\mathrm{LS}_1(n_{\mathrm{i}}) \geq \tilde{S}_{th} \,\big|\widehat{\omega}_1, \hat{\beta}_1\big) \qquad \textbf{4.29}$$

$$\widehat{T_2}\big(n_{\mathrm{j}}\big|\mathrm{n_k} = 0\big) = \mathrm{P}\big(\mathrm{LS}_2\big(n_{\mathrm{j}}\big) \geq \tilde{a}_{th}\big|\widehat{\omega}_2, \hat{\beta}_2\big) \qquad \textbf{4.30}$$

Where $\widehat{\omega}_1, \hat{\beta}_1, \widehat{\omega}_2$ and $\hat{\beta}_2$ are the a priori pdf of ω_1,ω_2, β_1 and β_2 respectively.

Given that $\widehat{\omega}_1$, ,$\widehat{\omega}_2$, $\hat{\beta}_1$and $\hat{\beta}_2$ are normal random variables, the degradation signal LS_1 and LS_2 computed at cycles n_{i} and n_{j} respectively, are normal variables as well [**59**][**47**][**61**] with mean variance given by:

$$\mu_{\mathrm{LS}_1}(n_{\mathrm{i}}) = \mu_{\omega 1} + \mu_{\beta 1} n_{\mathrm{i}}$$
$$\sigma^2{}_{\mathrm{LS}_1}(n_{\mathrm{i}}) = \sigma^2{}_{\omega 1} + \sigma^2{}_{\beta 1} n_{\mathrm{i}}{}^2 + 2\rho_1\sigma_{\omega 1}\sigma_{\beta 1} + \sigma_{r1}{}^2 \qquad \textbf{4.31}$$

$$\mu_{\mathrm{LS}_2}(n_\mathrm{j}) = \mu_{\omega 2} + \mu_{\beta 2} n_\mathrm{j}$$

$$\sigma^2{}_{\mathrm{LS}_2}(n_\mathrm{j}) = \sigma^2{}_{\omega 2} + \sigma^2{}_{\beta 2} n_\mathrm{j}{}^2 + 2\rho_2 \sigma_{\omega 2} \sigma_{\beta 2} + \sigma_{r2}{}^2 \qquad \textbf{4.32}$$

Remembering the Eq.4.29 and 4.30, we can write for $\widehat{T_1}$:

$$\widehat{T_1}(n_\mathrm{i}|\mathrm{n_k} = 0) = 1 - \mathrm{P}\big(\mathrm{LS}_1(n_\mathrm{i}) \le \tilde{S}_{th} \,|\widehat{\omega}_1, \hat{\beta}_1\big) =$$

$$= 1 - P\left(Z < \frac{\tilde{S}_{th} - \mu_{\mathrm{LS}_1}(n_\mathrm{i})}{\sqrt{\sigma^2{}_{\mathrm{LS}_1}(n_\mathrm{i})}}\right)$$

$$= \Phi\left(\frac{\tilde{S}_{th} - \mu_{\mathrm{LS}_1}(n_\mathrm{i})}{\sqrt{\sigma^2{}_{\mathrm{LS}_1}(n_\mathrm{i})}}\right) \qquad \textbf{4.33}$$

And for $\widehat{T_2}$:

$$\widehat{T_2}\big(n_\mathrm{j}\big|\mathrm{n_k} = 0\big) = 1 - \mathrm{P}\big(\mathrm{LS}_2\big(n_\mathrm{j}\big) \le \tilde{a}_{th} \,|\widehat{\omega}_1, \hat{\beta}_1\big) =$$

$$= 1 - P\left(Z < \frac{\tilde{a}_{th} - \mu_{\mathrm{LS}_1}(n_\mathrm{i})}{\sqrt{\sigma^2{}_{\mathrm{LS}_1}(n_\mathrm{i})}}\right)$$

$$= \Phi\left(\frac{\tilde{a}_{th} - \mu_{\mathrm{LS}_2}(n_\mathrm{j})}{\sqrt{\sigma^2{}_{\mathrm{LS}_2}(n_\mathrm{j})}}\right) \qquad \textbf{4.34}$$

Where Φ stands for the standard normal cdf. The domain of $\widehat{T_1}$and $\widehat{T_2}$, is ≤ 0 , thus can take on negative values, which is practically impossible from an implementation standpoint. Consequently, we use the truncated cdf for $\widehat{T_1}$ and $\widehat{T_2}$ with the constraint $\widehat{T_i} \ge 0$, i=1,2 which is given as:

$$\widehat{T_1} = \frac{\widehat{T_1} - \widehat{T_1}(n_\mathrm{i} = 0)}{\widehat{T_1}(n_\mathrm{i} = 0)}$$

$$\widehat{T_2} = \frac{\widehat{T_2} - \widehat{T_2}(n_j = 0)}{\widehat{T_2}(n_j = 0)} \quad \textbf{4.35}$$

As observed by [**47**], $\widehat{T_1}$ and $\widehat{T_2}$ are three parameter truncated Bernstein distributed random variables for which the first and second moment closed form don't exist[**63**]. As suggested by [**47**] the median is taken as the central moment. This can be justified, from one side by the not-existence of a closed form for the mean, and for the other hand, considering that the T_i pdfs are skewed and therefore the use of the median is more appropriate and conservative.

To compute the sum of the two random variables the Monte Carlo technique is followed, given the $\widehat{T_1}$ and $\widehat{T_2}$ numerical pdfs shown in Figure 50. The $\hat{\omega}_1, \hat{\beta}_1, \hat{\omega}_2$ and $\hat{\beta}_2$ a priori pdfs parameters are reported in Table 8.

	$\hat{\omega}_1$	$\hat{\beta}_1$	$\hat{\omega}_2$	$\hat{\beta}_2$	ϵ_1	ϵ_2
μ	-10.35	6.95e-009	-8.85	1.07e-007	0	0
σ^2	0.69	6.92e-035	47.65	3.55e-029	1.76e-008	1.5e-005
ρ	-0.1421		-0.2039			

Table 8 $\hat{\omega}_1, \hat{\beta}_1, \hat{\omega}_2$ and $\hat{\beta}_2$ a priori pdfs parameters

The pdfs are simply obtained differentiating the two cdfs with respect to n.

(a)

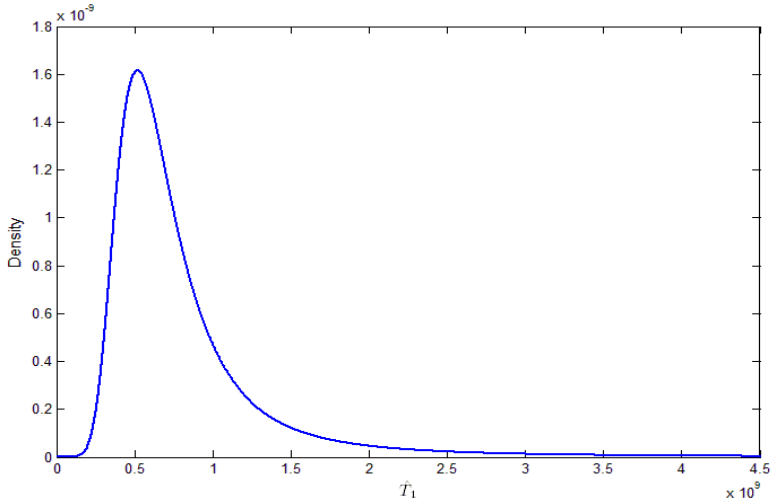

(b)

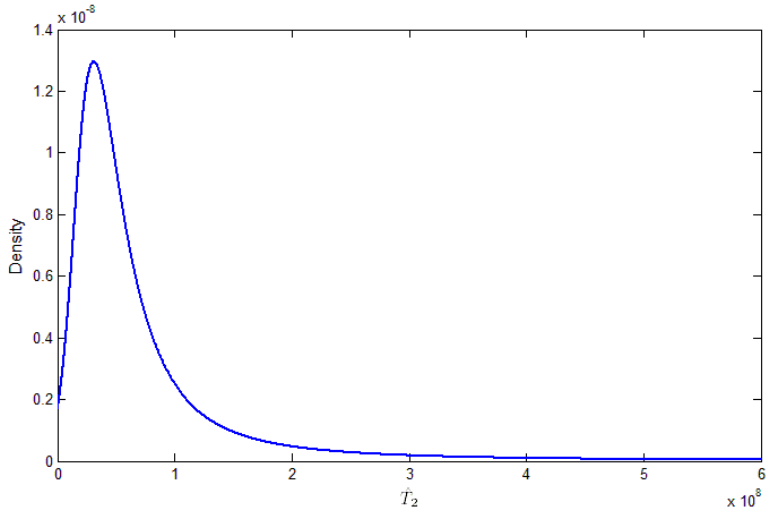

Figure 50 (a) $\widehat{T_1}$ pdf (b) $\widehat{T_2}$ pdf

Eventually the modeled a priori TTF is shown in Figure 51 compared to the simulated a priori TTF on a lognormal probability plot. The green circles belong to the simulated a priori TTF, while the black ones belong to the modeled a priori TTF.

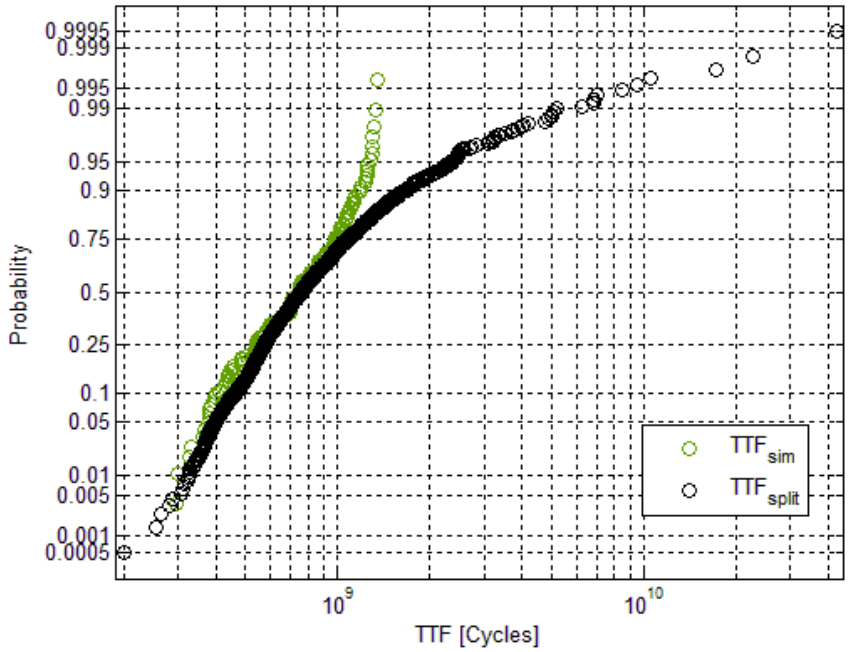

Figure 51 Simulated a priori TTF and a priori modeled TTF comparison – probability plot

A further comparison is between the two TTF pdfs is shown in Figure 52 in which both the cdfs are plotted. From the two figures can be observed that the left hand distributions' tail are similar, while for large values of TTF the two distributions differs. The modeled TTF has the right hand tail longer than the simulated one. However, for our purposes the left hand tail is much more important than the right one. For this reason the $\hat{\beta}_1$ and $\hat{\beta}_2$ normality assumption can be acceptable.

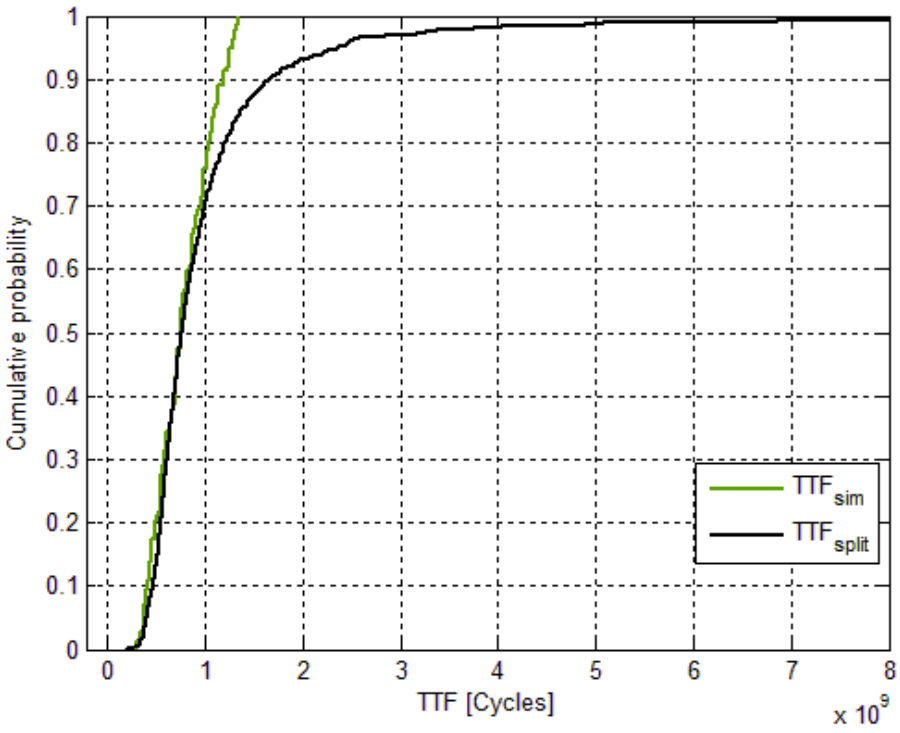

Figure 52 Simulated a priori TTF and a priori modeled TTF comparison – cdf

It is worth noting that if the two model's parameters are somehow correlated, It would be possible to update the second model's parameter instead of using the a priori information to compute the TTF till the threshold $\tilde{S}_{th}$ is reached. This situation would be valuable to exploit because better predictions could be performed since the beginning of the crack growth. Unfortunately this is not the case since the two pairs of coefficients are not significantly correlated as can be observed from Figure 53.

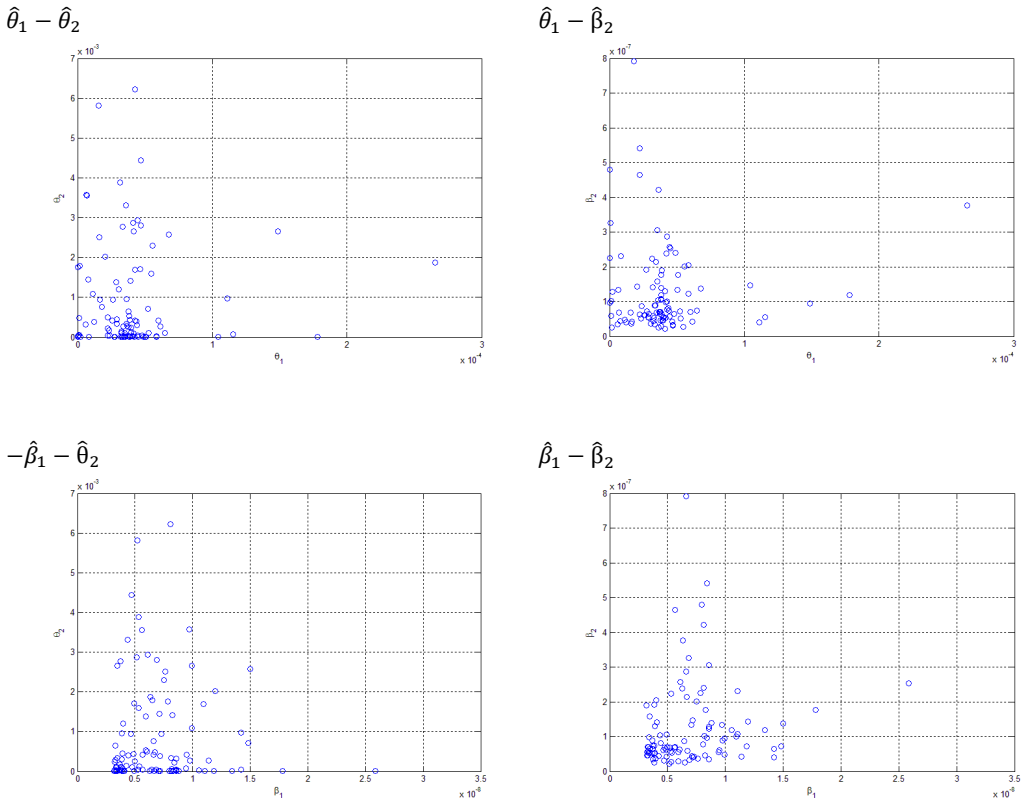

Figure 53 Correlations between the couple of model parameters

Now, once we have computed the a priori parameters' pdfs, we can write the equations that update these pdfs' parameters once obtained the signals $LS_{1,1}, \dots, LS_{1,k}$ or $LS_{2,1}, \dots, LS_{2,k}$ from the monitoring system, depending in which S interval the signals are. Since the problem statement is reduced to that explained in the paragraph 0, i just report the final formulas form which the updated pdfs parameters are obtained.

The models can be rewritten as:

$$\begin{cases} LS_1 = X_1[A]_1 & S \leq \tilde{S}_{th} \\ LS_2 = X_2[A]_2 & \tilde{S}_{th} \leq S \leq \tilde{a}_{th} \end{cases} \quad \textbf{4.36}$$

Where:

$$[A]_1 = \begin{bmatrix} \omega_1 \\ \\ \beta_1 \end{bmatrix} \quad X_1 = \begin{bmatrix} 1 & n_1 \\ \vdots & \vdots \\ 1 & n_n \end{bmatrix} \quad [A]_2 = \begin{bmatrix} \omega_2 \\ \\ \beta_2 \end{bmatrix} \quad X_2 = \begin{bmatrix} 1 & n_{1,2} \\ \vdots & \vdots \\ 1 & n_{n,2} \end{bmatrix}$$

At a cycle n_t, given the measures $LS_{i,1}$, $LS_{i,2}, \dots, LS_{i,t}$, $i = 1,2$ the updated $\omega_1, \beta_1, \omega_2, \beta_2$ pdfs parameters are:

$$\tilde{\mu}_1{}^T = \left(\left[\left(X_1{}^T X_1 \right)^{-1} X_1{}^T LS_1 \right]^T \frac{X_1{}^T X_1}{\sigma_{r1}{}^2} + \hat{\mu}_1{}^T \hat{\Sigma}_1{}^{-1} \right) \left(\frac{X_1{}^T X_1}{\sigma_{r1}{}^2} + \hat{\Sigma}_1{}^{-1} \right)^{-1} \quad \textbf{4.37}$$

$$\tilde{\Sigma}_1 = \left(\frac{X_1{}^T X_1}{\sigma_{r1}{}^2} + \hat{\Sigma}_1{}^{-1} \right)^{-1} \quad \textbf{4.38}$$

$$\tilde{\mu}_2{}^T = \left(\left[\left(X_2{}^T X_2 \right)^{-1} X_2{}^T LS_2 \right]^{T^T} \frac{X_2{}^T X_2}{\sigma_{r2}{}^2} + \hat{\mu}_2{}^T \hat{\Sigma}_2{}^{-1} \right) \left(\frac{X_2{}^T X_2}{\sigma_{r2}{}^2} + \hat{\Sigma}_2{}^{-1} \right)^{-1} \quad \textbf{4.39}$$

$$\tilde{\Sigma}_2 = \left(\frac{X_2{}^T X_2}{\sigma_{r2}{}^2} + \hat{\Sigma}_2{}^{-1} \right)^{-1} \quad \textbf{4.40}$$

Where:

$$\hat{\mu}_1 = [\mu_{\omega 1} \quad \mu_{\beta 1}] \qquad \hat{\mu}_2 = [\mu_{\omega 2} \quad \mu_{\beta 2}]$$

$$\hat{\Sigma}_1 = \begin{bmatrix} \sigma_{\omega 1} & \sigma_{\omega 1,\beta 1} \\ \sigma_{\omega 1,\beta 1} & \sigma_{\beta 1} \end{bmatrix} \quad \hat{\Sigma}_1 = \begin{bmatrix} \sigma_{\omega 2} & \sigma_{\omega 2,2} \\ \sigma_{\omega 2,\beta 2} & \sigma_{\beta 2} \end{bmatrix}$$

are the vectors of the a priori pdfs means and the covariance matrixes while:

$$\tilde{\mu}_1 = [\tilde{\mu}_{\omega 1} \quad \tilde{\mu}_{\beta 1}] \qquad \tilde{\mu}_2 = [\tilde{\mu}_{\omega 2} \quad \tilde{\mu}_{\beta 2}]$$

$$\tilde{\Sigma}_1 = \begin{bmatrix} \tilde{\sigma}_{\omega 1} & \tilde{\sigma}_{\omega 1,\beta 1} \\ \tilde{\sigma}_{\omega 1,\beta 1} & \tilde{\sigma}_{\beta 1} \end{bmatrix} \quad \tilde{\Sigma}_2 = \begin{bmatrix} \tilde{\sigma}_{\omega 2} & \tilde{\sigma}_{\omega 2,2} \\ \tilde{\sigma}_{\omega 2,\beta 2} & \tilde{\sigma}_{\beta 2} \end{bmatrix}$$

are the vectors of the a a posteriori pdfs means and the covariance matrixes .
Now, given the a posteriori pdfs' parameters the T_1 or T_2 distribution can be computed.
Remembering Eq.4.31 and 4.32 the updated mean and the variance of the degradation signal at a cycle n_i or n_j will be:

$$\tilde{\mu}_{\mathrm{LS}_1}(n_\mathrm{i}) = \tilde{\mu}_{\omega 1} + \tilde{\mu}_{\beta 1} n_\mathrm{i}$$

$$\tilde{\sigma}^2{}_{\mathrm{LS}_1}(n_\mathrm{i}) = \tilde{\sigma}^2{}_{\omega 1} + \tilde{\sigma}^2{}_{\beta 1} {n_\mathrm{i}}^2 + 2\tilde{\rho}_1 \sigma_{\omega 1} \tilde{\sigma}_{\beta 1} + {\sigma_{r1}}^2 \qquad \textbf{4.41}$$

$$\tilde{\mu}_{\mathrm{LS}_2}(n_\mathrm{j}) = \tilde{\mu}_{\omega 2} + \tilde{\mu}_{\beta 2} n_\mathrm{j}$$

$$\tilde{\sigma}^2{}_{\mathrm{LS}_2}(n_\mathrm{j}) = \tilde{\sigma}^2{}_{\omega 2} + \tilde{\sigma}^2{}_{\beta 2} {n_\mathrm{j}}^2 + 2\tilde{\rho}_2 \tilde{\sigma}_{\omega 2} \tilde{\sigma}_{\beta 2} + {\sigma_{r2}}^2 \qquad \textbf{4.42}$$

And therefore from Eq.4.33 and 4.34 the updated T_1 or T_2 pdf will be:

$$\tilde{T}_1(n_\mathrm{i} \mid LS_{1,1} \; LS_{1,2}, \dots, LS_{1,t}) = \Phi\left(\frac{\tilde{S}_{th} - \mu_{\mathrm{LS}_1}(n_\mathrm{i})}{\sqrt{\sigma^2{}_{\mathrm{LS}_1}(n_\mathrm{i})}}\right) \qquad \textbf{4.43}$$

$$\xRightarrow{\tilde{T}_1 \geq 0} \frac{\tilde{T}_1 - \tilde{T}_1(0)}{\tilde{T}_1(0)}$$

And for $\tilde{T}_2$:

$$\tilde{T}_2\left(n_j \middle| LS_{2,1}\ \ LS_{2,2}, \dots, LS_{2,t}\right) = \Phi\left(\frac{\tilde{a}_{th} - \mu_{LS_2}(n_j)}{\sqrt{\sigma^2{}_{LS_2}(n_j)}}\right) \quad \textbf{4.44}$$

$$\xRightarrow{\tilde{T}_2 \geq 0} \frac{\tilde{T}_2 - \tilde{T}_2(0)}{\tilde{T}_2(0)}$$

An Example:

Given a crack growth path shown in Figure 54, at each time step we can update the a priori TTF given in Figure 37, exploiting the information gained form monitoring the crack growth.

Using Eq. 4.37, 4.38 for the first part of the degradation pattern (T_1 in Figure 54) and the Eq.4.39 and 4.40 for the second part, we can compute the a posteriori $\hat{\omega}_1, \hat{\beta}_1, \hat{\omega}_2$ and $\hat{\beta}_2$ pdfs' parameters, that are the means and the standard deviations.

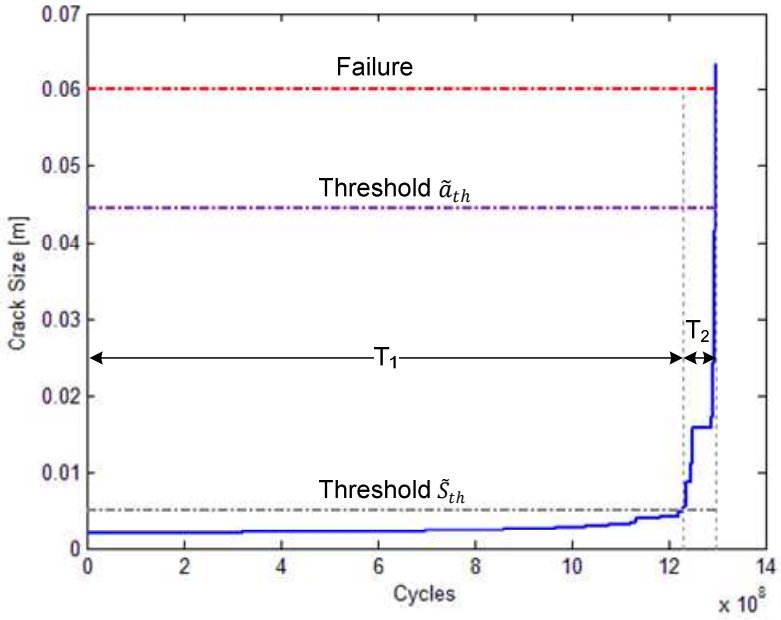

Figure 54 Crack growth path

From the initial cycle to that one that corresponds to a crack size of 5.1 mm the updated TTF is given by Eq.4.7 where T_2 is given by Eq.4.35, that is the a priori modeled T_2.

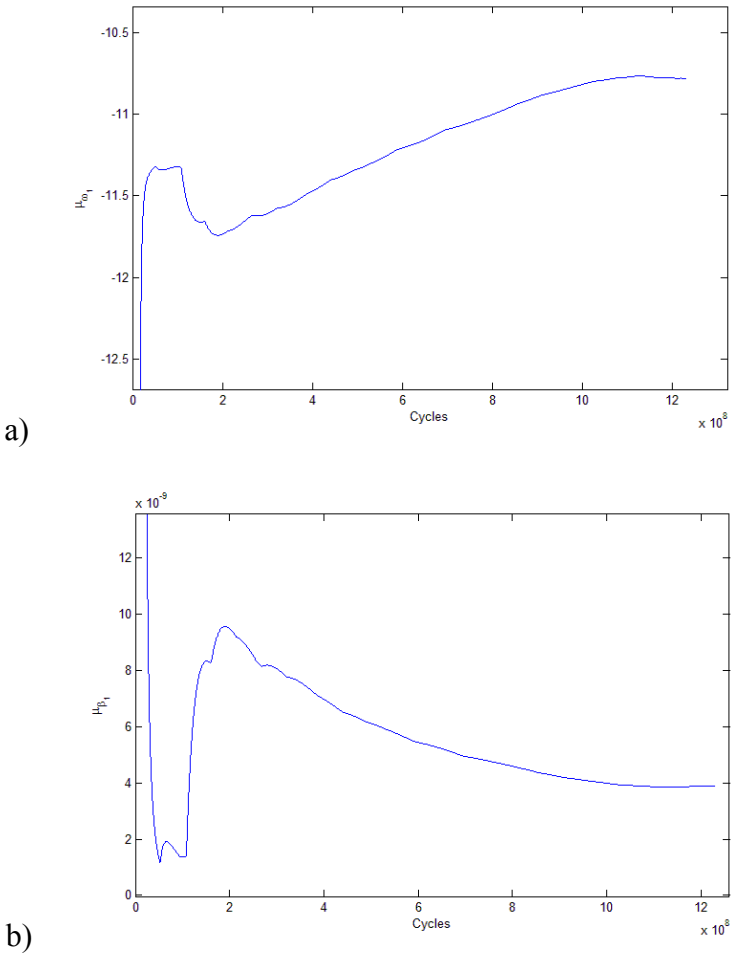

Figure 55 a) updated $\tilde{\mu}_{\omega 1}$ and b) updated $\tilde{\mu}_{\beta 1}$

Figure 55 a) shows the updated $\tilde{\mu}_{\omega 1}$ as a function of cycles, while the plot b) shows the updated $\tilde{\mu}_{\beta 1}$.

At each time step, given the updated $\tilde{\mu}_{\omega 1}$ and $\tilde{\mu}_{\beta 1}$ we can compute the a actual TTF where $\tilde{T}_1$ is given by the Eq.4.43. For each time step the TTF median and the 1st percentile is stored. These two values are plotted in Figure . As can be observed, cycle after cycle the predictions converge to the true TTF even before the second degradation phase. In this case, both the 1st percentile and the mean fall within the 5% error interval. The interval in which the TTF median and its

1st percentile lines are interrupted means that the predicted TTF falls beyond the timescale.

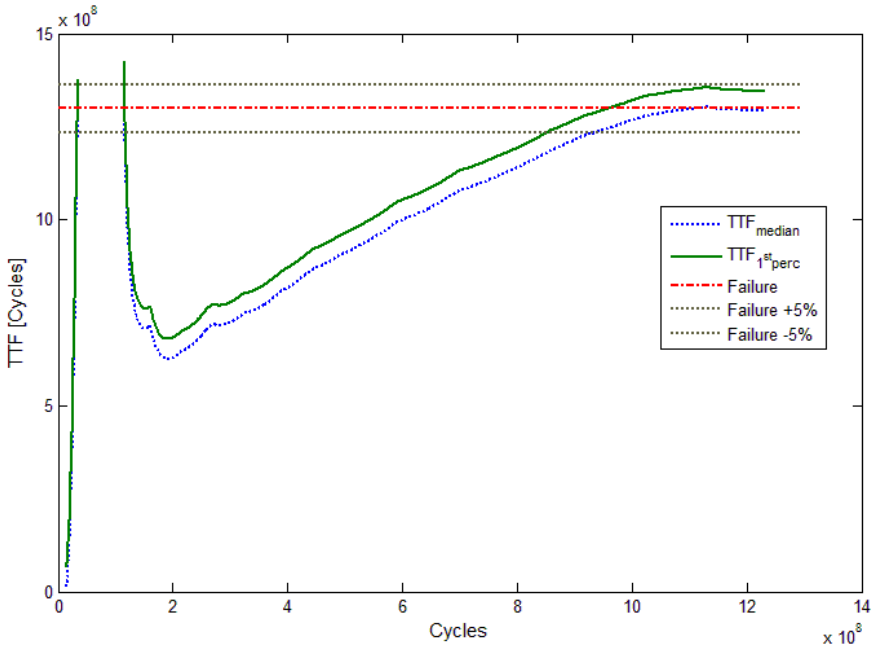

Figure 56 Predicted TTF - 1st phase

Once the threshold $\tilde{S}_{th}$ is passed, the TTF is equal to the cycle T_1, that is no more a random variable (it is deterministic), plus the predicted $\tilde{T}_2$.
$\tilde{T}_2$ is given by Eq.4.44, once computed the updated $\mu_{\beta 2}$, $\mu_{\omega 2}$ and the related variances given by Eq.4.39 and 4.40.
Figure 57 shows the updated $\mu_{\beta 2}$ and $\mu_{\omega 2}$ respectively.

a)

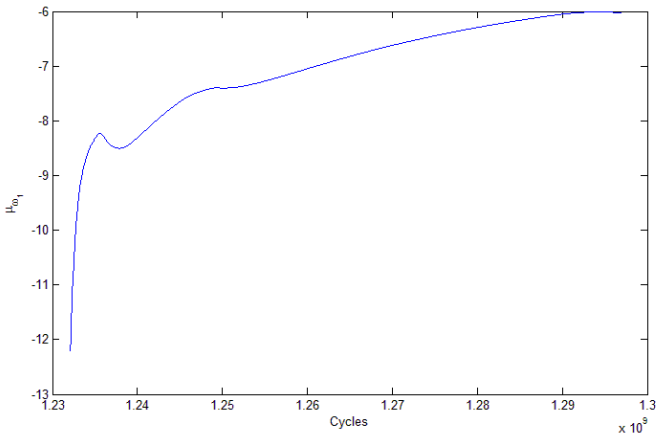

b)

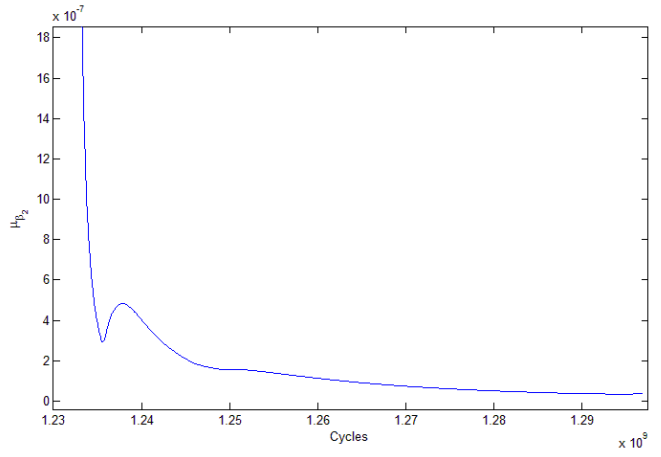

Figure 57 a) updated $\tilde{\mu}_{\omega 2}$ and b) updated $\tilde{\mu}_{\beta 2}$

As previously done for the first degradation phase, the TTF pdf can be computed using Eq.4.39, 4.40, 4.42 and eventually 4.44. The updated TTF median and its 1st percentile are shown in Figure 58.

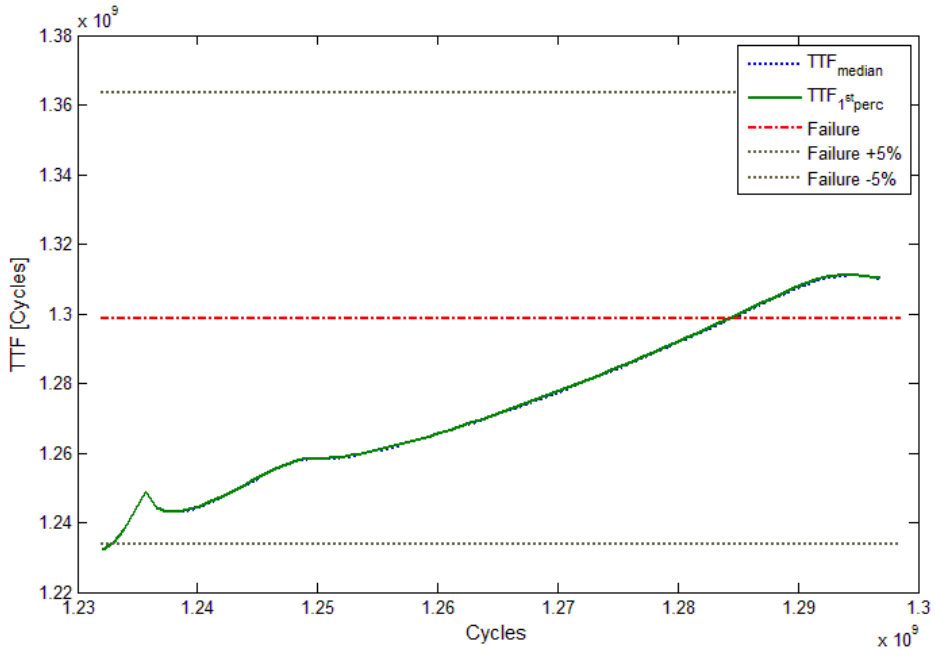

Figure 58 Predicted TTF – 2nd phase

Can be observed how the predictions converge to actual failure time. This time the prediction variances are smaller than those of the first phase. This is due to the fact that the 1st phase predictions include the uncertainties related to the a priori T_2 pdf.

4.4.3. Prognostic through the physical model

The same problem faced by the Bayesian prognostic model can be pursued through a recursive application of the crack growth model presented in paragraph 4.2. The physical phenomenon analyzed in this context has been faced by numerous researches, therefore numerous models have been proposed capable of describing and highlighting the main variables and their relations that influence the crack growth. The NASGRO model used in this context is recognized to be the most reliable to describe crack growth in railway axles[**78**][**69**][**81**], therefore can be used to predict accurately the TTF.

The main idea at the basis of this approach is that, once measured and estimated the actual crack size and the loads history, we can estimate the TTF through simulating the possible growth paths by using a Monte Carlo technique.

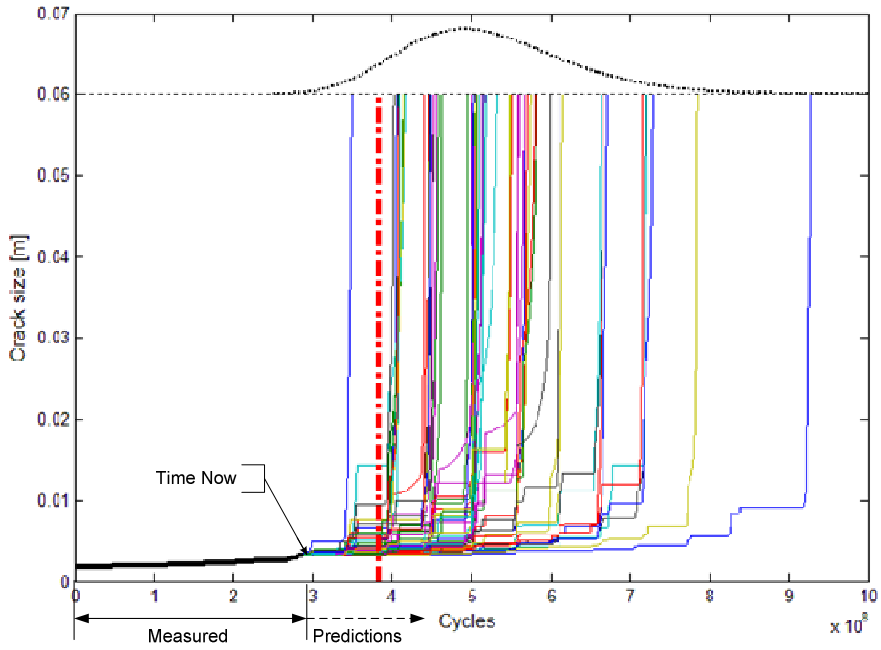

Figure 59 TTF prediction through the NASGRO crack growth model

This approach is shown in Figure 59. Let suppose that through the monitoring infrastructure we have measured the crack size at the time now, we can simulate the crack propagation considering as random variables the load applied and the SIF threshold and the initial crack size equal to the measured one. The functions plotted and originating from the time now, are some simulated crack growth paths. Starting from the crack growth paths set, it is possible to estimate the TTF pdf. In Figure 59 the black dotted line represents the predicted TTF pdf, while the red line represents the actual failure time.

The estimated TTF at each time step can be approximated by lognormal distribution, as shown in paragraph 4.2 and in Figure 60.

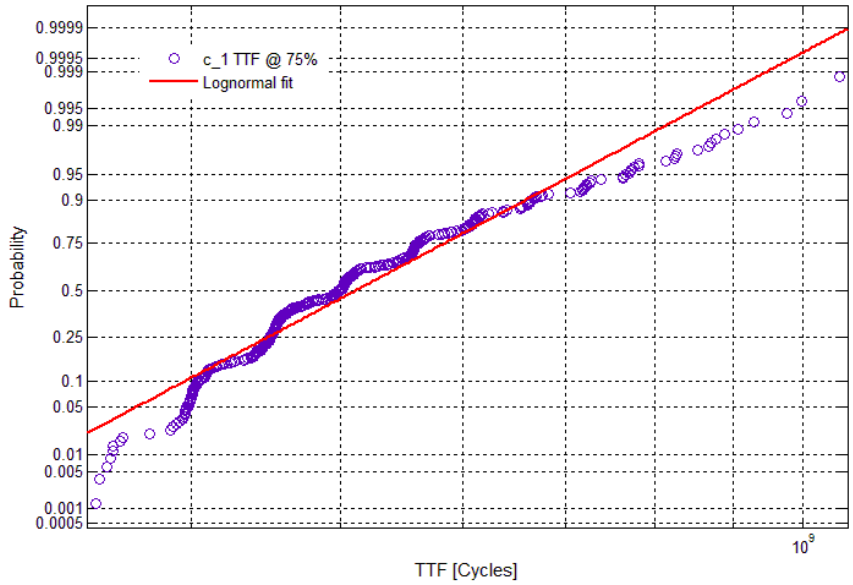

Figure 60 The approximated TTF probability plot

As in the Bayesian approach, at each time step, the TTF 1st percentile, the median and the TTF at 98% level of confidence is stored. However, for computational reasons, the TTF up dating times are set at the 5%, to the 99% of the actual TTF with a 5% gap. Figure 61 shows the TTF estimations at different time steps. Can be observed how the predictions converge to the actual failure. At the last updating time step all the TTF distribution falls into the 5% error interval.

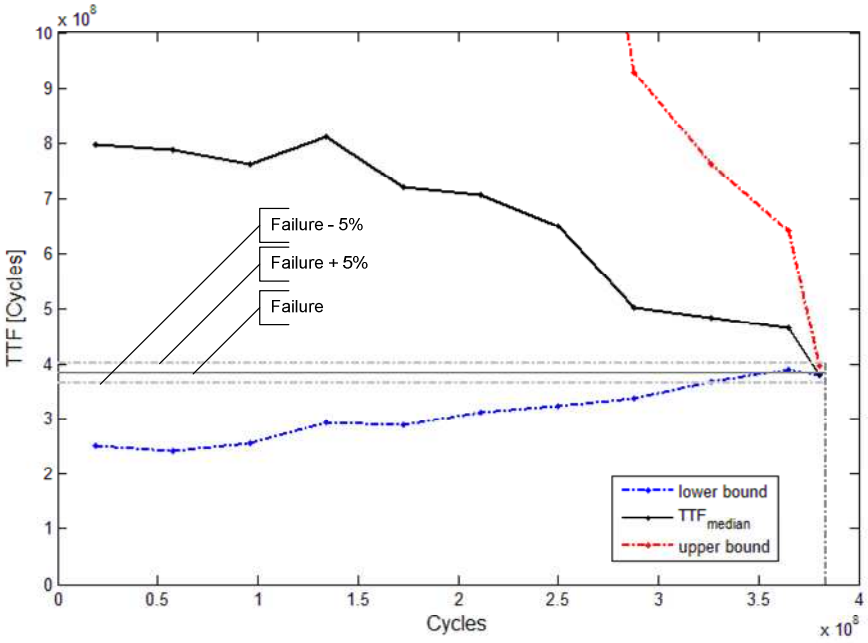

Figure 61 TTF predictions

Figure 62 shows how the confidence interval diminish as we approach to the actual failure. The green dotted line represents the difference between the TTF median and the TTF at the 0.01 confidence level, while the red dashed dotted line represents the TTF pdf upper bound, at the 0.99 confidence level.

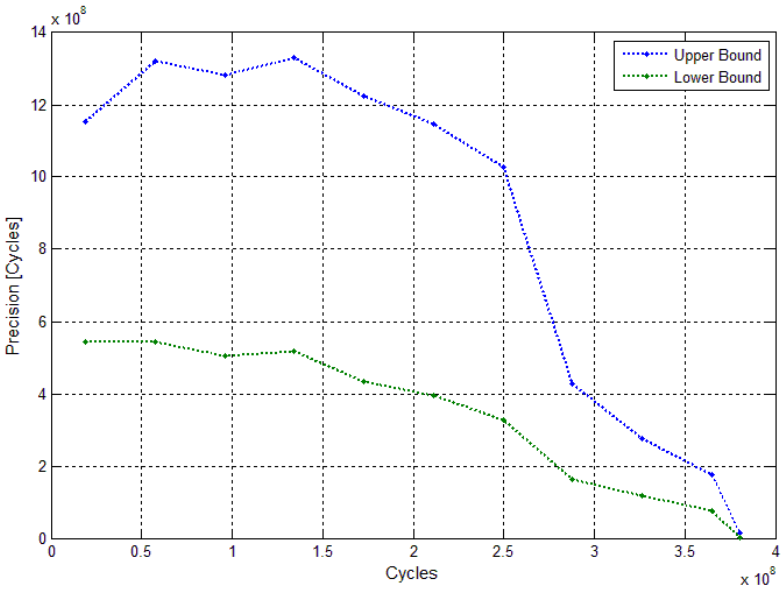

Figure 62 Estimated TTF at the 0.01 and 0.98 confidence level

4.4.4. The size error and the updating frequency effect on TTF predictions

In the case of the physical model, the size error and the updating frequency effect on the estimations can be approximately evaluated through simple geometrical considerations. The assessment of these effects on the predictions performances is an important issue since they characterize the monitoring and diagnostic equipment goodness. Higher size errors characterize low performance diagnostic, while lower updating frequency entails lower monitoring equipment cost.

In this case the effect of the updating frequency on the prediction performances is not relevant since the TTF estimation relies on just the last crack size measurement and not, as in the Bayesian case, on the complete set of measurements. The TTF updating frequency effect can be considerable when maintenance scheduling decisions is considered. By this point of view, high frequency updating is preferable since the decisions can be based on more updated TTF.

In this case we can apply a predictive maintenance policy similar to that one proposed by Kaiser et.al. in [**64**]. The stopping rule, i.e the cycle n_k at which the axle should be substituted, is defined as in Eq.4.45.

$$n_k \rightarrow TTF_{lb}(n_k) - n_k - \delta \leq 0 \qquad \textbf{4.45}$$

Where n_k is the first cycle at which the rule is verified, $TTF_{lb}(n_k)$ is the TTF prediction computed at a 0.01 confidence level at the cycle n_k, δ is the updating interval. From this simple rule is self-evident that the greater δ the lower n_k.

This simple rule can be easily understood by analyzing the graph shown in Figure 63. The blue line represents the estimated TTF at the 0.01 confidence level while the black dotted line represents the equality $n = TTF_{lb}$. The dashed line represents the equality $n = TTF_{lb} + \delta$. Therefore, for Eq. 4.45, the cycle n_k is the first intersection point of the TTF_{lb} (blue line) with the black dashed line. Particularly, referring to what stated in the previous chapters, the quantity $TTF_{lb}(n_k) - n_k$ is the RUL computed at the 0.01 confidence level (RUL_ in Figure 63). The main idea associated with this rule is that the axle can be safely run till it reaches the last TTF_{lb} estimation.

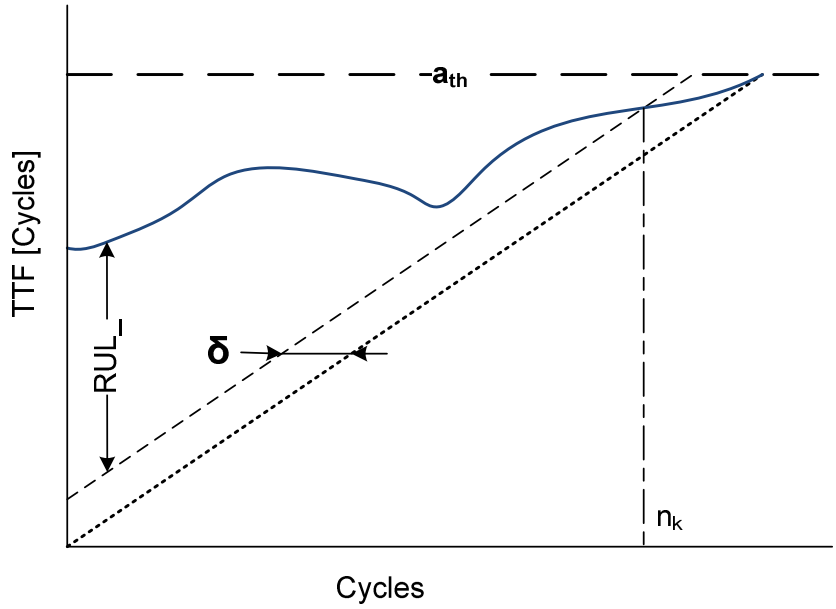

Figure 63 The effect of updating frequency on TTF predictions

The size error effect on the TTF predictions can be approximately computed making the hypothesis that the crack growth path can be approximated with an exponential function. Generally, as described in 4.4.1, the more the size error the lesser the threshold. The analysis framework is shown in Figure 64. Let us suppose that for a given size error , the failure threshold is set at the value a_{th} and that we are at the cycle n_i and we measure the crack size exp (LS_i). Through the method explained in paragraph 4.4.3, we can compute the TTF pdf (blue line) and therefore we know the TTF_{median} and the $TTF_{1^{st}p}$ at the 0.01 confidence level.

Next, suppose that the new size error is greater to the previous one, consequently, from Eq.4.17 keeping a_{max} constant, we obtain the failure threshold a_{th2} lower than a_{th}. This threshold shift causes a change in the TTF pdf parameters and therefore to the reference points TTF_{median} and $TTF_{1^{st}p}$.
The new reference points TTF'_{median} and $TTF'_{1^{st}p}$ computed at cycle n_i, thanks to the hypothesis made, can be computed as follows:

$$TTF'_{median} = TTF_{median} - \frac{\log a_{th} - \log a_{th2}}{\beta} \quad \textbf{4.46}$$

$$TTF'_{1^{st}p} = TTF_{1^{st}p} - \frac{\log a_{th} - \log a_{th2}}{\alpha} \quad \textbf{4.47}$$

Where:

$$\alpha = \frac{\log a_{th} - LS_i}{TTF_{1^{st}p} - n_i} \quad \textbf{4.48}$$

$$\beta = \frac{\log a_{th} - LS_i}{TTF_{1^{st}p} - n_i} \quad \textbf{4.49}$$

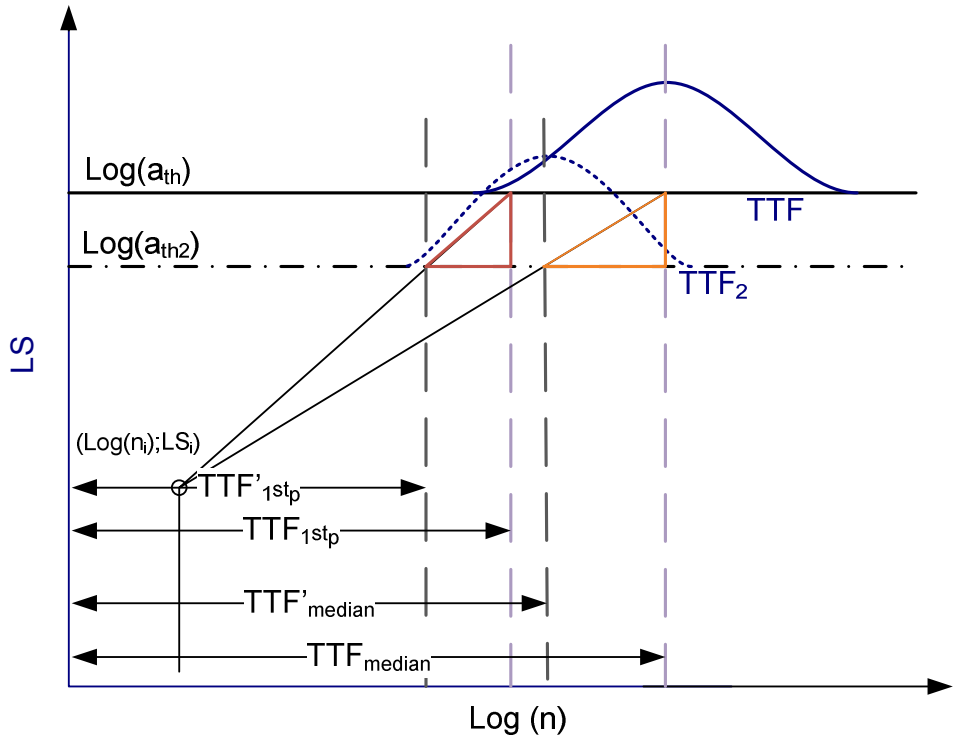

Figure 64 The error size effect on TTF predictions

The lower confidence interval $CI = (TTF_{median} - TTF_{1^{st}p})$, as stated in 1.2, decreases when the size error increases, i.e the prediction is more accurate. This can be easily demonstrated, subtracting term by term Eq. 4.46 with Eq. 4.47 we obtain:

$$CI' = CI - \Delta(\log a_{th})\left(\frac{1}{\beta} - \frac{1}{\alpha}\right) \qquad \textbf{4.50}$$

Since $\beta < \alpha$ and $\Delta(\log a_{th}) > 0$ for increasing size errors $CI' < CI$.

It is worth noting that, from Eq. 4.47, the ratio $\frac{TTF_{1^{st}p}}{TTF'_{1^{st}p}}$ is not linear with respect to the ratio $\frac{a_{th}}{a_{th2}}$ and from Eq.4.17 the ratio $\frac{a_{th}}{a_{th2}}$ is not a linear function of the size error ratio.

The updating frequency and size error combined effect on the cycle n_k normalized with respect the actual failure (i.e % of the life exploited) on particular crack growth curve is shown in Figure 65. As we can see the relationship between the size error and the ratio $\frac{n_k}{n_{failure}}$. As the size error increases, for a given updating frequency, the life exploited decreases, while the relationship between the updating frequency and the life exploited for a given size error is linear: the more frequent the TTF updating the greater the life exploited.

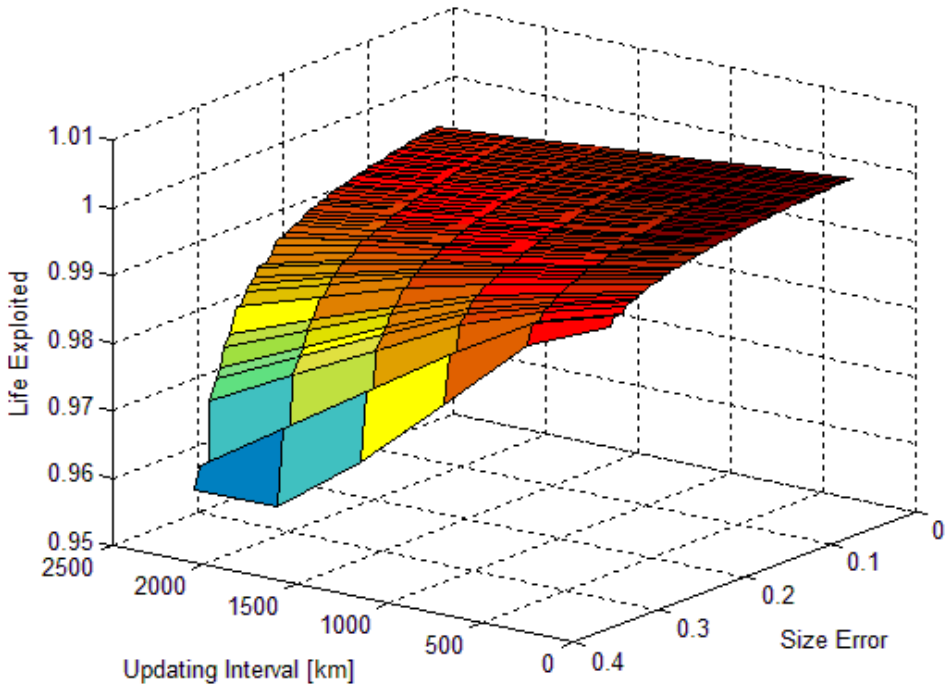

Figure 65 The updating frequency and size error combined effect

4.5. Results

Our goal, as stated in paragraph , is to assess the predictive performances of both the prognostic models and eventually highlight the differences between the predictive and preventive maintenance policy.

The probabilistic aspect of the issue has clearly arisen during the dissertation, therefore a reliable and a definitive answer to the questions proposed has to be given after numerous simulations that guarantee a reliable representation of the probabilistic aspects involved. However, some preliminary considerations can be outlined analyzing a limited number of instances.

The method used to select the instances analyzed is based on the stratified sampling technique. Particularly, the TTF pdf represented in Figure 37 has been divided in 10 equal spaced intervals, that corresponds to the bins shown in the same figure. For each bin a crack growth path was selected obtaining a set of 10 possible degradation curves as shown in Figure 28.

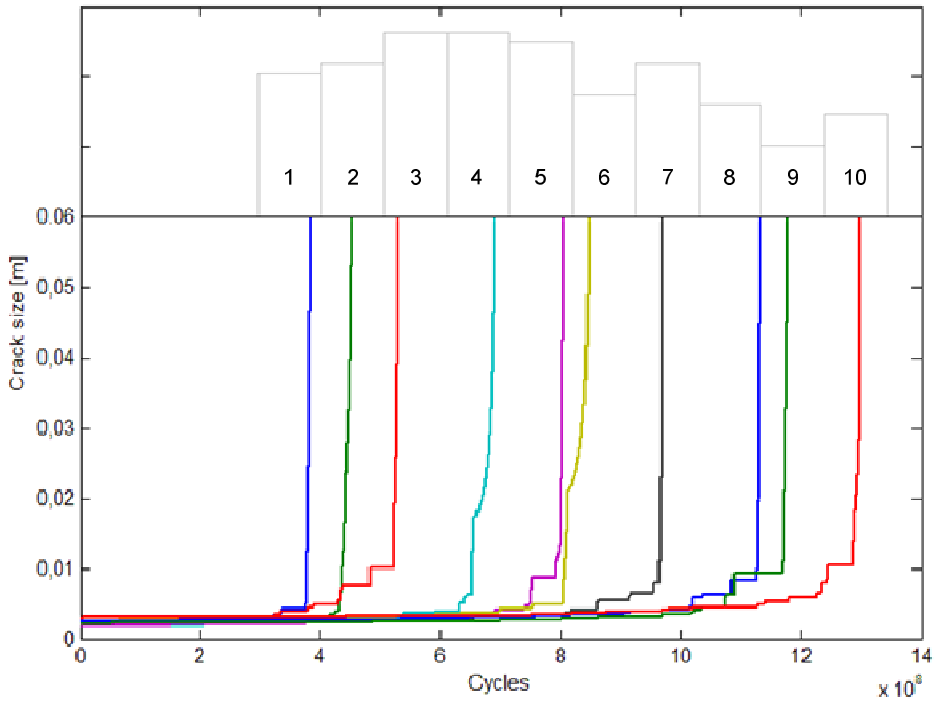

Figure 66 The 10 selected crack growth paths

For the whole set of track selected, the Bayesian prognostic algorithm and the physical model was applied. Moreover, the maximum number of inspections N_{insp} and the expected number of inspections $\overline{N_{insp}}$ was computed.

In order to evaluate the prognostic algorithms described, two metrics were used, one of which suggested by [**86**].
This metric, called Timeliness φ, exponentially weighs RUL prediction errors through an asymmetric weighting function. Penalizes the late predictions more than early prediction. The formula is:

$$\Phi(n) = \begin{cases} \exp\left(\frac{|z(n)|}{a}\right) & z \geq 0 \\ \exp\left(\frac{|z(n)|}{b}\right) & z \leq 0 \end{cases} \quad \textbf{4.51}$$

$$\varphi = \frac{1}{N}\sum_{n=1}^{N} \Phi(n) \quad \textbf{4.52}$$

Where $z(n) = TTF_{actual} - TTF_{median}(n)$ is the prediction error computed at cycle n, while a and b are two constants where $a > b$. In this case $a = 100$ and $b = 10$.

Ideally the perfect score is φ=1. To be comparable, the updating frequency has to be the same between the two algorithms, therefore the TTF predictions in the physical model case have been linearly interpolated.

The other metric chosen is simply the predictions percentage error computed at fixed time steps $n_k = 0.25FT,\ 0.5FT,\ 0.75FT,\ 0.98FT$, where FT is the cycle at which the failure occurs.

In the appendix (Chapter 7) the comparison of the predictions at different time steps and the PC_{DET} for each of 10 sampled paths can be found. Moreover, the size error and the updating frequency effect on the exploited life are plotted for each instance.

As can be noticed form these figures, both the algorithms' predictions converge to the actual failure time. The information about the actual degradation path increase as time elapses, resulting in an improved knowledge about the actual TTF. Better knowledge of the crack growth behavior allow more accurate predictions. The advantage of continuous monitoring with respect to the a priori information is clearly evident observing Figure 67. It shows the TTF pdf obtained from the prognostic algorithms described and the a priori TTF pdf (black line). It is clearly noticeable how prognostics can improve the knowledge on the actual failure path followed by an individual axle.

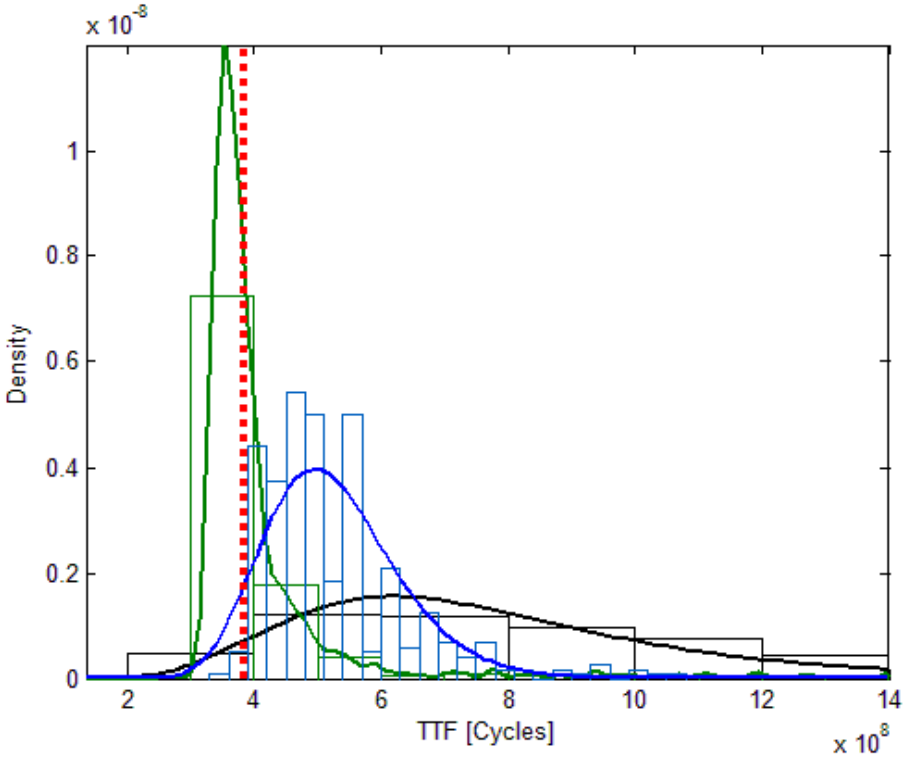

Figure 67 Comparison of the a priori TTF pdf and the updated TTF pdf obtained from the prognostics algorithms described (green-Bayesian, blue physical based model, black - a priori)

However, substantial differences among the two prognostic approach exists. Particularly, what differs is the distribution of the prediction errors along the degradation timeline and the prediction confidence interval. The last statement is evident observing the figures in the appendix in which the predictions paths are compared. In all the instances selected the physical model confidence interval is larger than that one computed by the Bayesian approach.

However, the most important differences among the two approaches have to be evaluated in term of the prediction errors. The following graphs display the prediction errors for both the algorithms and for the whole crack growth track set at fixed residual life percentile (i.e 0.25, 0.5, 0.75, 0.98). The same information are displayed in a tabular form in Table 9. The percentage prediction error is simply calculated as:

$$err\% = \frac{FT - TTF_{median}}{FT} 100 \qquad \textbf{4.53}$$

From the graphs can be concluded that:

1. Physical model prediction errors decrease approaching the FT
2. Bayesian algorithm prediction errors decreases till the 75° percentile of the residual lifetime, while at 98% the errors are greater that in the 75 percentile
3. Physical model predictions are lower for FT near the average (bins 3,4,5)
4. Bayesian predictions seems to outperform the physical model predictions for till the 75th percentile, while for the 98th the physical model predictions are more accurate.

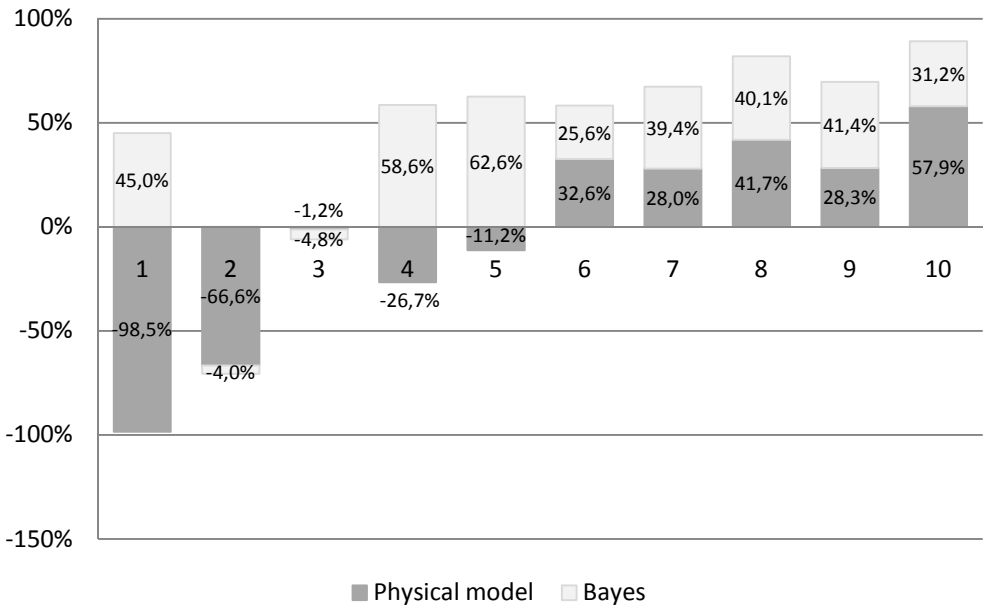

Figure 68 Percentage prediction error @ 25% FT

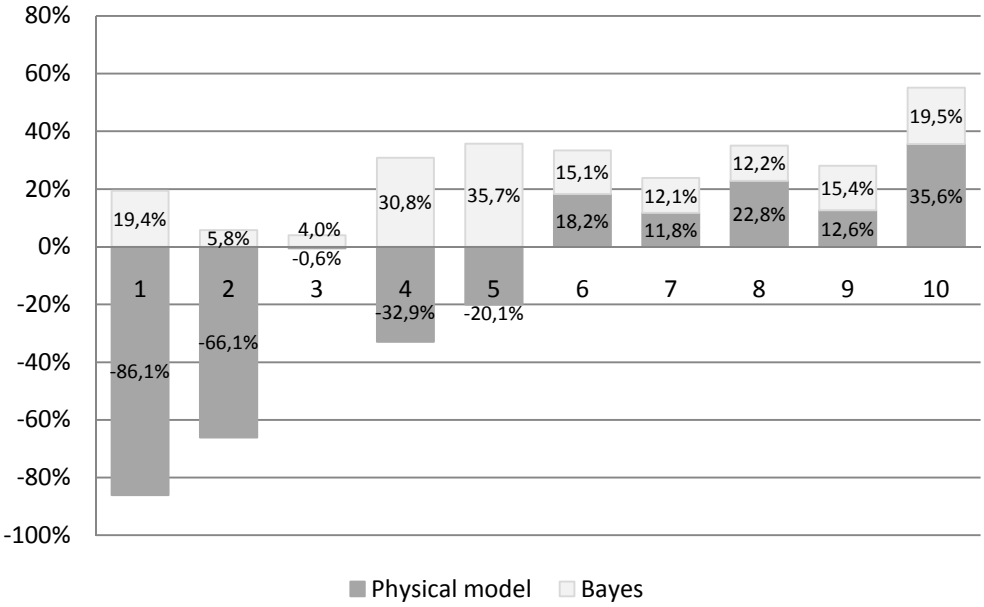

Figure 69 Percentage prediction error @ 50% FT

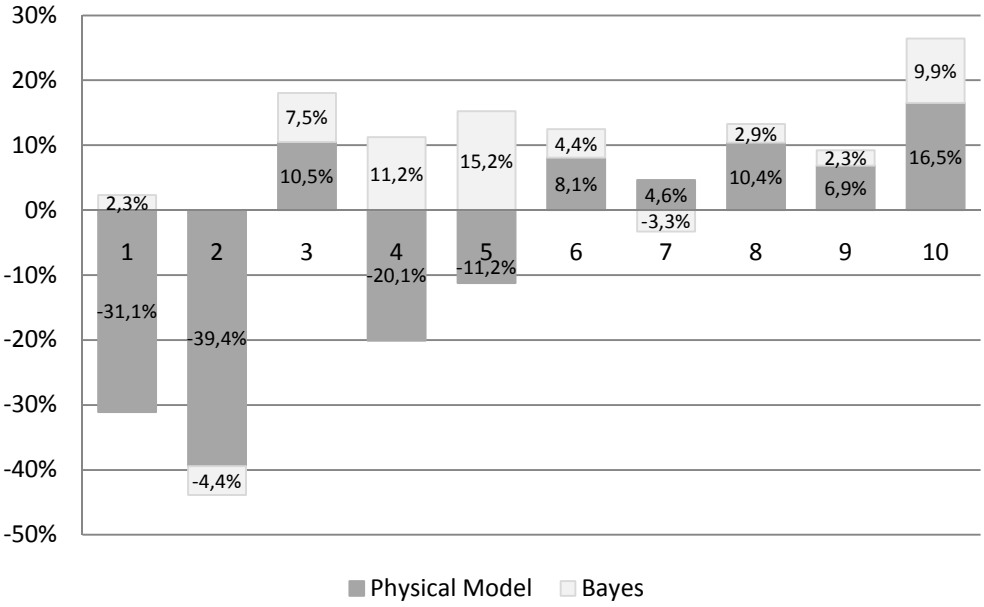

Figure 70 Percentage prediction error @ 75% FT

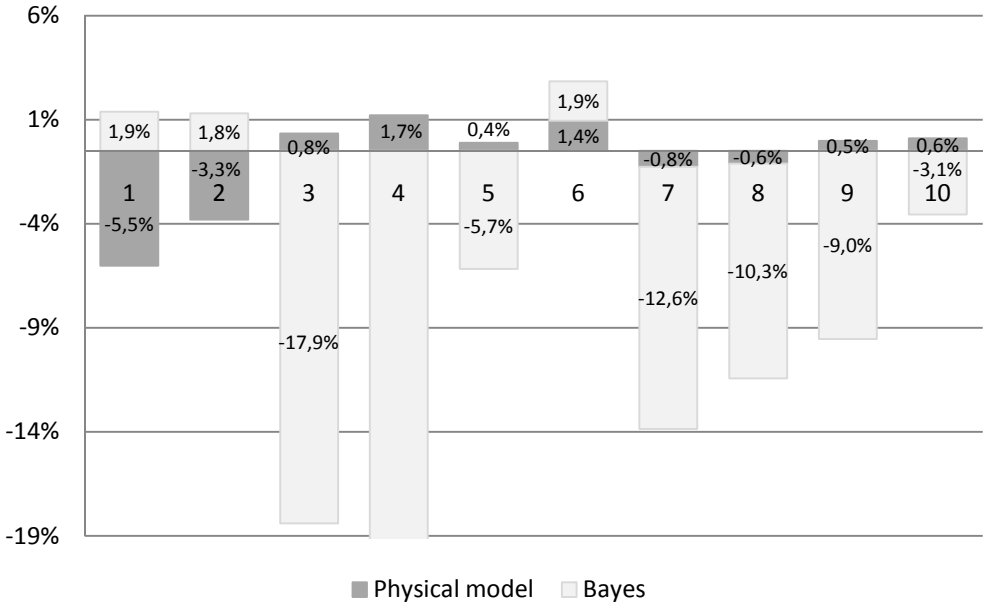

Figure 71 Percentage prediction error @ 98% FT

% Life	Model	c_1	c_2	c_3	c_4	c_5
25	Physical model	-98,50%	-66,59%	-1,20%	-26,69%	-11,19%
	Bayes	44,95%	-3,96%	-4,85%	58,58%	62,57%
50	Physical model	-86,08%	-66,11%	-0,55%	-32,95%	-20,08%
	Bayes	19,36%	5,77%	4,00%	30,77%	35,70%
75	Physical model	-31,09%	-39,44%	10,52%	-20,11%	-11,21%
	Bayes	2,31%	-4,42%	7,53%	11,24%	15,22%
98	Physical model	-5,52%	-3,31%	0,84%	1,72%	0,39%
	Bayes	1,87%	1,81%	-17,90%	-40,00%	-5,68%

% Life	Model	c_6	c_7	c_8	c_9	c_10
25	Physical model	32,56%	27,98%	41,74%	28,29%	57,91%
	Bayes	25,64%	39,37%	40,14%	41,39%	31,19%

50	Physical model	18,24%	11,76%	22,84%	12,63%	35,59%
	Bayes	15,11%	12,08%	12,15%	15,37%	19,54%
75	Physical model	8,09%	4,64%	10,39%	6,87%	16,52%
	Bayes	4,38%	-3,27%	2,87%	2,34%	9,91%
98	Physical model	1,44%	-0,76%	-0,61%	0,48%	0,61%
	Bayes	1,90%	-12,61%	-10,32%	-9,04%	-3,06%

Table 9 Percentage prediction errors

General considerations can be drafted form the conclusive graph in Figure 72 that display the mean squared percentage error among the whole set for each residual life percentile. The statements of the list above are confirmed.

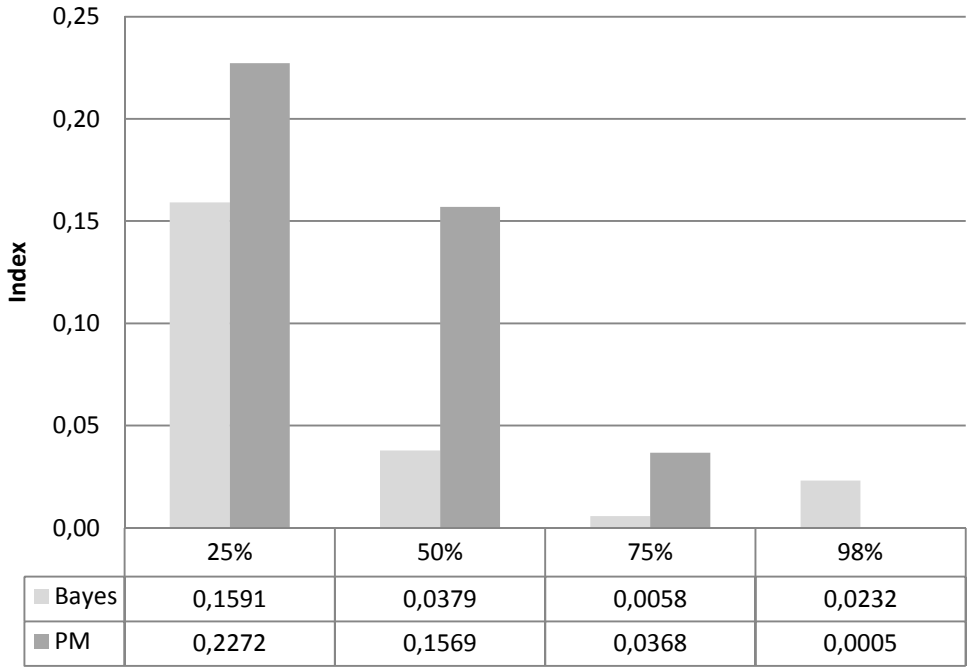

Figure 72 MS of the percentage prediction errors for each residual life percentile

Using the other metric chosen, expressed by Eq.4.52 the results displayed in Table 10 are obtained. The main difference between the metric defined before, is that this metric considers the whole set of predictions and not only those that corresponds to particular moments. The results found are very similar among the

two approaches. The physical model index is slightly smaller than the Bayesian one.

	Physical model	Bayes	NDI - max	NDI - mean
c_1	1,07595	1,02061	34	33,24
c_2	1,05471	1,00486	40	39,49
c_3	1,00225	1,02235	47	42,41
c_4	1,02188	1,01337	61	58,98
c_5	1,01014	1,01547	71	68,61
c_6	1,00199	1,00774	75	73,04
c_7	1,00143	1,00769	86	82,14
c_8	1,00251	1,00787	100	96,19
c_9	1,00163	1,00240	105	100,35
c_10	1,00355	1,00484	115	110,70
MS	**1,01791**	**1,01074**		

Table 10 Results – φ, N_{insp} and $\overline{N_{insp}}$

The last two columns of Table 10 reports respectively the maximum non destructive inspections number and the expected NDI number. The last result is obtained multiplying the NDI cumulative number with the corresponding PC_{DET}. Obviously, the expected NDI number increases as the FT increases. The NDI number that should be performed to guarantee a 99% chance to detect a crack before it reaches the length of 6cm is relevant. As a consequence, the availability of the asset is highly affected from this maintenance policy. The loose of availability and the numerous maintenance activities imply a considerable maintenance costs build up.

In Figure 73 the effect of an increase of the size error is displayed[8], considering the updating frequency of 90 km. Can be noticed that generally, as previously stated, the greater the size error, the lower the life exploited. However, the life exploited reduction is not relevant. An increase of 3 times of the size error

[8] Computed considering the physical model predictions only

causes a life exploited reduction of about 5% on average. For the figures in appendix can be noticed that the effect of the updating frequency is lower with respect to the error size effect.

The scarce effect of this important variables to the exploited life is due to the fact that an increase of the size error cause a reduction of the threshold a_{th} that however corresponds to a negligible life loss reduction thanks to the high crack growth rate that characterize the last part of the degradation phase. Greater effects shall be noticed when the size error is large enough to force the threshold a_{th} to be set at crack sizes at which the growth rate is lower (i.e at the end of the first degradation phase).

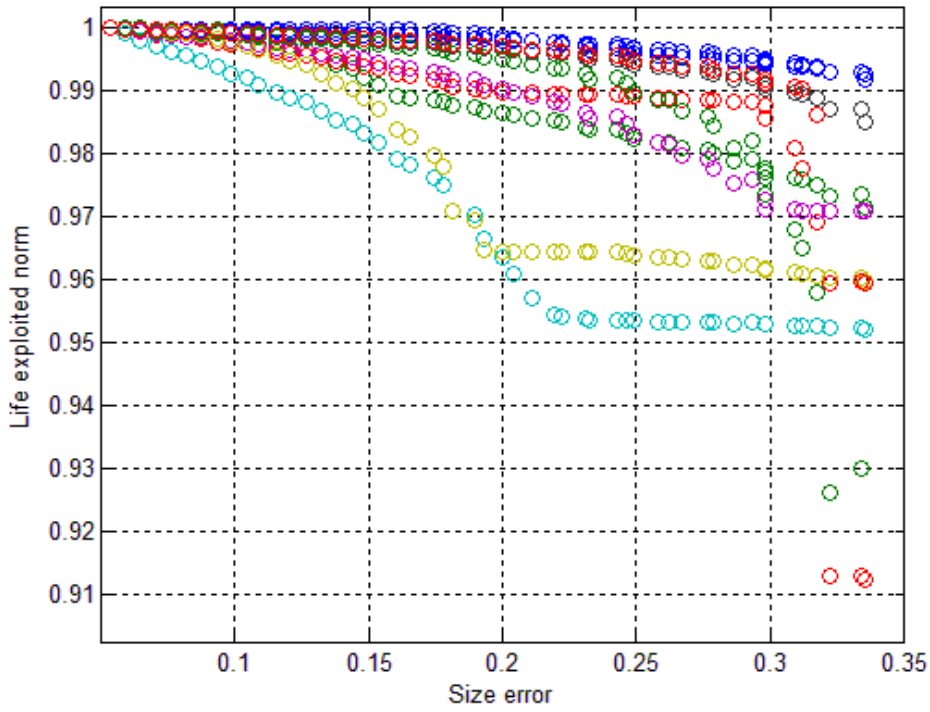

Figure 73 The size error effect on life exploited given $\delta = 90\ km$[9]

[9] Life exploited is normalized with respect to the life exploited that corresponds to the first size error considered

5. Conclusions

The objective of this thesis research was to propose an integrated approach to a condition based maintenance policy in order to preliminary assess its benefits and to understand the main variables that influence the overall approach performance. Moreover, an explanatory study was carried out to evaluate the possibility to introduce prognostic concepts into railway axle maintenance management.

It is argued that in order to assess completely the benefits of a CMB approach an integrated framework that integrate the technical issues, the maintenance scheduling and replacement decision policy and the spare part supply chain design is necessary. A linkage between low-level degradation-based sensor data with upper-level decision models, is necessary for improving the decision-making process.

The degradation Bayesian modeling framework presented in [**59**] for computing RULs of partially degraded components is presented. Since no available signals were available, the degradation signals from functioning components were artificially generated and then used to continuously/periodically update RUL distributions in real-time. The assumption made in this step is the exponential shape of the degradation pattern, condition that is often reached in most of the mechanical components These RUL distributions are used to compute, at each time step, the optimal scheduling and replacement times assuming a discontinuous component utilization, such as in the case of an aircraft LRU. The resulting replacement and scheduling policies are therefore driven by the underlying degradation process.

The results of several simulations were used to design a single-unit (S,1-S) spare parts supply chain. A comparison between different maintenance policies are then carried out. Simulations' results with different LT show a better exploitation of the component's life in a CBM scenario, resulting in an increased system availability with respect to a SM scenario. Besides, a certain degradation of performances and some misbehaviors are observed for high LT values. The main explanation is that in this condition the system is forced to schedule maintenance basing on an early and unreliable RUL estimation, since Bayesian

prediction needs a certain assessment time in order to reach high precision and accuracy. As for depot stock level, the related cost index follows a nonlinear trend, indicating an optimum for LT equal to 350 hrs and substantial savings with respect to scheduled maintenance scenario. Simulations in CBM scenarios, based on different LTs, shows a generally increase of the system availability and lower maintenance tasks frequency.

The opportunity to introduce prognostics maintenance policy into the railway axle maintenance management was also investigated. Through a reliable probabilistic crack growth model a comparison between a prognostic maintenance approach based on Bayesian probabilistic theory, a prognostic maintenance approach based on the same crack growth physical model and the classical preventive maintenance policy based on regular NDT was carried out. The probabilistic crack growth model considers the SIF as a random normal variable and a random load history derived from measured load spectra. The diagnostic-monitoring infrastructure precision was described by a size error, directly derived from the calibration curve of an ultrasonic NDT. Assuming the hypothesis introduced in chapter 4, the results suggests that further research should be conducted validating the approach proposed on a real case study. As matter of facts both the prognostic algorithms described guarantee an average absolute predictions errors lower than 50 % at 25% of the actual axle life. The later predictions guarantees lower prediction errors, approaching the 7% on average. Earlier predictions errors are generally lower for the Bayesian prognostic algorithm than those computed through the physical model. Whereas, for later predictions the physical model seem to provide more accurate RUL estimations. However, the gap between predictions error computed by the two models are, on average, comparable. The effect of the updating frequency and the size error on predictions errors in case of prognostic physical model algorithm scenario and therefore, on the overall approach performance (life exploited with a determined reliability threshold) is assessed as well. The results show that the higher the size error and the lower updating frequency the lower life exploited. However the effect of updating frequency and size error in terms of life exploited is limited till the maximum crack size threshold, derived from the error size of the diagnostic infrastructure, becomes lower than about 5 mm, i.e the crack size at which the crack growth rate significantly increases.

Generally speaking, a CBM approach needs a deep system/component knowledge. This need implies high investment costs to perform experimental

tests (high fixed costs). System/component knowledge in high safety requirement environments, such as in the aviation industry, has to be known before commissioning for obvious safety reasons. Low Accuracy PHM May Be Worse Than No PHM. Costs and the benefits resulting from a prognostic approach could be distributed differently across the actors involved, therefore an "integrator" that manages all the process is suggested or partnership between the main actors involved committed to share the investment costs. Moreover it is worth noting that a trade off exists between system usage pattern and the resulting benefits, higher usage allows a better return on investment but lowers t_{ADV} , i.e the main prognostic benefits driver.

After all these considerations, it is possible to sum up the results in the matrix displayed in Figure 74. Profitability of a PHM (CBM) approach can be thought as a function of two variables:

- Component criticality
- Easiness to acquire data of component's failure modes

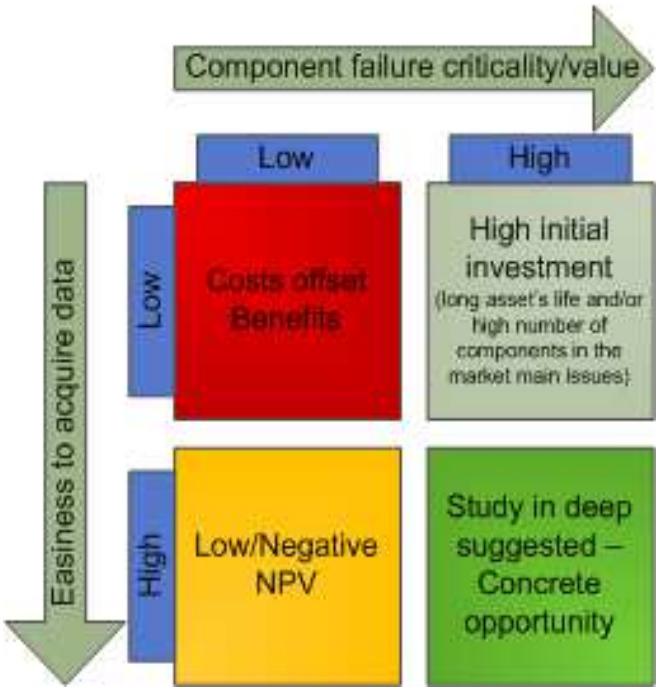

Figure 74: PHM applicability

Difficulties to describe and acquire data on the component' failure behavior imply high R&D costs while the components criticality and value can boos the benefits allowed by a PHM approach. The case in which a PHM approach is suggested is the case in which it is easy to acquire and data and knowledge on the component failure behavior and in which the component monitored and maintained is critical for the whole system availability and/or it has a very high value. In the other two situations further investigation aimed to better estimate the costs and the benefits involved is suggested.

6. References

[1] F.L. Lewis, M. Roemer, A. Hess and B. Wu G. Vachtsevanos, *Intelligent Fault Diagnosis and Prognosis for Engineering Systems*. New York: John Wiley & Sons Inc., 2006.

[2] A. Mehr, I. Tumer and W. Chen C. Hoyle, "On Quantifying Cost-Benefit of ISHM in Aerospace Systems," in *IEEE Aerospace Conference*, 2007, pp. 1-7.

[3] A.Hess and L.Fila B. Byer, "Writing a convincing cost benefit analysis to substantiate autonomic logistics," in *Proceedings of the IEEE Aerospace Conference*, vol. 6, Big Sky, MT, 2001, pp. 3095-3103.

[4] R. Abujamra, A.K.S. Jardine, D. Lin and D. Banjevic J. Lee, "An integrated platform for diagnostics, prognostics and maintenance optimization," in *The IMS '2004 International Conference on Advances in Maintenance and in Modeling, Simulation and Intelligent Monitoring of Degradations*, Arles, France, 2004.

[5] D. Lin and D. Banjevic K.S. A. Jardine, "A review on machinery diagnostics and prognostics implementing condition-based maintenance," *Mechanical Systems and Signal Processing*, vol. 20, pp. 1483–1510, 2006.

[6] B.J. Gilmartin, K.Bongort and A. Hess S.J. Engel, "Prognostics, The Real Issues Involved With Predicting Life Remaining," in *Proceedings IEEE Aerospace Conference*, vol. 6, 2000, pp. 457-469.

[7] G.Yang K.Yang, "Degradation reliability assessment using severe critical values," vol. 5, pp. 85-95, 1998.

[8] A.H. Christer, "Operational research applied to industrial maintenance and replacemen," *Developments in Operational Research*, pp. 31-58, 1984.

[9] N.S Arumugadasan M.H Monplaisir, "Maintenance decision support: analyzing crankcase lubricant condition using markov process modeling," *Journal of the Operational Research Society*, vol. 45, pp. 509-518, 1994.

[10] R.Dekker F.P.A Coolen, "Analysis of a 2-phase model for optimization of condition monitoring intervals," *IEEE Transactions on Reliability*, vol. 55, pp. 505-511, 1995.

[11] J.M. van Noortwijk M.J. Kallen, "Optimal periodic inspection of a deterioration process with sequential condition states," *International Journal of Pressure Vessels and Piping*, vol. 83, no. 4, pp. 249-255, 2006.

[12] K.S Trivedi D.Chen, "Optimization for condition-based maintenance with semi-Markov decision process," *Reliability Engineering and System Safety*, vol. 90, no. 1, pp. 25-29, 2005.

[13] H.M. Mitchell, P.S Ansell K.D. Glazebrook, "Index policies for the maintenance of a collection of machines by a set of repairmen," *European Journal of Operational Research*, vol. 165, no. 1, pp. 267-284, 2005.

[14] J. Knezevic H. Saranga, "Reliability prediction for condition-based maintained systems," *Reliability Engineering and System Safety*, vol. 71, no. 2, pp. 219-224, 2001.

[15] A. Loskiewicz-Buczak and R.E Uhrig I.E Alguindigue, "Monitoring and diagnosis of rolling element bearings using artificial neural networks," *IEEE Transactions on Industrial Electronics*, vol. 40, no. 2, pp. 209-217,

1993.

[16] V.K Jain V.K., and Rama Rao Ch V.V., S.K Choudhury, "On-line Monitoring of Tool Wear in Turning Using a Neural Network," *International Journal of Machine Tools & Manufacture*, vol. 39, no. 3, pp. 489-504, 1999.

[17] J.R McDonald C.Booth, "The Use of Artificial Neural Networks for condition Monitoring of Electrical Power Transformers," *Neurocomputing*, vol. 23, pp. 97-109, 1998.

[18] D.J Evan and B.Jones D. Bansal, "A real-time predictive maintenance system for machine systems," *International Journal of Machine Tools & Manufacture*, vol. 44, pp. 759-766, 2004.

[19] M.D. Pandey S.K. Sinha, "Probabilistic neural network for reliability assessment of oil and gas pipelines," *Computer-Aided Civil and Infrastructure Engineering*, vol. 17, no. 5, pp. 320-329, 2002.

[20] H.J Shyur J.T Luxhoj, "Comparison of proportional hazards models and neural networks for reliability estimation".

[21] D.Banjevic, and A.K.S Jardine D.Lin, "Using principal components in a proportional hazards model with applications in condition-based maintenance," *Journal of the Operational Research Society*, vol. 57, no. 8, pp. 910-919, 2006.

[22] D.R Cox, "Regression models and life tables," *Journal of the Royal Statistical Society, B*, vol. 34, pp. 187-220, 1972.

[23] M.Anderson A.K.S. Jardine, "Use of concomitant variables for reliability estimation," *Maintenance Management International*, vol. 5, no. 2, pp. 135-140, 1985.

[24] P.M Anderson and D.S Mann A.K.S. Jardine, "Application of the Weibull proportional hazards model to aircraft and marine engine failure data," *Quality Reliability Engineering International*, vol. 3, no. 2, pp. 77-82, 1987.

[25] P. Ralston, N. Reid and J. Stafford A.K.S. Jardine, "Proportional hazards analysis of diesel engine failure data," *Quality & Reliability Engineering International*, vol. 5, no. 3, pp. 207-216, 1989.

[26] V. Makis and A.K.S Jardine Y. Zhan, "Adaptive Model for Vibration Monitoring of Rotating Machinery Subject to Random deterioration," *Journal of Quality in Maintenance Engineering*, vol. 9, no. 4, pp. 351-375, 2003.

[27] U. Westber D. Kumar, "Maintenance scheduling under age replacement policy using proportional hazars model and TTT-plotting," *European Journal of Operational Research*, vol. 99, pp. 507-515, 1997.

[28] B.B. Fawzi, D.F. Percy and H.E Ascher K.A.H. Kobbacy, "A full history proportional hazards model for preventive maintenance scheduling," *Quality & Reliability Engineering International*, vol. 13, pp. 187-198, 1997.

[29] V. Makis, D. Banjevic, D. Braticevic and M. Ennis A.K.S Jardine, "A decision optimization model for condition-based maintenance," *Journal of Quality in Maintenance Engineering*, vol. 4, no. 2, pp. 115-121, 1998.

[30] S.Yacout and M.S Ouali A. Ghasemi, "Optimal condition based maintenance with imperfect information and the proportional hazards model," *International Journal of Production Research*, vol. 45, no. 4, pp. 989-1012, 2007.

[31] K.R.M Rao P.V.N Prasad, "Reliability models of repairable systems considering the effect of operating conditions," in *Proceedings of the Annual Reliability and Maintainability Symposium*, 2002, pp. 503-510.

[32] H.J. Shyur J.T Luxhoj, "Comparison of proportional hazards models and neural networks for reliability estimation," *Journal of Intelligent Manufacturing*, vol. 8, no. 3, pp. 227-234, 1997.

[33] J.L Coetzee, D. Banjevic, A.K.S. Jardine and V. Makis P.J. Vlok, "Optimal component replacement decisions using vibration monitoring and the proportional-hazards model," *Journal of the Operational Research Society*, vol. 53, no. 2, pp. 193-202, 2002.

[34] Modeling accelerated life testing based on mean, "Modeling accelerated life testing based on mean residual life," *International Journal of Systems Science*, vol. 36, no. 11, pp. 689-696, 2005.

[35] N.Z. Gebraeel A.H. Elwany, "Sensor-driven prognostic models for equipment replacement and spare parts inventory," *IIE Transactions (Institute of Industrial Engineers)*, vol. 40, no. 7, pp. 629-639.

[36] M. Hamada and C. Chiao S.Tseng, "Using degradation data to improve fluorescent lamp reliability," *Journal of Quality Technology*, vol. 27, pp. 363-369, 1995.

[37] A.Jeang K.Yang, "Statistical surface roughness checking procedure based on a cutting tool wear," *Journal of Manufacturing Systems*, vol. 13, no. 1, pp. 1-8, 1994.

[38] B. Roylance and J.Moore K. B. Goode, "Development of a predictive model for monitoring condition of a hot strip mill," in *IoM Steel Division Annual Meeting N°2*, vol. 25, 1998, pp. 42-46.

[39] D.C Swanson, "A general prognostic tracking algorithm for predictive maintenance," in *IEEE Aerospace Conference Proceedings*, vol. 6, 2001, pp. 2971- 2977.

[40] A.Hoyland K.A Doksum, "Models for variable-stress accelerated life testing experiments based on Wiener processes and the inverse Gaussian distribution," *Technometrics*, vol. 34, no. 1, pp. 74-82, 1992.

[41] G. Whitmore, "Estimating degradation by a Wiener diffusion process subject to measurement error," *Lifetime Data Analysis*, vol. 1, pp. 307-319, 1995.

[42] J.Lee, "Measurement of machine performance degradation using a neural network model," *Computer Industry*, vol. 30, no. 3, pp. 193-209, 1996.

[43] K.Nezu Y.Shao, "Prognosis of remaining bearing life using neural networks," *Proceedings of the Institution of Mechanical Engineers, Part I: Journal of Systems and Control Engineering*, vol. 214, no. 3, pp. 217-230, 2000.

[44] M. Lawley N.Z. Gebraeel, "Life distributions from component degradation signals: a neural net approach," *IEEE transactions on automation science*

and engineering, vol. 5, no. 1, pp. 153-163, 2008.

[45] P. Mohan R.B Chinnam, "Online reliability estimation of physical systems using neural networks and wavelets," *Journal of Smart Engineering System Design*, vol. 4, no. 4, pp. 253-264, 2002.

[46] W.Meeker C.Lu, "Using degradation measures to estimate a time-to-failure distribution," *Technometrics*, vol. 25, no. 2, pp. 161-174, 1993.

[47] M. Lawley, R. Li, and J. K. Ryan N. Gebraeel, "Life distributions from component degradation signals: A Bayesian approach," *IIE Trans.*, vol. 37, no. 6, pp. 543–557, 2005.

[48] L. Bennett, C. Ligetti, J. Banks and S. Nestler J. Hines, "Cost-Benefit Analysis Trade-Space Tool as a Design-Aid for the U.S. Army Vehicle Health Management System (VHMS) Program," in *Annual Conference of the Prognostics and Health Management Society*, San Diego, 2009, pp. 1-18.

[49] Z. Williams, "Benefits of IVHM: an analytical approach," in *Proceedings of the 2006 IEEE Aerospace Conference*, Big. Sky, Montana, 2006, pp. 1-9.

[50] M.E Malley, "A Methodology for Simulating the Joint Strike Fighter's (JSF) prognostics and Health Management System," 2001.

[51] A. Mehr, I. Tumer and W. Chen C. Hoyle, "On quantifying cost-benefit of ISHM in aerospace systems," in *ASME 2007 International Design Engineering Technical Conferences*, 2007, pp. 1-10.

[52] D.A. Murphy R.M. Kent, "Health Monitoring System Technology Assessments Ð Cost Benefits Analysis," Hampton, Virginia, 2000.

[53] K.L Feldman, S.Ghelam, P. Sandborn, M.Glade and B.Foucher E. Scanff, "Life cycle cost impact of using prognostic health management (PHM) for helicopter avionics," *Microelectronics Reliability*, vol. 47, pp. 1857-1864, 2007.

[54] D.J Haas C.G Schaefer Jr, "A Simulation Model To Investigate the Impact of Health and Usage Monitoring Systems (HUMS) on Helicopter Operations and Maintenance," in *Proceedings American Helicopter Society 58˚th Annual Forum*, 2002.

[55] N.Z. Gebraeel K.A. Kaiser, "Predictive maintenance management using sensor-based degradation models," *IEEE Transactions on Systems, Man, and Cybernetics Part A:Systems and Humans*, vol. 39, no. 4, pp. 840-849, 2009.

[56] J.J Luna, "Metrics, Models, and Scenarios for Evaluating PHM Effects on Logistics Support," in *Proceedings PHM Conference 2009*, San Diego.

[57] N.K.Srinivasan S.K.Upadhya, "Availability of weapon systems with multiple failures and logistic delays," *International Journal of Quality & Reliability Management*, vol. 20, no. 7, pp. 836-846.

[58] M.Bazargan, and R.N. McGrath P Gupta, "Simulation Model for Aircraft Line Maintenance," in *Proceedings Planning Reliability and Maintainability Symposium*, 2003.

[59] J. Pan N. Gebraeel, "Prognostic Degradation Models for Computing and Updating Residual Life Distributions in a Time-Varying Environment,"

IEEE Transaction on Reliability, vol. 57, no. 4, pp. 539-549, 2008.

[60] J. Lee, J. Lin and G.Yu H. Qiu, "Robust performance degradation assessment methods for enhanced rolling element bearing prognostics," *Advanced Engineering Informatics*, vol. 17, no. 3-4, p. 2003.

[61] W.Q. Meeker C.J. Lu, "Using Degradation Measures to Estimate a Time-to-Failure Distribution," *American Society for Quality*, vol. 35, no. 2, pp. 161-174, 1993.

[62] A. F. M. Smith D. V. Lindley, "Bayes estimates for the linear model," *Journal of the Royal Statistical Society, Series B, Statistical*, vol. 34, no. 1, pp. 1–41, 1972.

[63] M Ahmad and T.S Mirza A.K Sheikh, "Renewal Analysis Using Bernstein Distribution," *Reliability Engineering*, vol. 5, pp. 1-19, 1983.

[64] K.A. Kaiser N.Z Gebraeel, "Predictive Maintenance Management Using Sensor-Based Degradation Models," *IEEE Transactions on Systems, Man, and Cybernetics, Part A: Systems and Humans*, vol. 39, no. 4, pp. 840-849, 2009.

[65] J.Tierno A.Khalak, "Influence of prognostic health management on logistic supply chain," in *Proceedings of the 2006 American Control Conference*, Minneapolis, 2006, pp. 3737-3742.

[66] K.F. Simpson Jr, "In-Process Inventories," *Operations Research*, vol. 6, no. 6, pp. 863-873, 1958.

[67] S.P.Willems S.C Graves, "Strategic Safety Stock Placement In Supply Chains," in *Proceedings of the 1996 MSOM Conference*, 1996.

[68] EN13103, "Railway applications – wheelsets and bogies – non powered axles – design method," 2001.

[69] M. Vormwald, C. Andersch U. Zerbst, "The development of a damage tolerance concept for railway components and its demonstration for a railway axle," *Engineering Fracture Mechanics*, vol. 72, pp. 209–239, 2005.

[70] D.S. Hoddinot, "Railway axle failure investigations and fatigue crack growth monitoring of an axle," *Proceedings of the Institution of Mechanical Engineers, Part F: Journal of Rail and Rapid Transit*, vol. 218, pp. 283–292, 2004.

[71] D.H. Stone C.P. Lonsdale, "North american axle failure experience," *Proceedings of the Institution of Mechanical Engineers, Part F: Journal of Rail and Rapid Transit*, vol. 218, no. 4, pp. 293–298, 2004.

[72] S. Beretta M. Carboni, "Effect of probability of detection upon the definition of inspection intervals for railway axles," *Proceedings of the Institution of Mechanical Engineers, Part F: Journal of Rail and Rapid Transit*, vol. 221, no. 3, pp. 409-417, 2007.

[73] K. Madler, H. Hintze U. Zerbst, "Fracture mechanics in railway applications—an overview," *Engineering Fracture Mechanics*, vol. 72, pp. 163–194, 2005.

[74] S.Hillmansen R.A. Smith, "A brief historical overview of the fatigue of railway axles," *Proceedings of the Institution of Mechanical Engineers,*

Part F: Journal of Rail and Rapid Transit, vol. 218, no. 4, pp. 267-277, 2004.

[75] A.S.Kiremidjianb K.Ortiza, "Stochastic modeling of fatigue crack growth," *Engineering Fracture Mechanics*, vol. 29, no. 3, pp. 317-334, 1988.

[76] B.M. Hillberry, P.K.Goel D.A. Virkler, "The statistical nature of fatigue crack propagation," *ASME, Transactions, Journal of Engineering Materials and Technology*, vol. 101, pp. 148-153, 1979.

[77] F. Kozin J.L Bogdanoff, *Probabilistic models of cumulative damage*. New York: John Wiley & Sons, 1985.

[78] M. Carboni S. Beretta, "Experiments and stochastic model for propagation lifetime of railway axles," *Engineering Fracture Mechanics*, vol. 73, pp. 2627–2641, 2006.

[79] Anonymus, Fracture Mechanics and Fatigue Crack Growth 4.2, 2006.

[80] M.Carboni S.Beretta, "Simulation of fatigue crack propagation in railway axles," *J ASTM Int*, vol. 2, no. 5, pp. 1-14, 2005.

[81] M. Carboni, S. Cantini, A. Ghidini S. Beretta, "Application of fatigue crack growth algorithms to railway axles and comparison of two steel grades," *Proceedings of the Institution of Mechanical Engineers, Part F: Journal of Rail and Rapid Transit*, vol. 218, no. 4, 2004.

[82] M.Carboni S.Beretta, "Rotating vs. plane bending for crack growth in railway axles," in *ESIS-TC24 Meeting*, Geesthacht, 2005.

[83] M. Madia, M.Schoedel and U.Zerbst S.Beretta, "SIF solutions for cracks at notches under rotating bending," in *Proceedings of the 16th European Conference on Fracture (ECF16)*, Alexandropoulos, 2006.

[84] E. Gassner, "Performance fatigue testing with respect to aircraft design," in *Fatigue in Aircraft Stuctures*. New York: Academic Press, 1956.

[85] J. Schijve, *Fatigue of structures and materials*. Dordrecht: Kluwer Academic Publishers, 2001.

[86] J. Celaya, E.Balaban, K. Goebel, B. Saha, S. Saha, and M. Schwabacher A.Saxena, "Metrics for Evaluating Performance of Prognostic Techniques," in *International Conference on prognostics and health management* , Denver, CO, 2008, pp. 1-17.

7. Appendix

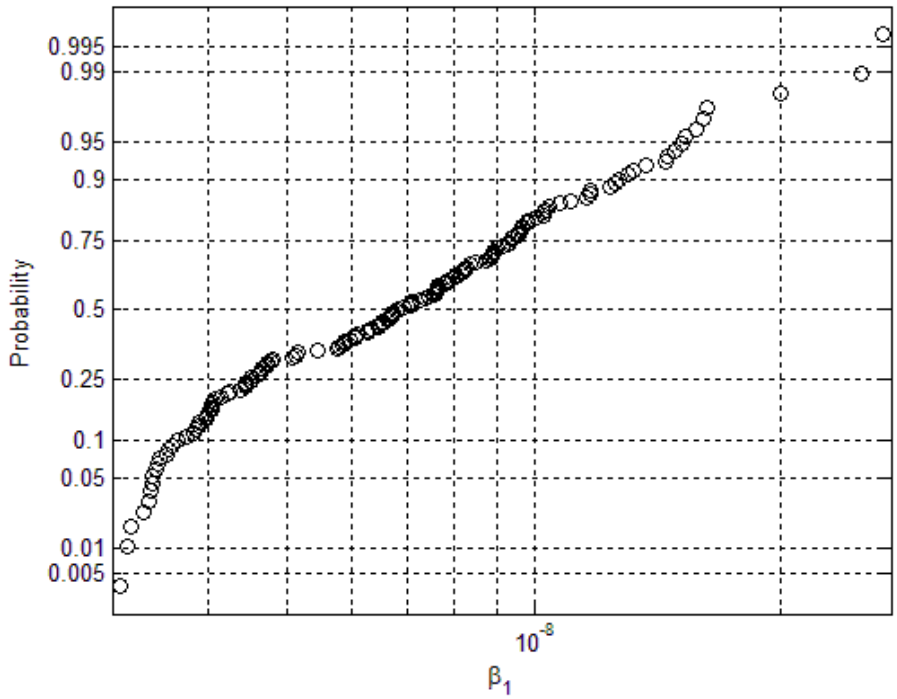

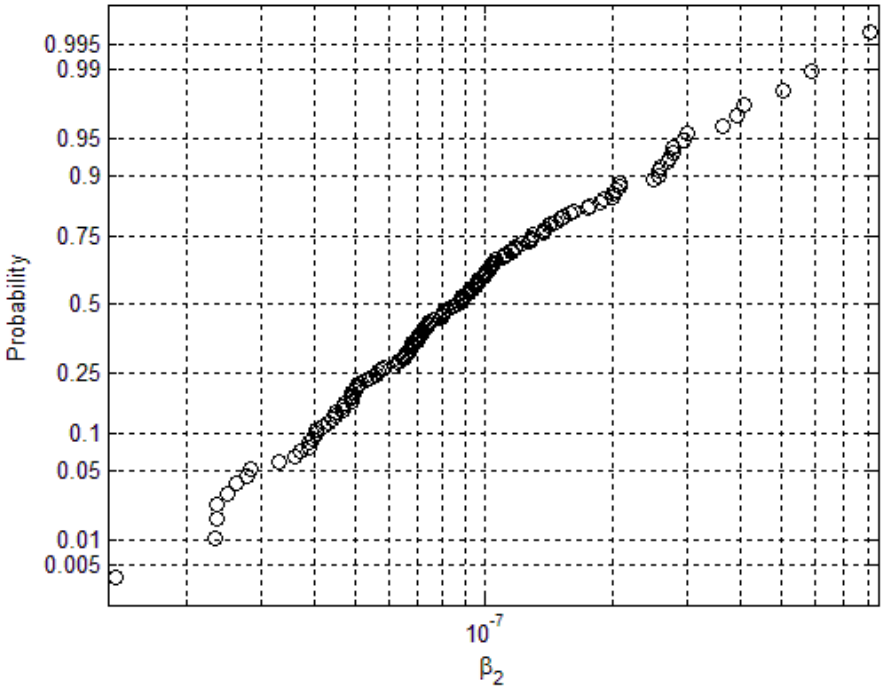
0.995
0.99
0.95
0.9
0.75
0.5
0.25
0.1
0.05
0.01
0.005
Probability
10^-7
β2

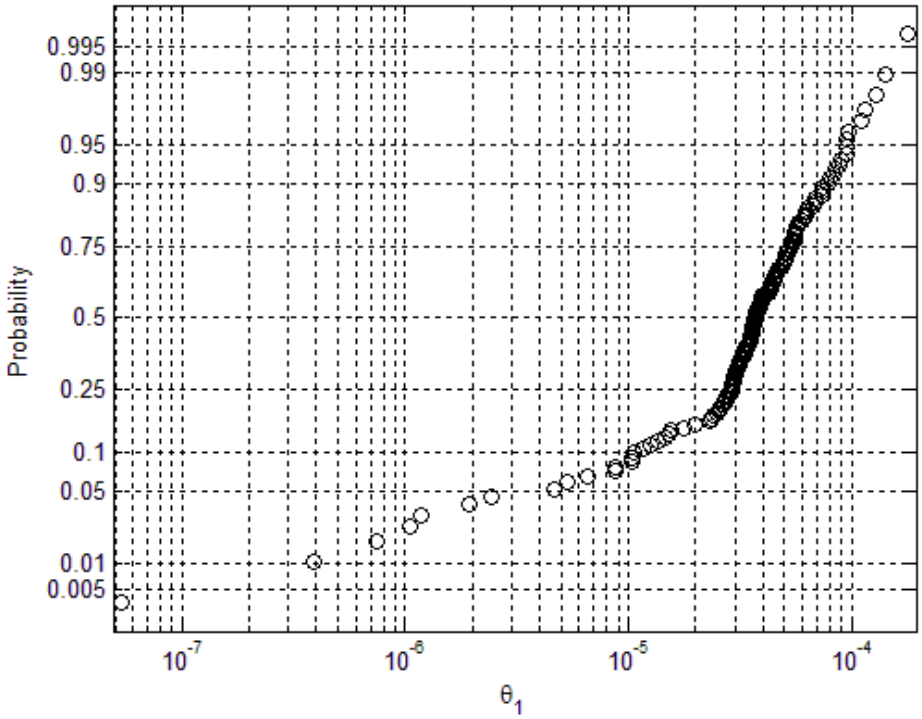
0.995
0.99
0.95
0.9
0.75
0.5
0.25
0.1
0.05
0.01
0.005
Probability
10^-7
10^-6
10^-5
10^-4
θ1

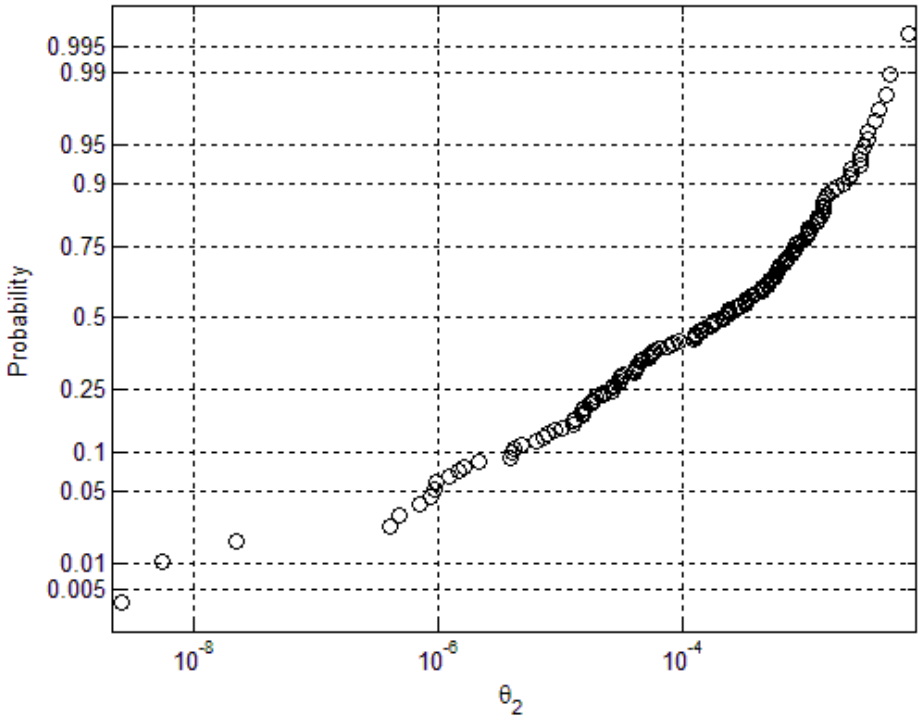
0.995
0.99
0.95
0.9
0.75
0.5
0.25
0.1
0.05
0.01
0.005
Probability
10^-8
10^-6
10^-4
θ2

C1[10]

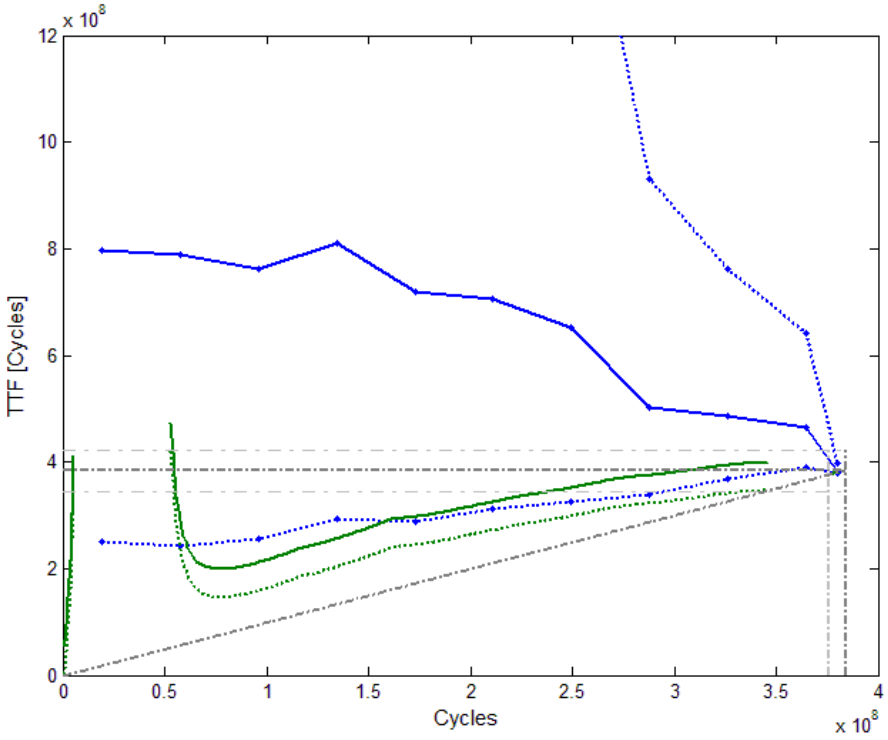

[10] Blue line: Physical model TTF estimation with confidence bounds (dotted)

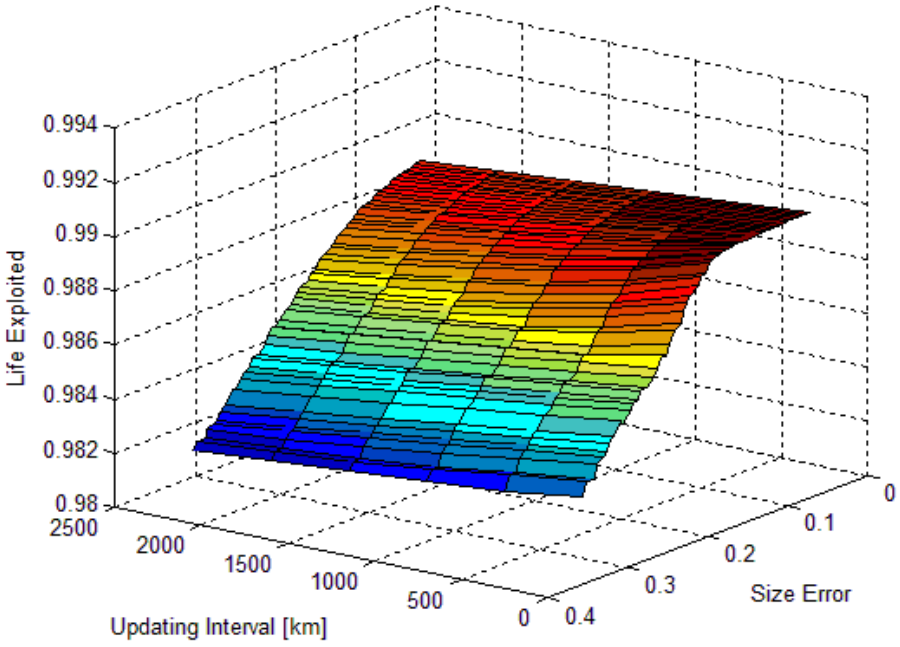

Green Line: Bayesian model TTF estimations with lower confidence bound (dotted)

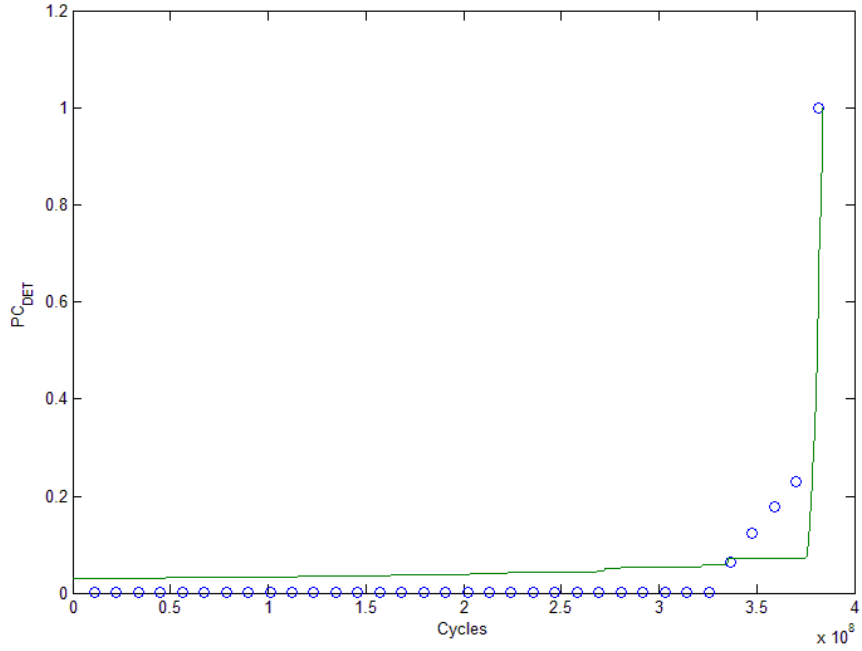
1.2
1
0.8
0.6
0.4
0.2
0
PC_{DET}
0
0.5
1
1.5
2
2.5
3
3.5
4
Cycles
x 10^8

C2

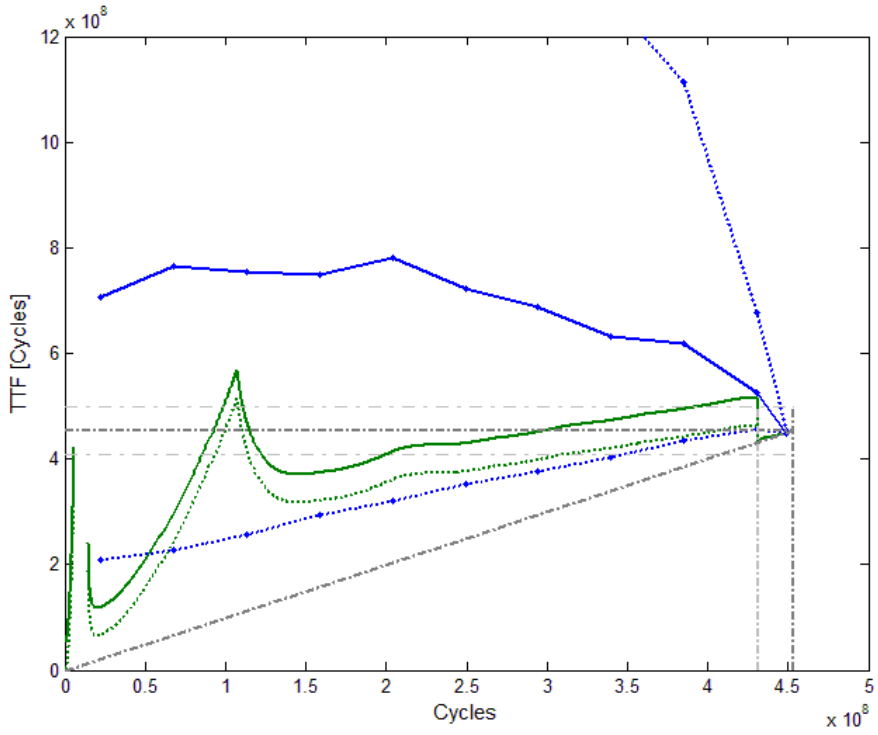
x 10^8
12
10
8
6
4
2
0
TTF [Cycles]
0
0.5
1
1.5
2
2.5
3
3.5
4
4.5
5
Cycles
x 10^8

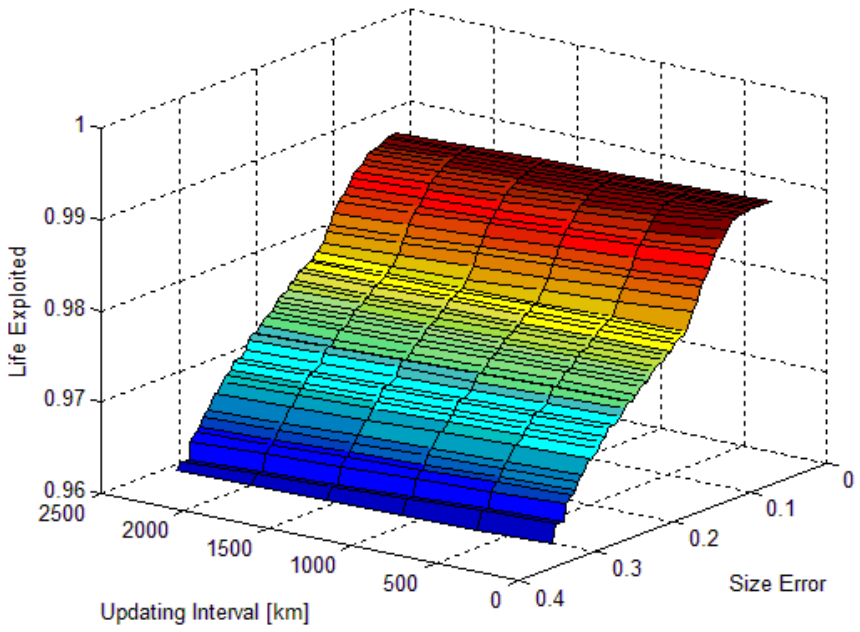
1
0.99
0.98
0.97
0.96
Life Exploited
2500
2000
1500
1000
500
0
Updating Interval [km]
0
0.1
0.2
0.3
0.4
Size Error

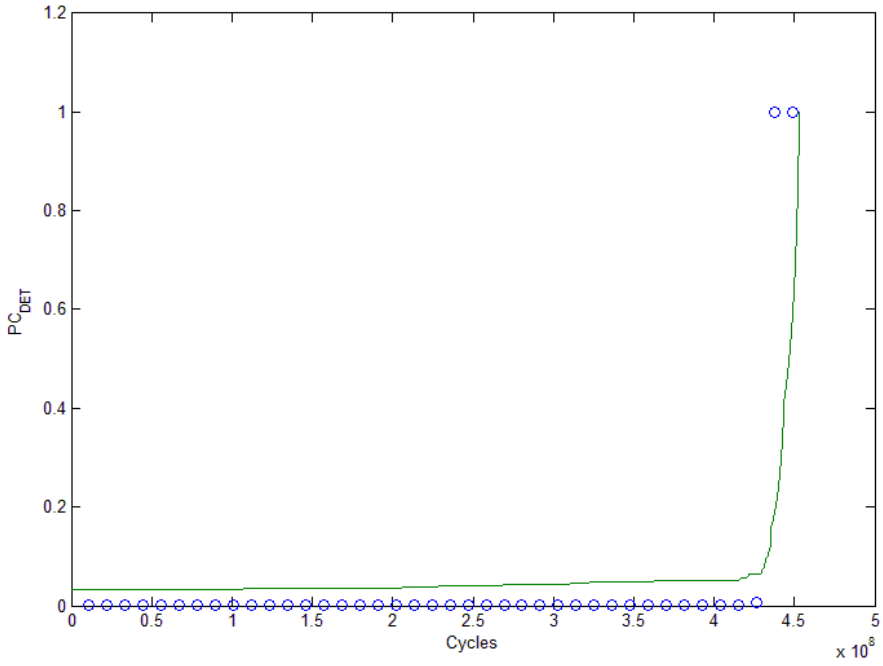
1.2
1
0.8
0.6
0.4
0.2
0
PC_DET
0
0.5
1
1.5
2
2.5
3
3.5
4
4.5
5
Cycles
x 10^8

C3

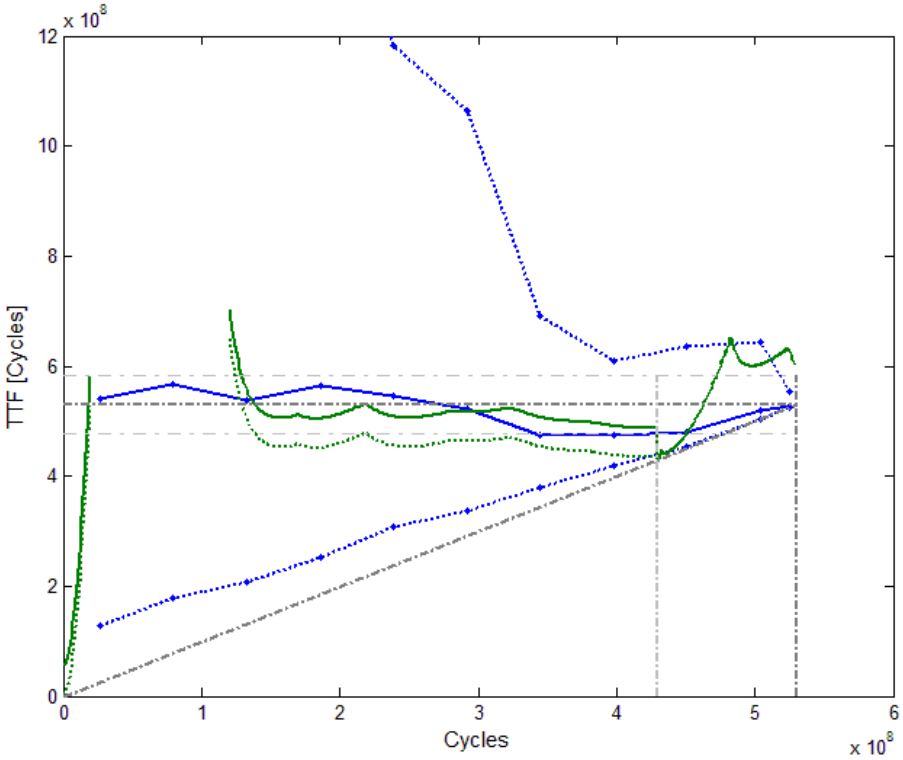

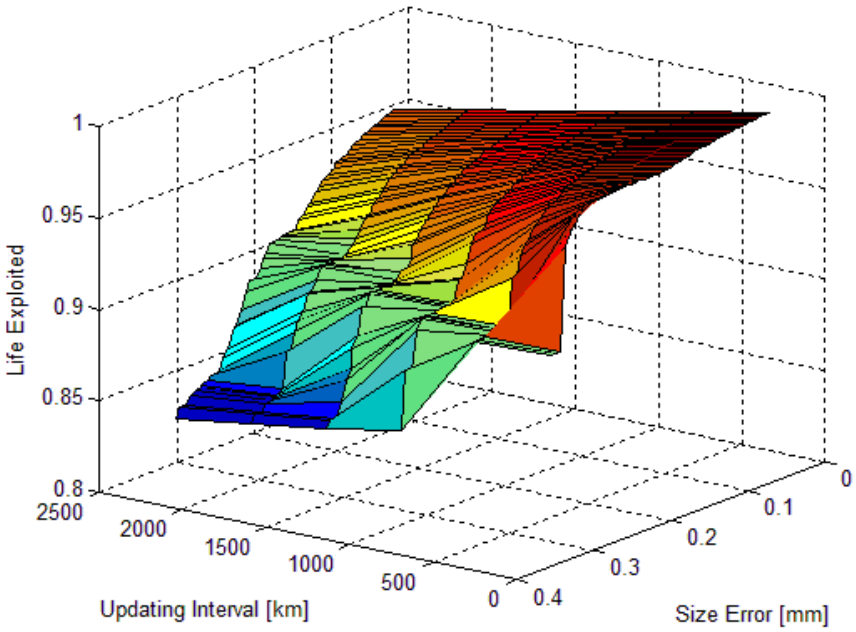
Life Exploited
1
0.95
0.9
0.85
0.8
2500
2000
1500
1000
500
0
Updating Interval [km]
0
0.1
0.2
0.3
0.4
Size Error [mm]

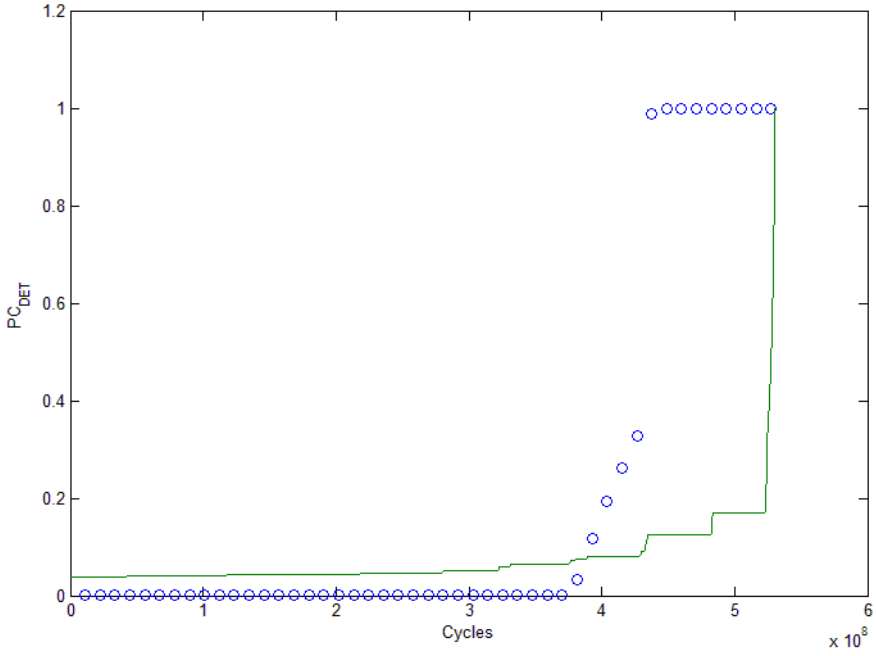
1.2
1
0.8
0.6
0.4
0.2
0
PC_DET
0
1
2
3
4
5
6
Cycles
x 10^8

C4

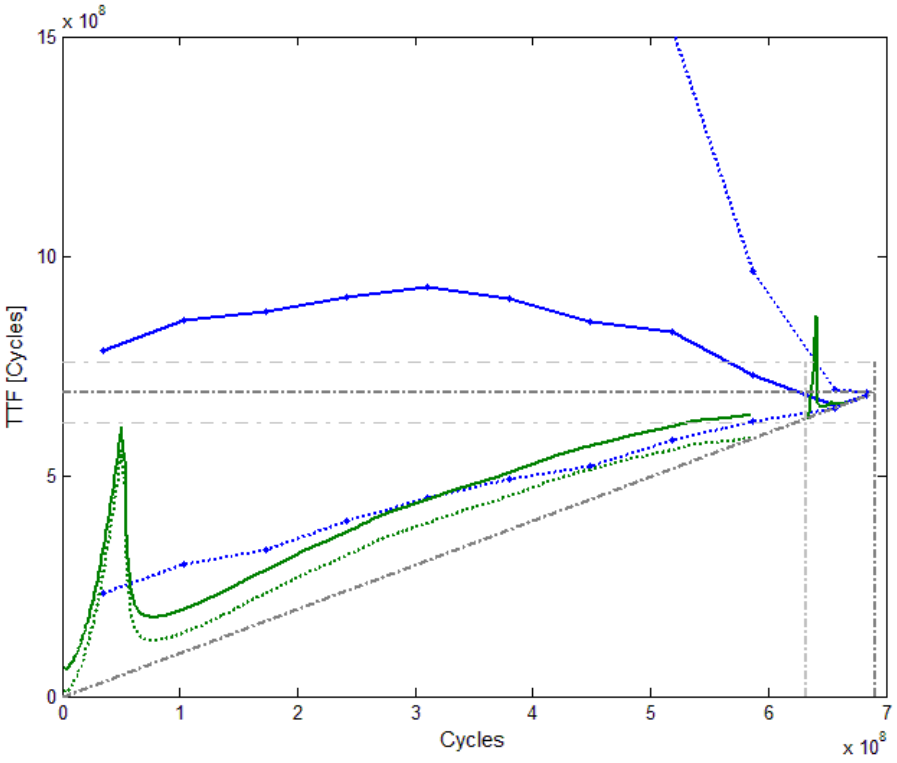

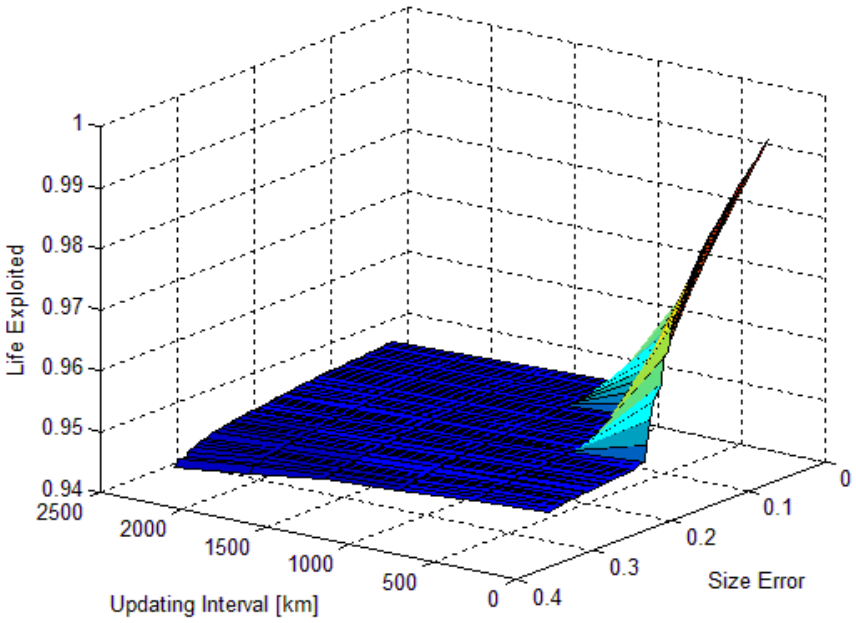
Life Exploited
1
0.99
0.98
0.97
0.96
0.95
0.94
2500
2000
1500
1000
500
0
Updating Interval [km]
0
0.1
0.2
0.3
0.4
Size Error

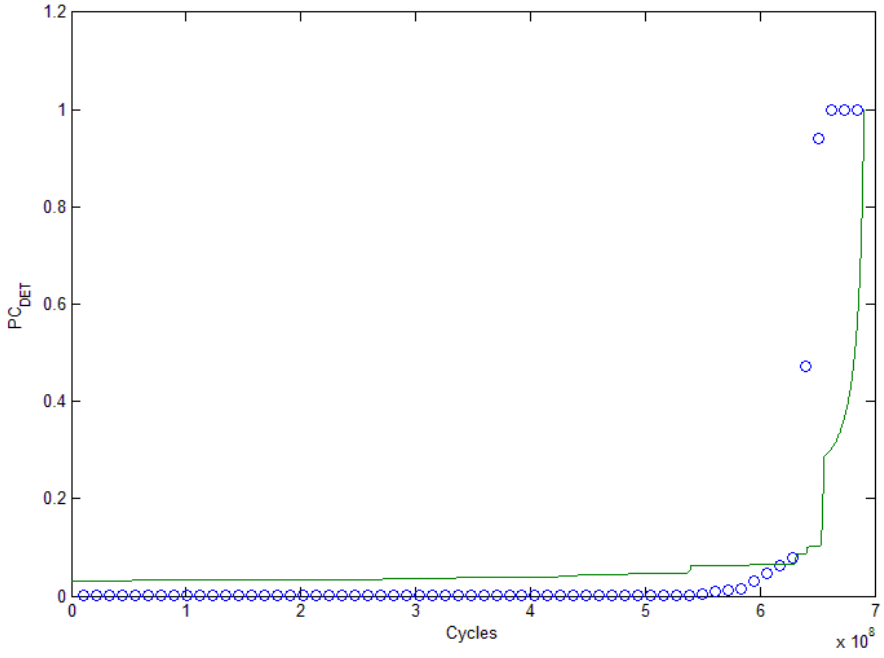
1.2
1
0.8
0.6
0.4
0.2
0
PC_DET
0
1
2
3
4
5
6
7
Cycles
x 10^8

C5

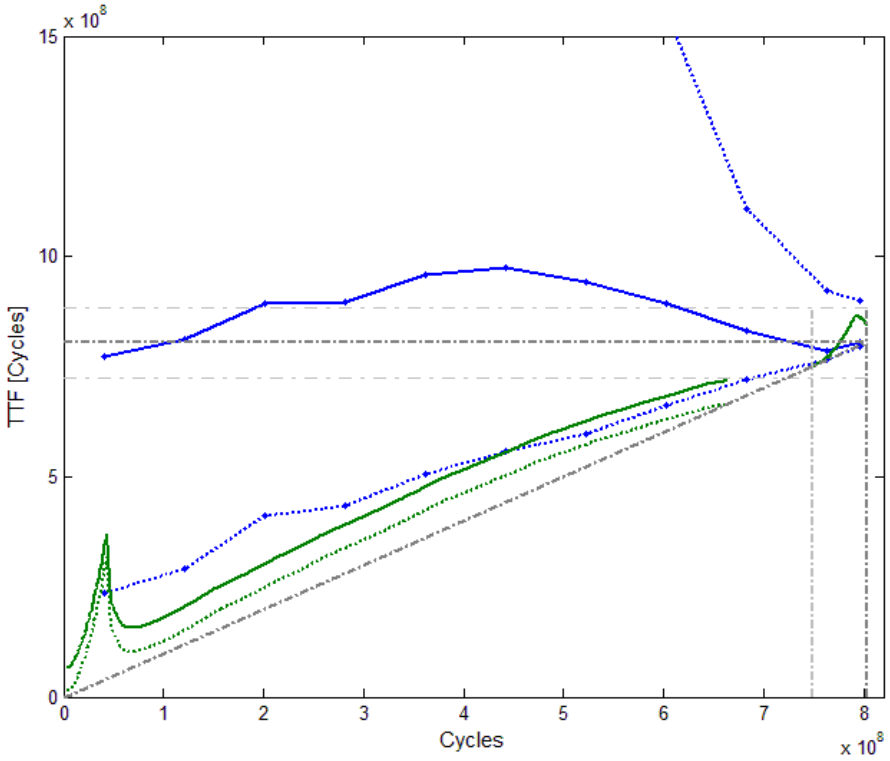

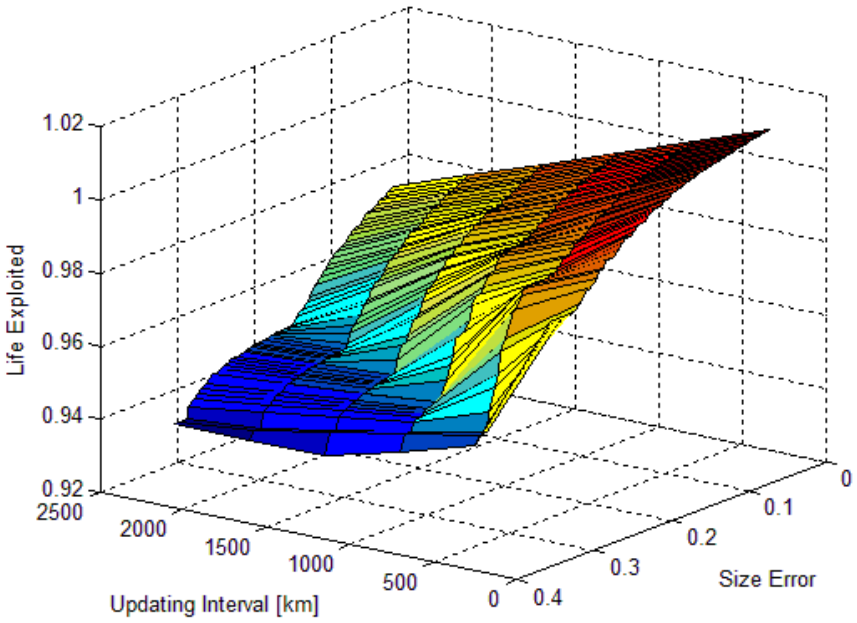
Life Exploited
1.02
1
0.98
0.96
0.94
0.92
2500
2000
1500
1000
500
0
Updating Interval [km]
0
0.1
0.2
0.3
0.4
Size Error

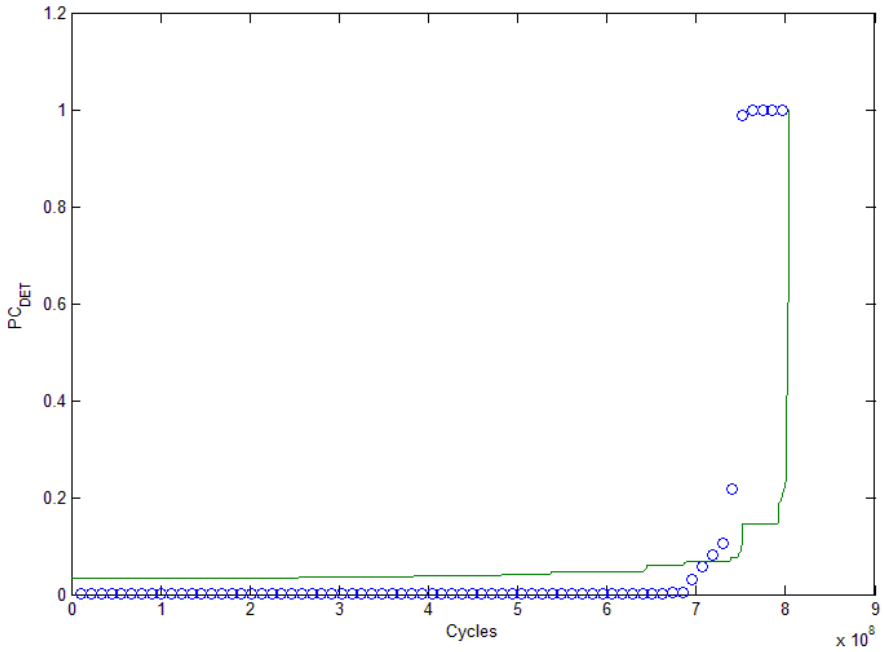
PC_DET
1.2
1
0.8
0.6
0.4
0.2
0
0
1
2
3
4
5
6
7
8
9
Cycles
x 10^8

C6

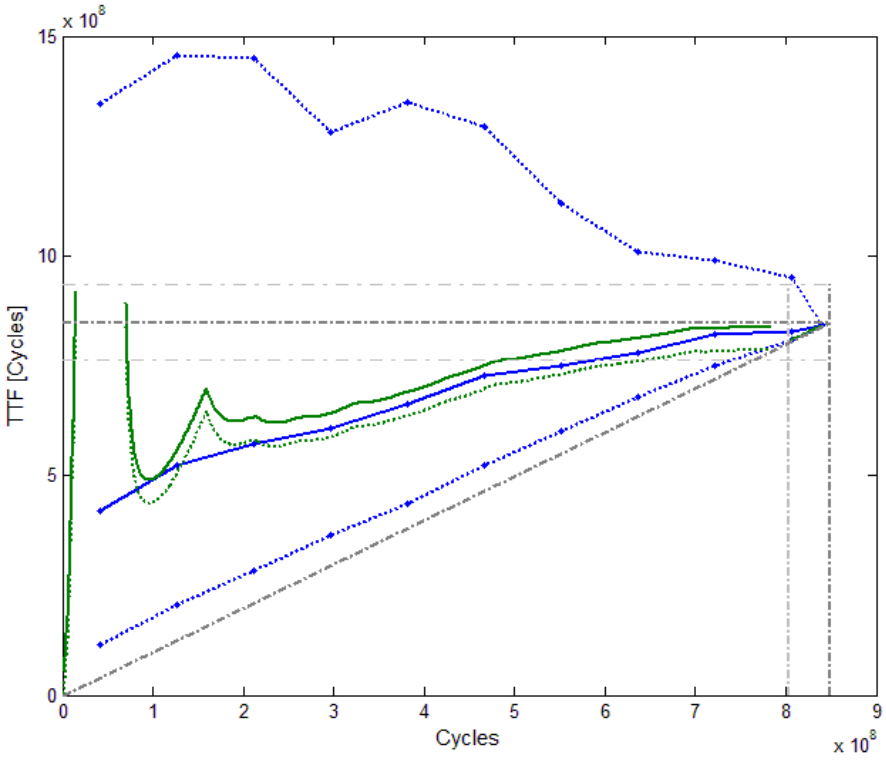

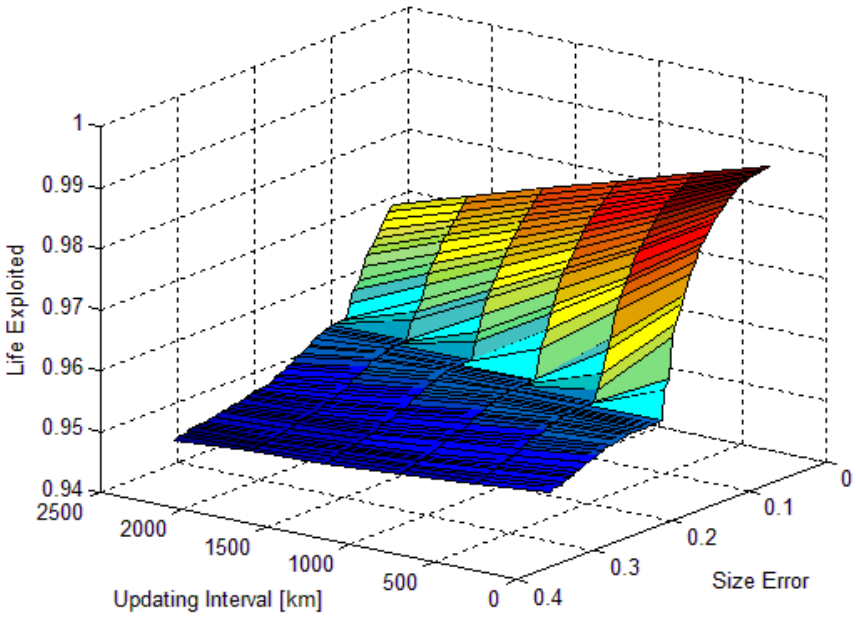
Life Exploited
1
0.99
0.98
0.97
0.96
0.95
0.94
2500
2000
1500
1000
500
0
Updating Interval [km]
0
0.1
0.2
0.3
0.4
Size Error

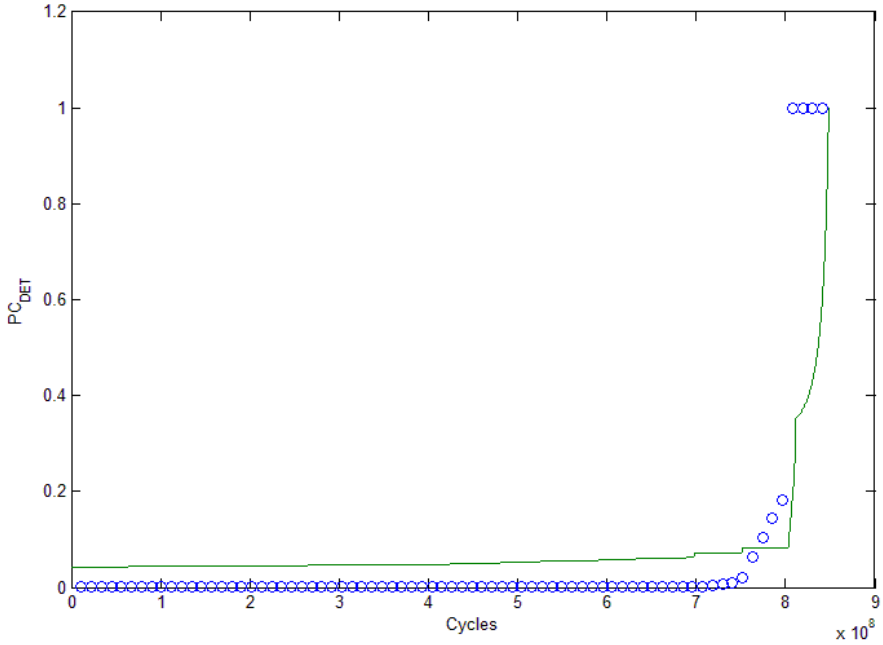
1.2
1
0.8
0.6
0.4
0.2
0
PC_DET
0
1
2
3
4
5
6
7
8
9
Cycles
x 10^8

C7

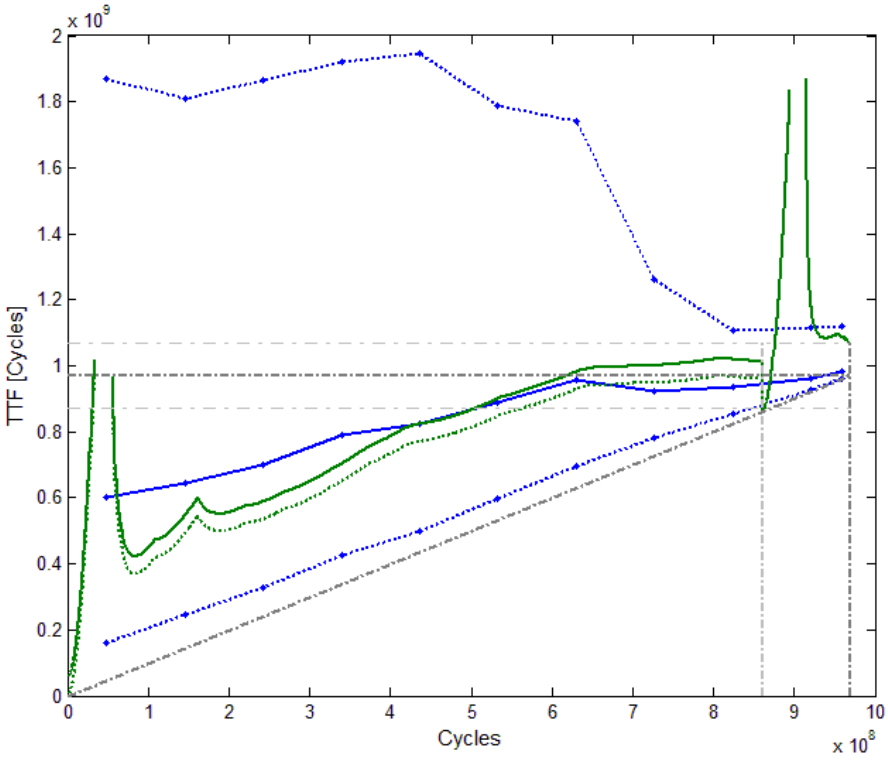
x 10^9
2
1.8
1.6
1.4
1.2
1
0.8
0.6
0.4
0.2
0
TTF [Cycles]
0
1
2
3
4
5
6
7
8
9
10
Cycles
x 10^8

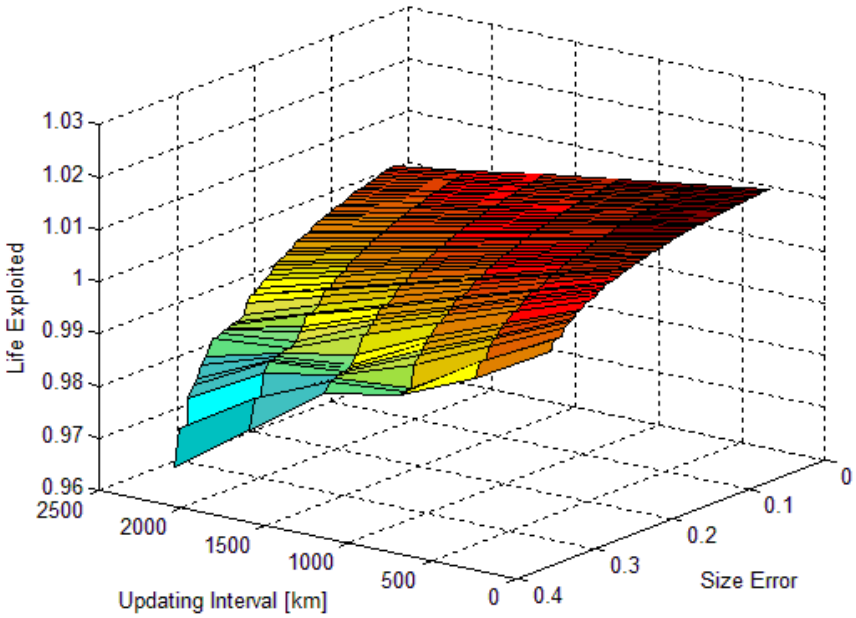
Life Exploited
1.03
1.02
1.01
1
0.99
0.98
0.97
0.96
2500
2000
1500
1000
500
0
Updating Interval [km]
0
0.1
0.2
0.3
0.4
Size Error

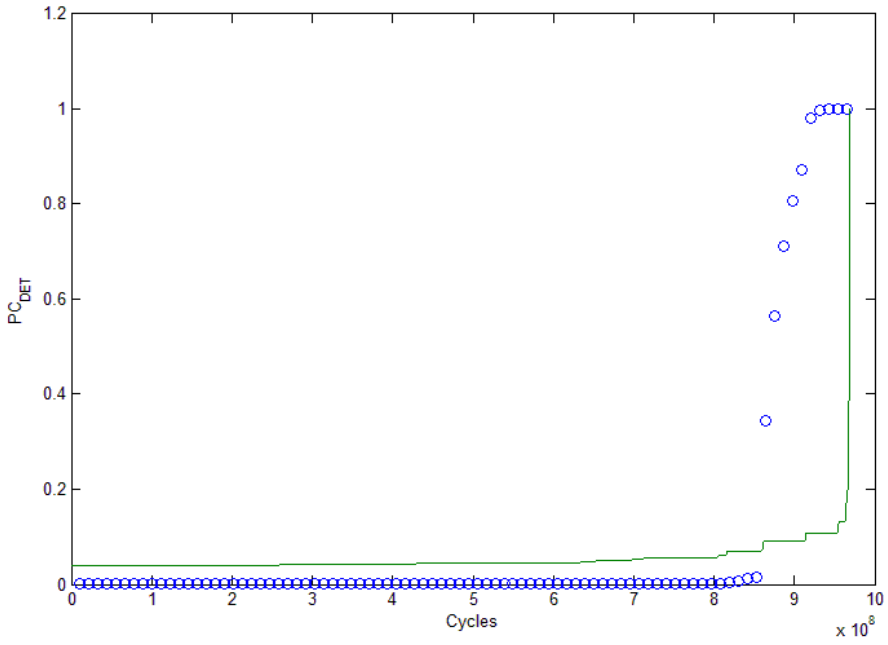
PC_DET
1.2
1
0.8
0.6
0.4
0.2
0
0
1
2
3
4
5
6
7
8
9
10
Cycles
x 10^8

C8

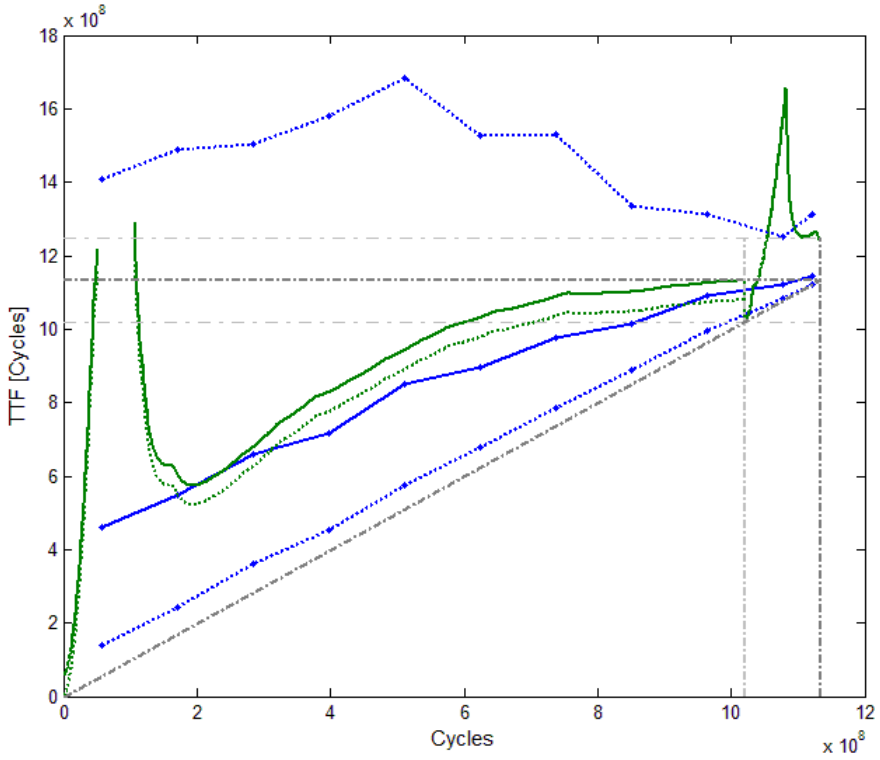

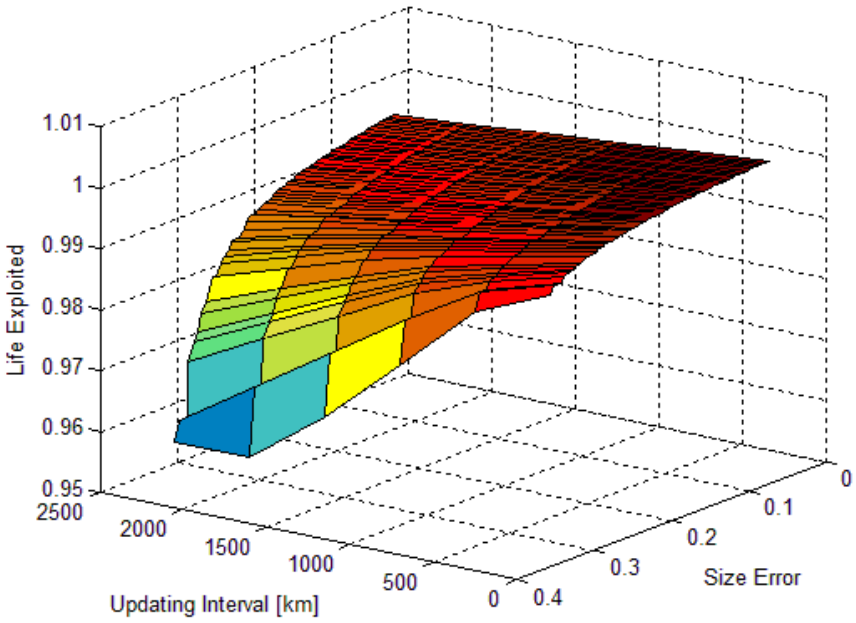
Life Exploited
1.01
1
0.99
0.98
0.97
0.96
0.95
2500
2000
1500
1000
500
0
Updating Interval [km]
0
0.1
0.2
0.3
0.4
Size Error

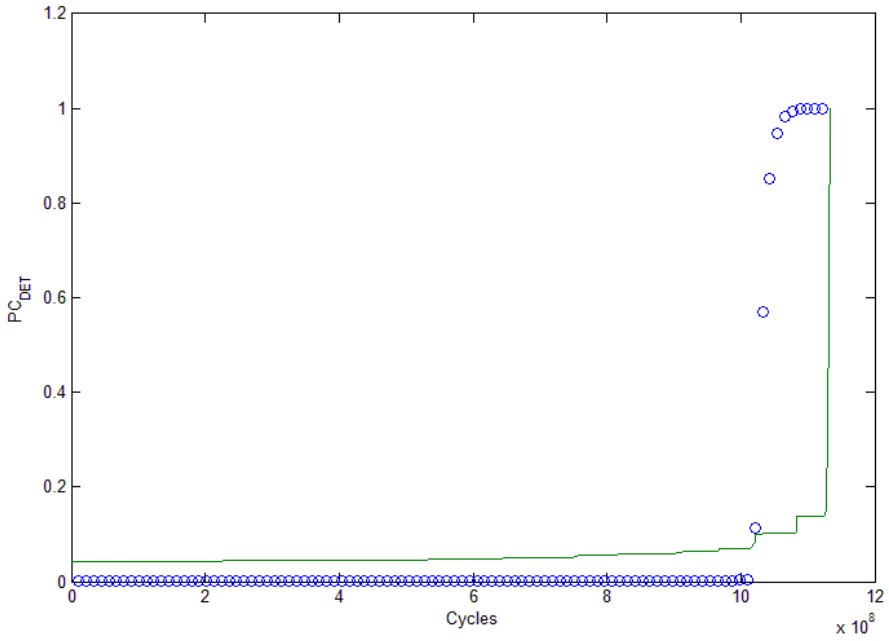
PC_DET
1.2
1
0.8
0.6
0.4
0.2
0
0
2
4
6
8
10
12
Cycles
x 10^8

C9

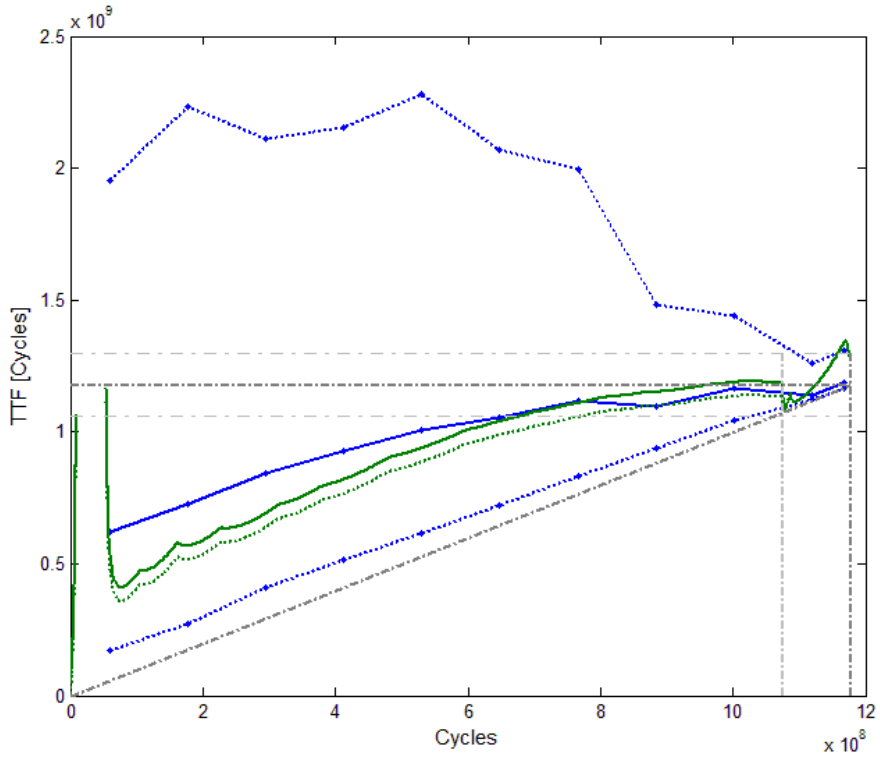
x 10^9
2.5
2
1.5
1
0.5
0
TTF [Cycles]
0
2
4
6
8
10
12
Cycles
x 10^8

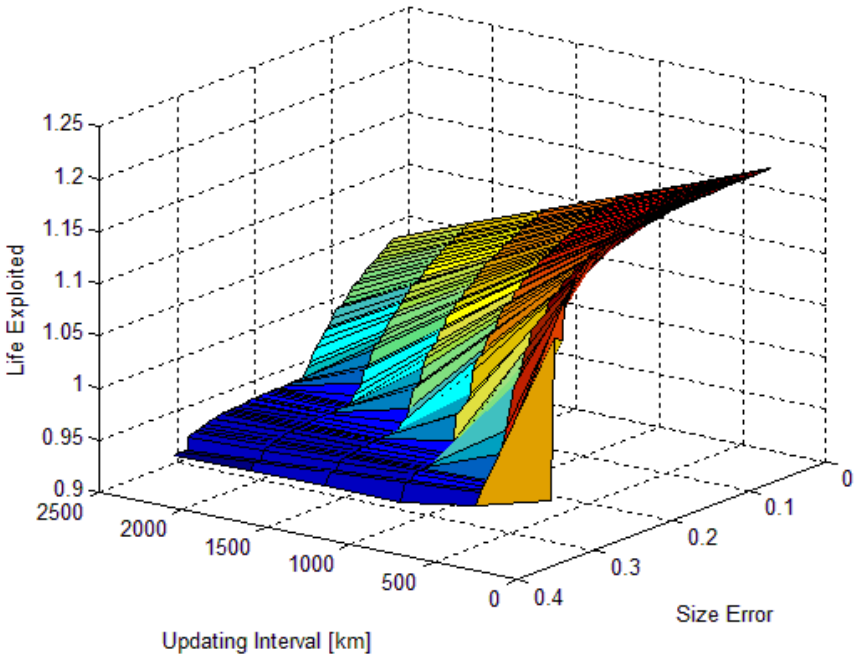
1.25
1.2
1.15
1.1
1.05
1
0.95
0.9
Life Exploited
2500
2000
1500
1000
500
0
Updating Interval [km]
0
0.1
0.2
0.3
0.4
Size Error

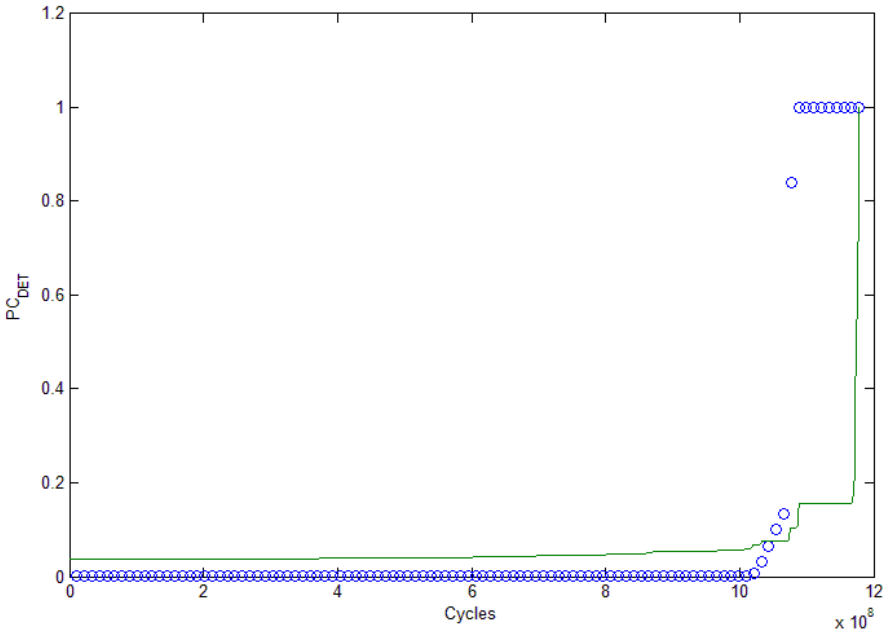
1.2
1
0.8
0.6
0.4
0.2
0
PC_{DET}
0
2
4
6
8
10
12
Cycles
x 10^8

C10

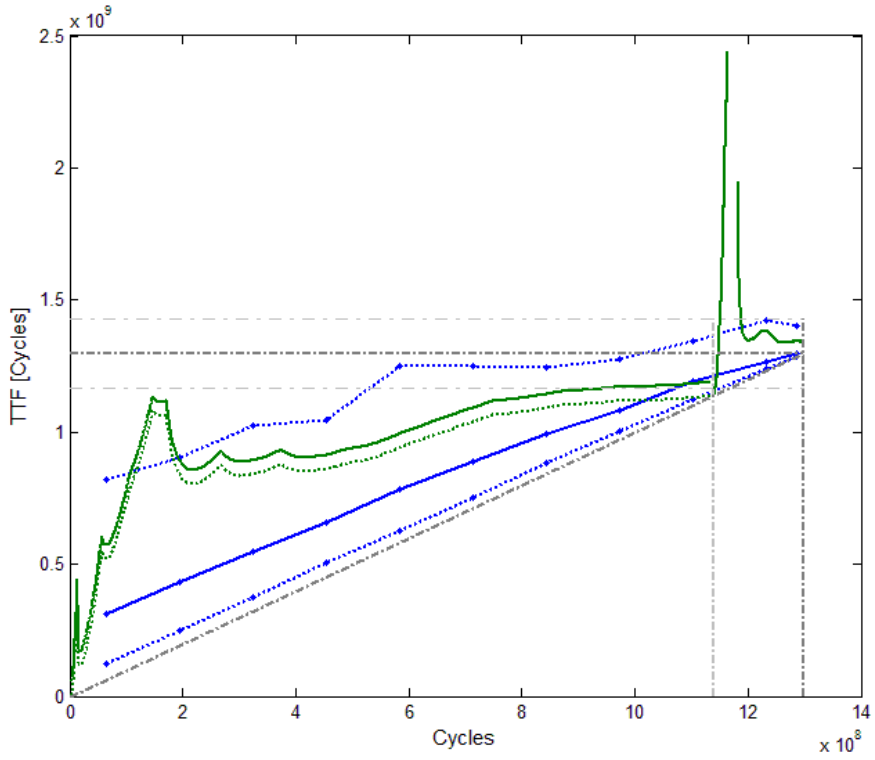
x 10^9
2.5
2
1.5
1
0.5
0
TTF [Cycles]
0
2
4
6
8
10
12
14
Cycles
x 10^8

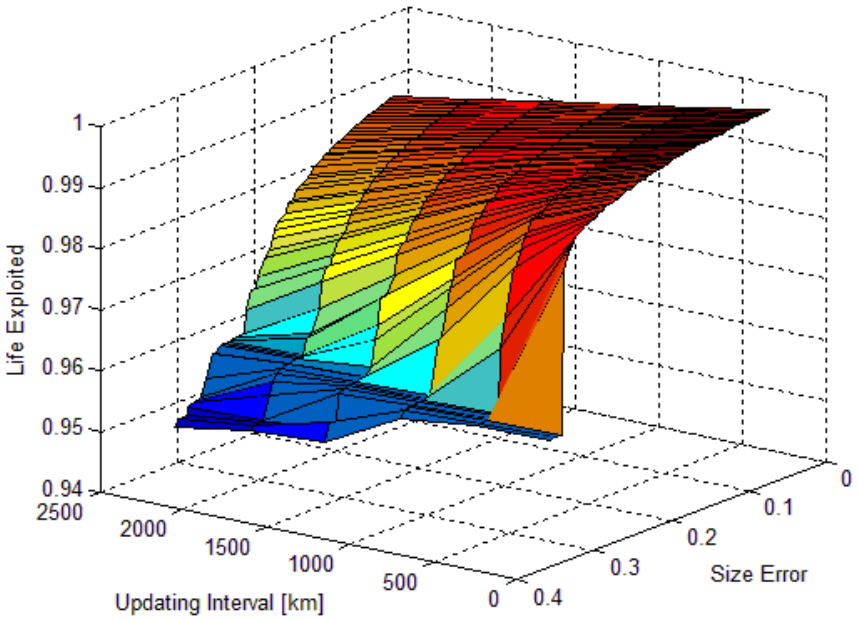
1
0.99
0.98
0.97
0.96
0.95
0.94
Life Exploited
2500
2000
1500
1000
500
0
Updating Interval [km]
0
0.1
0.2
0.3
0.4
Size Error

m

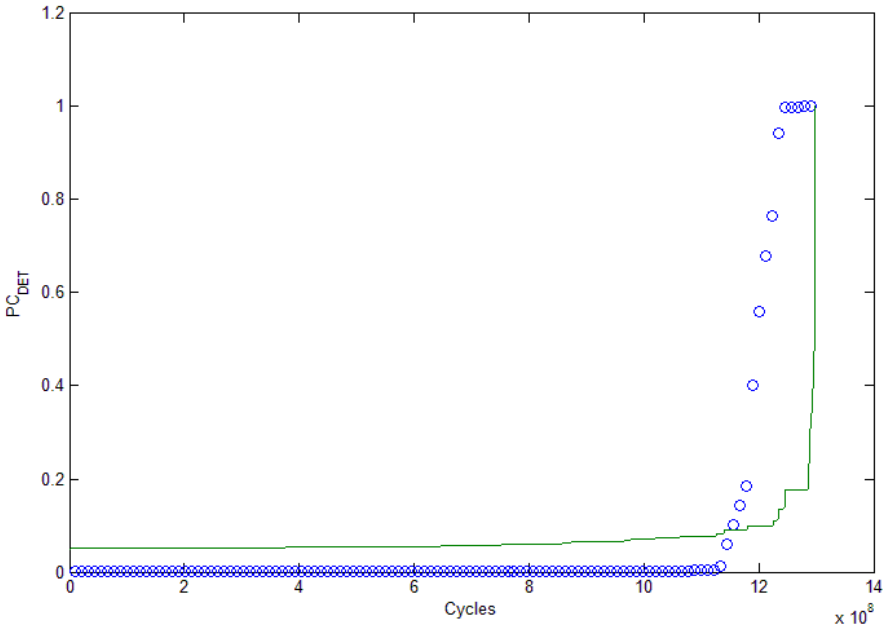
1.2
1
0.8
0.6
0.4
0.2
0
PC_{DET}
0
2
4
6
8
10
12
14
Cycles
x 10^8